DISSERTATION

submitted to the
Combined Faculties for Natural Sciences and Mathematics
of the Ruperto Carola University Heidelberg, Germany
for the degree of
Doctor of Natural Science

Presented by

Johanna Zierow, Diploma in biochemistry

Born in: Rostock, Germany
Oral examination: June, 22nd 2018

Investigation of liver sinusoidal endothelial cells - characterisation and application of new transgenic mouse models

Referees: Prof. Dr. Jonathan Sleeman
Prof. Dr. Sergij Goerdt

Parts of this thesis have been published

"*GATA4-dependent organ-specific endothelial differentiation controls liver development and embryonic hematopoiesis.*"

Géraud C*, Koch PS*, Zierow J*, Klapproth K, Busch K, Olsavszky V, Leibing T, Demory A, Ulbrich F, Diett M, Singh S, Sticht C, Breitkopf-Heinlein K, Richter K, Karppinen SM, Pihlajaniemi T, Arnold B, Rodewald HR, Augustin HG, Schledzewski K, Goerdt S.

Journal of Clinical Investigation, 127(3):1099-1114; March 2017

Acknowledgement

I would like to express my gratitude to Prof. Goerdt and Prof. Géraud for giving me the opportunity to join the laboratory and for providing me with these exciting PhD topics. I want to thank for their supervision and their scientific advises.

I want to thank Prof Sleeman for being my first supervisor, for reviewing this thesis and supporting me during the Thesis Advisory Committee meetings over the years.

Dr. Ruiz de Almodovar for her interest in this work and her advises during my Thesis Advisory Committee meetings.

Prof. Stöcklin for his interest in this work and for getting on board with my Thesis Defense Committee.

I want to thank Dr. Schledzewski and Dr. Koch for always encouraging me, and for their intellectual and practical support.

I would like to thank my cooperation partner Dr. Klapproth and Dr. Busch. The cooperation could not have been more productive and fruitful than it has been. Thank you both for the scientific input.

Of course, I want to thank all my collegues and former lab members. I really had a wonderful time together with you. You are supportive, funny and open-minded people. I want to thank especcialy Mrs. Demory for her excellent technical help and support over the years.

My greatest gratitude goes to my family who has always supported me, encouraged me and helped me through all my ups and down over the past years.

Last, but no least, I want to thank my friends from Rostock, Frankfurt, Berlin, and Ludwigshafen who accompanied me on my scientific journey, always listened to me complaining about my life and spent so many cheerful evenings and weekends together.

Abstract

Liver sinusoidal endothelial cells (LSECs) constitute organ-specific microvascular endothelial cells (ECs) with unique phenotypical and functional characteristics. They form a discontinuous endothelial sheet at the interface between the blood stream and the hepatocytes and are the most permeable vascular barrier of the mammalian body. LSECs express endocytosis receptors that clear blood borne waste molecules and ensure thereby tissue homeostasis. Under pathological conditions they participate in development and progression of chronic liver diseases or promote liver regeneration through secretion of angiocrine factors.

So far, most of LSEC research performed with mouse models relies on transgenic mice that demonstrated off-target effects in a variety of vascular beds. *In vitro* cell culture techniques only enable short-term cultivation of LSECs due to the subsequent dedifferentiation and are therefore of limited utility. To target the microvasculature of the liver more specifically transgenic mouse models were generated in which the bacteriophage-derived recombinase Cre is controlled by promoter elements of LSEC characteristic proteins. Two different founders of the Stab2-cre mouse and one founder of the Clec4g-cre mouse were characterised by reporter mouse models. All of three transgenic mouse lines demonstrated recombination in LSECs, but also in arterial and venous liver ECs. Apart from the liver, the Stab2- and Clec4g-cre mice target sinusoidal endothelial beds of other organs. A transgene activity in subpopulations of haematopoietic cells has been observed in two of three mouse lines. The pattern of Cre activity was time-dependent. Stab2-cre founder 2 mouse for example showed sinusoidal EC activity during development that broadened to most ECs in other organs during adulthood. Therefore, the transgenic mouse models can be advantageous when manipulating LSEC specific protein expression or using them for cell fate tracking. An appropriate model should be selected depending on the gene of interest and the developmental period to be investigated. In comparison to conventional and inducible endothelial transgenic mouse lines these mouse models exhibit reduced off-target effects in ECs of other organs and homogenous Cre activity in LSECs, respectively.

GATA4 was identified in a cluster of transcription factors (TFs) overexpressed in rat LSECs compared to rat lung microvascular ECs. GATA4 has a fundamental role during cardiac development and in cardiac ECs precluding the analysis of GATA4 in LSECs by conventional endothelial Tek- or Cdh5-cre mice. Consequently, investigation of the function of GATA4 in LSECs required a transgenic mouse line that would induce GATA4 loss in LSECs but not in the developing heart. Therefore, Stab2-cre founder 2 mouse was utilised to generate a conditional GATA4 knockout in LSECs. The knockout mouse demonstrated embryonic lethality with a reduced size of the fetal liver (FL) and a impaired hepatic vasculature. The FL endothelium transformed from discontinuous liver sinusoids to continuous capillaries. The capillarized ECs impaired the immigration of haematopoietic stem and progenitor cells (HSPCs) into the FL leading to lethal anaemia. Together, the data identify GATA4 as a master regulator for liver sinusoidal EC specification and for acquisition of organ-specific vascular competence supporting liver development. Finally, the results establish a role of the FL sinusoidal endothelium on maturation of HSPCs.

Zusammenfassung

Lebersinusendothelzellen sind organspezifische mikrovaskuläre Blutgefäßzellen mit einzigartigen phänotypischen und funktionellen Merkmalen. Sie bilden ein diskontinuierliches Endothelzellblatt an der Grenze zwischen dem Blutstrom und den Hepatozyten und sind die durchlässigste vaskuläre Barriere im Säugetierkörper. Lebersinusendothelzellen exprimieren Endozytose-Rezeptoren, die durch Blut übertragene Abfallmoleküle klären und dadurch die Gewebehomöostase sicherstellen. Unter pathologischen Bedingungen sind sie an der Entwicklung und an der Progression von chronischen Lebererkrankungen beteiligt, oder fördern die Leberregeneration durch die Sekretion von angiokrinen Faktoren.

Bisher basierte der Großteil der Lebersinusendothelzellforschung mit Mausmodellen auf transgenen Mäusen, die „Off-Target-Effekte“ in einer Vielzahl von Gefäßbetten zeigten. In-vitro-Zellkulturtechniken ermöglichen aufgrund der nachfolgenden Dedifferenzierung nur eine kurzfristige Kultivierung von Lebersinusendothelzellen und sind daher nur von begrenztem Nutzen. Um gezielt die kleinen Blutgefäße der Leber anzusteuern, wurden spezifisch transgene Mausmodelle erzeugt, in denen die von Bakteriophagen stammende Rekombinase Cre durch Promotorelemente von lebersinusendothelzellcharakteristischen Proteinen kontrolliert wird. Zwei verschiedene Gründer der Stab2-cre-Maus und ein Gründer der Clec4g-cre-Maus wurden durch Reporter-Mausmodelle charakterisiert. Alle drei transgenen Mauslinien zeigten eine Rekombination in Lebersinusendothelzellen, aber auch in arteriellen und venösen Leberendothelzellen. Neben der Leber steuern die Stab2- und Clec4g-cre-Mäuse Sinusendothelzellen anderer Organe an. In zwei von drei Mauslinien wurde eine Transgenaktivität in Subpopulationen von hämatopoetischen Zellen beobachtet. Das Muster der Cre-Aktivität war zeitabhängig. Beispielsweise zeigte die Stab2-cre Gründermaus 2 während der Entwicklung eine Aktivität in Sinusendothelzellen, die sich im Erwachsenenalter auf die meisten Blutgefäßzellen in anderen Organen ausweitete. Die transgenen Mausmodelle können daher vorteilhaft sein, um die lebersinusendothelzellspezifische Proteinexpression zu manipulieren oder um das Zellschicksal nachzuverfolgen. Ein geeignetes Modell sollte in Abhängigkeit von dem zu interessierenden Gen und der zu untersuchenden Entwicklungsperiode ausgewählt werden. Im Vergleich zu konventionellen und induzierbaren endothelialen transgenen Mauslinien zeigen diese Mausmodelle reduzierte „Off-Target-Effekte“ in Blutgefäßzellen anderer Organe bzw. homogenere Cre-Aktivität in Lebersinusendothelzellen.

GATA4 wurde in einem Cluster von Transkriptionsfaktoren identifiziert, die -im Vergleich zu mikrovaskulären Blutgefäßzellen der Rattenlunge- in Lebersinusendothelzellen der Ratte überexprimiert waren. GATA4 spielt eine fundamentale Rolle bei der Herzentwicklung und in kardialen Blutgefäßzellen, was die Analyse von GATA4 in Lebersinusendothelzellen durch konventionelle endotheliale Tek- oder Cdh5-cre-Mäuse ausschloss. Folglich erforderte die Untersuchung der Funktion von GATA4 in Lebersinusendothelzellen eine transgene Mauslinie, die einen GATA4-Verlust in Lebersinusendothelzellen induzieren würde, jedoch nicht in dem sich entwickelnden Herzen. Daher wurde Stab2-cre Gründermaus 2 verwendet, um einen bedingten GATA4 Knockout in Lebersinusendothelzellen zu generieren. Die Knockout-Maus zeigte eine embryonale Letalität mit einer reduzierten Größe der fetalen Leber und einem

beschädigten Lebergefäßsystem. Das fetale Leberendothel transformierte von diskontinuierlichen Lebersinusoiden in kontinuierliche Kapillare. Das kapillarisierten Gefäß beeinträchtigte die Einwanderung von hämatopoetischen Stamm- und Vorläuferzellen in die fetale Leber, was zur letalen Anämie führte. Zusammengenommen identifizieren die Daten GATA4 als Hauptregulator für die Spezifikation der Lebersinusendothelzellen und für den Erwerb von organspezifischer Gefäßkompetenz, die die Leberentwicklung unterstützt. Zu guter Letzt zeigen die Ergebnisse eine Rolle der sinusoidalen fetalen Leberblutgefäßzellen bei der Reifung von hämatopoetischen Stamm- und Vorläuferzellen.

Table of Contents

1. Introduction

1.1. Vasculature

The vasculature forms a hierarchical network that extends through the organism and connects thereby distant organs and supports the underlying tissues. The inner lining is formed by ECs which vary enormously in structure and morphology to ensure proper function (Figure 1). The vasculature can be classified in macro- and microvasculature and will be discussed more in detail in the following section.

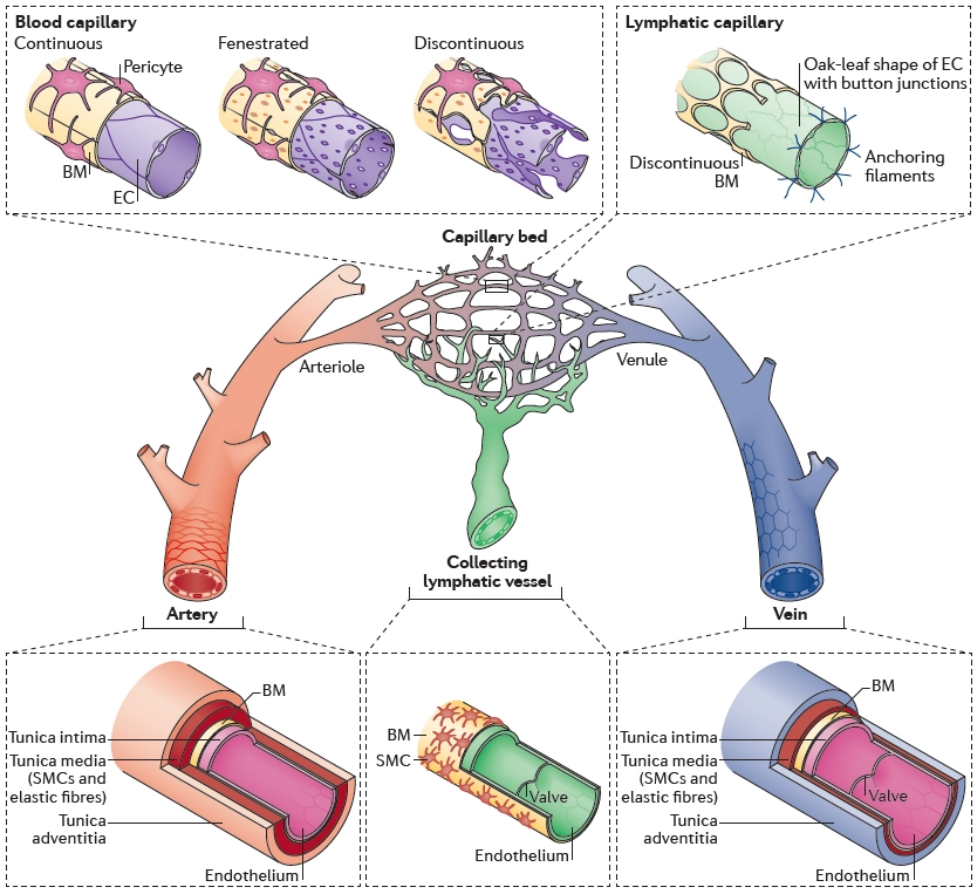

Figure 1: Organization and anatomy of the vasculature.
The hierarchical vascular network is comprised of arteries, veins, and interconnected capillaries as well as the lymphatic system. The macrovascular system (bottom of the image) connects distant organs whereas the microvasculature (top of the image) including arterioles, capillaries and venules, interacts with the underlying tissue. ECs - endothelial cells, BM - basement membrane; SMCs - smooth muscle cells. From Potente and Mäkinen [1].

1.1.1.Macrovasculature

The macrovascular system comprises the large vessels and with a diameter of more than 100 µm. The following section gives a brief overview about arterial and venous as well as lymphatic vessels.

1.1.1.1. Arterial and venous vessels

Arteries and veins constitute the macrovascular system. They are characterized by a continuous lining of ECs, a basement membrane and layers of smooth muscle cells (Figure 1) [1]. Arteries have thick walls and pulsate. The long and narrow ECs are lined in the direction of the blood flow and are characterized by tight inter-cellular junctions. Typical markers include ephrinB2, Delta-like ligand 4, neuropilin 1, Hey1 and Hey2. Veins, on the contrary, have thin walls, valves, and do not pulsate. The ECs are shorter and wider and are lined opposite to the blood flow. The tight junctions are less complex with regard to the inter-cellular molecules and protein composition. Specific markers include ephrinB4, neuropilin 2 and COUP-TF 2 [2]. Arteries transport well oxygenated blood to the organs and veins collect low-oxygenated blood from the organs, except for the pulmonary circulation, where the situation is reversed and arteries transport low-oxygenated blood and veins transport well oxygenated blood. [3].

1.1.1.2. Lymphatic vessels

Lymphatic vessels transport fluids from the pre-collecting lymphatic vessels and the microvascular lymphatic capillaries. The lymphatic system is coupled to the blood vascular system as extravasated fluid and macromolecules are collected and returned to the blood circulation at the left venous angle [1]. Lymphatic ECs of the vessels are characterised by a continuous basement membrane and perivascular smooth muscle cells which form zipper-like junctions that prevent leakage and ensure proper delivery to the lymph nodes (LNs) (Figure 1). The luminal valves are comprised of ECs with a unique spindle-like morphology that prevents retrograde lymph flow. Although lymphatic vessels are predominantly involved in immune cell trafficking they also play a role in intestinal fat absorption and cholesterol transport [4]. Compared to the blood vascular system, the lymphatic flow is slow and irregular and the transport is unidirectional. Lymphatic ECs derive from venous EC and their development is regulated by the TF PROX-1. Typical markers include, besides PROX-1, lymphatic vessel endothelial hyaluronan receptor 1 (LYVE1) and podoplanin.

1.1.2.Microvasculature

Opposite to the macrovascular system, which is responsible for the transfer of solutes to distant body parts, the microvasculature comprises vessels with smaller diameter that participate in the microcirculation of tissues and organs. Besides the microvascular lymphatic capillaries, the microvasculature comprises arterioles, venules and capillaries (Figure 1). Arterioles branch from the arteries into the capillaries and function in the regulation of the vascular tone, whereas venules collect blood from the capillaries and drain into the veins [1]. With a diameter of less than 10 µm and a thin wall consisting of only one layer of ECs the capillaries possess the largest surface of the vasculature and are responsible for the major exchange between blood and organ. Capillaries display the most diverse phenotype within the vascular tree as they vary in structure and function and are highly adopted towards the need of the underlying tissue. As a result, the phenotype of the capillaries may be continuous and either non-fenestrated or fenestrated, or discontinuous [2].

1.1.2.1. Continuous, non-fenestrated capillaries

Continuous, non-fenestrated capillaries are typically found in the heart, lung, and blood brain barrier. They are characterised on the abluminal side by the presence of a continuous basement layer that is 60 to 100 nm thick, composed of collagen type IV proteins and glycoproteins. On the luminal side an anionic glycocalyx matrix layer contributes to the endothelial barrier function. The transvascular flow occurs either via tight connected interendothelial clefts that allow for the passage of molecules with less than 1 nm in diameter [5] or via caveolae that transport larger substances [6]. High abundance of the junctional protein platelet endothelial cell adhesion molecule, also known as CD31, and expression of the basement membrane protein collagen IV enables the identification of continuous, non-fenestrated capillaries by immunological staining procedures.
Thus, continuous, non-fenestrated capillaries contribute to a restricted exchange of substance between the blood stream and the underlying tissue.

1.1.2.2. Continuous, fenestrated capillaries

Continuous, fenestrated capillaries are predominantly found in endocrine glands, intestinal mucosa and kidney glomeruli. Similar to the continuous, non-fenestrated capillaries they possess on the abluminal side a continuous basement membrane and on the luminal side an anionic glycocalyx matrix. Additionally, they are equipped with transcellular pores, so called fenestrations, which extend completely through the cell and are of approximately 70 nm in diameter. The majority of those fenestrae possess a non-membranous diaphragm across their opening which contributes to an increased permeability of small solutes and increases the size selectivity of transported substances. The density of fenestrations in EC vary between the vascular beds, in the rat jejunum for example the fenestral density is almost twice as high as in the pancreas [6]. The diaphragm

is mainly composed of the plasmalemma vesicle-associated protein (PLVAP) and is induced by vascular endothelial growth factor (VEGF) [5].
Thus, the presence of fenestrated EC enhances the transcellular flow and contributes to an increased filtration and transendothelial transport.

1.1.2.3. Discontinuous capillaries

Discontinuous capillaries, also known as sinusoids, are found in the bone marrow (BM), liver, LN, and spleen. They discriminate from the continuous capillary type by the lack of a basement membrane and a thin or partly irregular luminal glycocalyx layer [5]. Characteristics of sinusoidal EC in the BM, liver, LN, and spleen will be elaborated in the following section.

1.1.2.3.1. Bone marrow

The BM is the primary site for haematopoiesis in the adult organism and apart of delivery of oxygen and nutrients, the blood vessels serve as a vascular niche to support maintenance and differentiation of HSPCs. Two types of microvasculature, namely arterioles and sinusoidal EC, were observed to affect HSPCs different and were investigated by Itkin *et al.* in 2016 [7]. The BM sinusoids were characterised by low levels or lack of adherens and tight junction molecules VE-Cadherin and zona occudens-1, high levels of E-selectin and a diameter of 25 µm compared to a diameter of 5 µm in BM arterioles. Cells with high intracellular reactive oxygen species levels that induce HSPC mobilization and differentiation were detected adjacent to BM sinusoids. The lower blood flow due to the wider vessel lumen, the higher permeability due to fenestrations and loose junctions define the BM sinusoids as the exclusive site of rolling and adhesion of haematopoietic cells as well as transendothelial migration of mature leukocytes and immature HSPCs opposite to the BM arterioles which sustain HSPC quiescence.

1.1.2.3.2. Liver

The liver is responsible for the clearance of the blood and immune surveillance. The discontinuous capillaries in the liver form a sinusoidal network in which well-oxygenated blood from the hepatic artery and low-oxygenated, nutrient rich blood from the portal vein (PV) merges and drains into the central vein (CV). The sinusoids of liver will be discussed in more detail in section 1.1.3.

1.1.2.3.3. Lymph node

The LNs participate in the immune defence and are characterised by a network of lymphatic sinuses in close contact to immune cells and stromal cells. The lymph arrives via the afferent vessels into the subcapsular sinus, is transported to the cortical and medullary sinus and exits the LN via the efferent lymphatic vessels. High-endothelial venules (HEVs) represent the entry site for circulating lymphocytes [4]. The LN sinuses are composed of two major cell types, the discontinuous EC and macrophages, which express a unique set of

scavenger receptors and lectin like proteins. By a comparative gene expression profiling and immunohistochemistry Martens *et al.* described Stabilin- (Stab)2 to be exclusively expressed by sinusoidal EC, whereas other molecules, such as LYVE1 or CD169, showed an expression by both cell types lining the LN sinuses. The receptors mediated the binding and endocytosis of hyaluronan and carbohydrate structures which were increased or aberrant expressed on tumour cells, respectively. As a result, the LN sinuses participate in the clearance of antigens or adhesion of tumour cells during metastasis progression [8]. A study published by Iftakhar-E-Khuda *et al.* compared the transcriptome of ECs lining the sinuses of afferent and efferent lymphatic capillaries [9]. The authors identified CD169 and the macrophage scavenger receptor 1 to be exclusively expressed by the sinusoids of the subcapsular sinus whereas Endomucin was shown to be specific for sinusoidal EC of the cortical and medullary sinus. This differential protein expression pattern supported the function of the afferent lymphatic vessel to mediate the binding of lymphocytes and controlling thereby the entry into the parenchyma.

1.1.2.3.4. Spleen

The spleen collects antigen from the blood, is involved in immune responses to blood-borne pathogens and participates in the recycling of iron and in b-cell maturation [10]. The incoming blood drains via a network of branching arterial vessels into smaller arterioles and is then transported into venous sinusoids. Two distinct anatomic structures are present in the spleen, the white and the red pulp, separated by the marginal zone. The white pulp shows smaller branches of arterial capillaries and comprises the t-cell zone and b-cell follicle and promotes thereby a large interface for the immune defence. Most arterial capillaries terminate into the splenic sinusoids in the red pulp [11]. Characteristically, the sinusoidal ECs in the red pulp have a discontinuous phenotype but comprise a thin anionic glycocalyx and show low levels of phago-endocytosis. Sinusoidal ECs have a cuboidal phenotype and the interendothelial junctions are located at the apical and basal side up to 3 µm apart. On the abluminal side, stress fibres run in parallel to the cellular axis and connect the EC to the extracellular matrix (ECM) and guide erythrocytes into the sinuses through the interendothelial slits [5].

1.1.3. Liver sinusoidal endothelial cells

The liver receives blood from the arterial and venous vessels which is then filtered by the sinusoids and exits through the CV. The liver is comprised of the liver parenchymal cells, the hepatocytes, the non-parenchymal cells, including the Kupffer cells, stellate cells and sinusoidal ECs, and the biliary epithelial cells. LSECs separate the blood stream from the hepatocytes and are characterised by the perisinusoidal space, the so-called space of Dissé, in which the stellate cells reside, whereas the Kupffer cells, the liver resident macrophages, patrol in the lumen of the sinusoids (Figure 2) [12] .

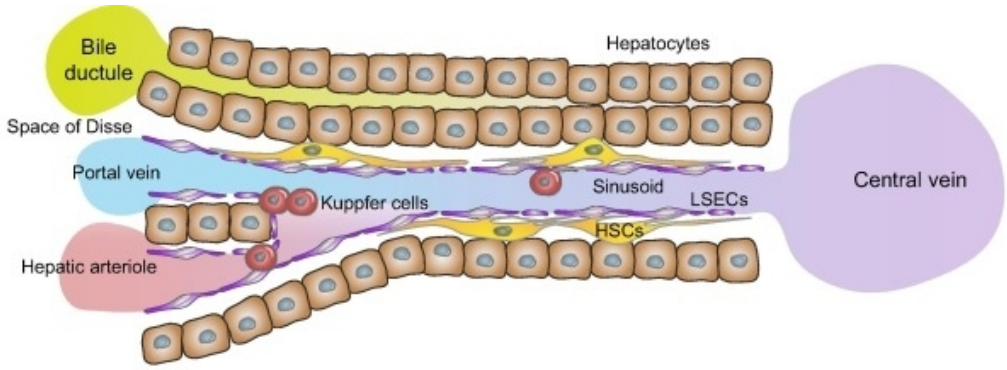

Figure 2: Schematic view of the sinusoids in the mammalian liver.
Blood drains from the PV and the hepatic artery in the liver sinusoids and leaves through the CV. The bile runs in the opposite direction and is collected in the bile duct. The liver resident macrophages, Kupffer cells, the ECs and the hepatic stellate cells constitute the sinusoids. The space of Dissé separates the LSECs and the hepatocytes. HSC – hepatic stellate cells. From Iwakiri *et al.* [13]

1.1.3.1. Phenotypical features

The LSECs comprise approximately 50% of the non-parenchymal cells of the liver. They are characterised by open fenestrations that occupy 6% to 8% of the endothelial surface, are of 100 – 150 nm in diameter and arranged in sieve plates. LSECs are connected by intercellular junctions, display no gaps [14], lack a basement membrane and are devoid of a glycocalyx matrix fibres within the fenestrae [2].
The presence of fenestrations in LSECs correlate with the presence of membrane rafts [15], so called microdomains in the cell membrane [16]. Svistounov *et al.* [15] applied three-dimensional structured illumination fluorescence light microscopy to investigate fenestrations in a primary culture of LSECs. Membrane rafts appeared in the perinuclear region in contrast to the fenestrations that were observed in the cellular periphery. Following treatment with several drugs, the numbers of membrane rafts were increased or decreased leading to a decrease or increase in the formation of fenestrations, respectively. By that the authors demonstrated an inverse relationship of membrane rafts and fenestrations and improved the understanding of those highly dynamic structures [15].

Typically, if studying LSECs *ex vivo* one encounters the problem that LSECs are difficult to isolate and rapidly lose their phenotype upon culture. Several methods regarding isolation from human, rat, porcine, or murine livers were published over the last

years and were critically discussed by the community [14]. Some of the points of criticism included that the antibodies applied for isolation were not commercially available [17], the isolation resulted in impurities [18] or markers for isolation were not chosen properly [19]. Similar controversy occurs with regard to the cultivation of LSECs [14]. Few scientists claim that LSECs can be cultivated and can be applied for experiments from a commercially available cell line [20] which is in contrast to the claim that LSECs die upon culture due to toxic effects of the serum supplemented to the growth medium [21], or that LSECs cannot be cultivated due to the lack of the liver specific microenvironment [22]. The latter statement is supported by several publications that demonstrate a decrease or loss of fenestrations already after one day in culture [14,23], loss of marker protein expression upon cultivation [24] and an impaired ability to perform endocytosis after several days in culture [25]. In order to circumvent these problems, one can either utilize LSECs for the analysis within a few hours after isolation, use tissue sections or apply *in vivo* methods to study LSEC functions.

In a comprehensive study Géraud *et al.* analysed the molecular components of LSEC junctions on human and rat liver sections [26]. Adherens junctions are cell-cell connections that are directly linked to the actin cytoskeleton [16] and were observed in LSECs by the high abundance of VE-Cadherin and the intracellular interaction partners α- and β-catenin as well as p120 catenin and plakoglobin. Tight junctional protein complexes function as barrier between neighbouring ECs [16] and are typically not found in human and rat liver sinusoids which was evident by the absence of occludin. However, the junctional adhesion molecule A was expressed in human and rat LSECs [26]. Therefore, LSECs can be identified by the classical adherens junction molecules, such as VE-Cadherin or β-catenin, or by the tight junction protein junctional adhesion molecule A. In addition to that, LSECs express cell surface marker that are also found in other sinusoidal capillary beds, like Stab2 [27] or LYVE1 [8].

1.1.3.2. Origin and formation

During the 80s and 90s, new insights in the field of liver development derived from ultrastructural analysis in human, rat, and mouse FLs. By using electron microscopy, the formation of the liver sinusoids was monitored during onset of liver organogenesis or during the phase of liver growth. Despite differences regarding the presence of fenestrations or gaps, the FLs showed remarkably common characteristics across mammalian species. During onset of liver formation, the sinusoids of the rat FL demonstrated a continuous EC lining, which were devoid of a basal lamina and had low numbers of diaphragmed fenestrations [28]. Murine sinusoids were characterised by a continuous sheet of ECs with the presence of tight junctional complexes [29]. In human, the primitive intrahepatic capillaries were defined as $CD31^{+}$ ECs between the hepatic cords which differentiated into $CD31^{low}$ $Laminin^{low}$ sinusoids or into $CD31^{+}$ $Laminin^{+}$ PV EC during onset of liver formation [30]. In the phase of liver growth, the sinusoids of fetal rat liver were still lined by continuous EC with diaphragmed fenestrations that were then gradually outnumbered until birth by fenestrations without diaphragms [28]. The murine sinusoids started to adopt a discontinuous endothelial phenotype with partially fenestrations [29]. In human, the phenotype of the FL vasculature resembles the adult

phenotype as sinusoidal ECs completely lack CD31 and Laminin expression [30]. Human, rat and mouse LSECs show hereby a high degree of plasticity because the liver sinusoids switch from a continuous to discontinuous endothelial phenotype during gestation.
Despite their continuous phenotype, the FL sinusoidal capillaries already express marker of adult LSECs [31]. The first ECs of the developing liver showed no vascular lumen and occasionally expressed Stab2. The increase of sinusoidal EC within the FL was accompanied by an increase of LYVE1 and Stab2 expression. During liver growth, $Stab2^+$ and $LYVE1^+$ EC were observed in the fetal sinusoids as well as in the large vessels, nevertheless, expression of LYVE1 and Stab2 in arterial and venous EC was diminished after birth.
Combination several transgenic mouse models allowed Zhang *et al.* to track liver ECs during development and demonstrated that the liver vasculature is derived from endocardial cells of the sinuous venosus [32]. The authors showed that during onset of liver formation, descendants of endocardial cells were involved in the formation of the initial liver endothelium. The cells accounted for approximately 40% of the liver EC during liver growth and persisted until the adulthood. Timed induction of the reporter system proved that the descendant cells contributed to the liver vasculature during the time of formation of the liver bud indicating a common endothelial origin hepatic and cardiac ECs.

1.1.3.3. Functional characteristics

LSECs possess high a phago-endocytic capacity which is facilitated by the expression of endocytosis receptors. So far, three main types of endocytosis receptors have been described in LSECs, the scavenger receptor, the mannose-receptor and the Fc-gamma receptor [33]. The mannose-receptor, CD206, binds to terminal mannose residues and internalizes substrates in a Ca^{2+} dependant manner. CD206 consists of an N-terminal cysteine-rich domain, a fibronectin type II domain, and several C-type lectin-like domains [34]. The Fc-gamma receptor IIb, CD32b, is involved in the binding and uptake of the Fc domain of immunoglobulin G and participates thereby in immunological functions [33]. The extracellular part of CD32b consists of two highly glycosylated Ig-like domains and the intracellular part is characterised by an immunoreceptor tyrosine-based inhibition motif [35]. Of the scavenger receptors, a variety has been discovered to be expressed in LSECs or in other cell types such as macrophages, dendritic cells or natural killer cells. Based on their function they were classified into ten groups (SR-A to SR-J) [36]. The macrophage scavenger receptor type I and II belong to the class A scavenger receptors, SR-A, and is a homotrimeric transmembrane protein with an extracellular scavenger receptor cysteine-rich domain and a collagen-like domain [37]. In LSECs, it internalises β-amyloid, heat shock proteins, surface molecules of Gram-positive and Gram-negative bacteria, and hepatitis C viruses [38]. The platelet glycoprotein 4 belongs to the class B scavenger receptors, SR-B, [36] and consists of two short intracellular domains at both termini and a large extracellular domain with a hydrophobic sequence where lipid ligands bind [39]. Besides fatty acid uptake, it facilitates the internalisation of apoptotic cells and amyloid proteins [40]. The hyaluronan receptors Stab1 and Stab2 are grouped into the class H scavenger receptors, SR-H [36]. Stab1 and Stab2 are both multidomain proteins consisting of fasciclin, epidermal

growth factor- (EGF) like and Laminin-type EGF-like domains as well as a linker region and share about 40% homology [41]. Stab2 is the primary receptor for hyaluronan and is responsible for the uptake of heparin, chondroitin sulphate, dermatan sulphate, non-glycosaminoglycan, acetylated low-density lipoprotein, pro-collagen propeptides and advanced glycation end products [42,43]. Stab1 mediates the endocytosis of acetylated low-density lipoprotein, Gram-positive and Gram-negative bacteria [41,42,44]. Other receptors with known scavenging functions are for example the c-type lectin domain family 4 member G (CLEC4G) or LYVE1.

Implication of the scavenger receptors on tissue homeostasis was emphasized by Schledzewski *et al.* who genetically inactivated the hyaluronan receptors Stab1 and Stab2 [45]. While single knockouts of Stab1 or Stab2 did not cause any gross abnormalities, the double knockout resulted in a decreased survival rate and a perisinusoidal liver fibrosis. Although no metabolic dysfunction of the liver was observed, the authors determined severe defects of the kidney function. Detailed analysis revealed a glomerular fibrosis and a proteinuria that was caused most likely by circulating, yet, unidentified factors.

Over the past years, the liver sinusoidal endothelium became more and more recognised as key players in instructing neighbouring cells and participating in regeneration, metabolism and liver formation. Pioneering work in this field derived from S. Rafii and colleagues who defined the term 'angiocrine' as "vascular niche-derived paracrine factors" [46] and emphasized the critical role of the endothelium on tissue homeostasis. LSECs secrete angiocrine factors and promote liver regeneration. Ding *et al.* demonstrated the contrasting function of the C-X-C chemokine receptors type 4 (CXCR-4) and type 7 (CXCR-7) in LSECs during acute and chronic liver injury [47]. After acute liver damage, CXCR7 induced the upregulation of the TF Id1 that lead to a secretion of angiocrine factors from LSEC which were known to promote angiogenesis and trigger liver regeneration. After chronic liver damage, however, signalling from fibroblast growth factor (FGF) receptor 1 induces upregulation of CXCR-4 which inhibited Id1 and caused an increase of ECM proteins and induced a pro-fibrotic niche. Besides the balance of CXCR-4 and CXCR-7 signalling on liver regeneration, angiopoietin-2 was identified to control liver regeneration in a spatiotemporal manner [48]. During the first phase of liver regeneration, hepatocyte proliferation was ensured by low levels of LSEC-derived angiopoietin-2. However, during the second phase of regeneration the increase of angiopoietin-2 expression from LSECs is necessary to promote angiogenesis. These findings underline LSECs as highly dynamic structures in orchestrating organ regeneration and highlight their function on liver homeostasis.

1.1.3.4. Pathological aspects

In a healthy and physiological surrounding, LSECs participate in a variety of processes. Under pathological conditions, however, LSECs can engage the initiation and progression of liver diseases, for example through the transformation of their sinusoidal phenotype, activation of quiescent stellate cells, or promotion of cancer progression [49].

LSECs display a unique phenotype along the microvascular bed as they are characterised by fenestrations and discontinuity. Loss of these characteristics, i.e. the reduction of

fenestrations, the formation of a basement membrane and the change in the marker expression profile, is called capillarization *in vivo* or dedifferentiation *in vitro*. It classifies early events during various liver diseases and many researchers attempted to gain insight into the mechanism. However, if studying liver sinusoidal capillarization as an isolated process in mouse models, problems can occur due to secondary effects that distort the results. Lao *et al.* circumvented this pitfall by applying sodium arsenite to the mice which was reported to induce hepatic capillarization without the subsequent fibrotic events [50]. Proteome profiling of treated versus untreated mice identified, among others, disabled homolog 2 (Dab2) to be upregulated in dedifferentiated LSECs. Dab2 mediates endocytosis of the VEGF receptor and the increased Dab2 expression correlated with an increased VEGF signalling as well as increased VEGF receptor endocytosis during dedifferentiation in LSECs. However, VEGF was reported to maintain LSEC differentiation [51], consequently Lao *et al.* hypothesized that the Dab2 mediated VEGF receptor endocytosis dominated over the VEGF concentration effect during LSEC dedifferentiation [50].

Capillarization of LSECs is a result of toxic liver injury, non-alcoholic steatohepatitis or alcoholic liver injury and can progress further into chronic liver disease [52]. The phenotypical liver fibrosis is characterised by an accumulation of ECM in the perisinusoidal and periportal area. Fibrosis can develop into cirrhosis or liver failure and is reversible until a specific time point after which the only effective treatment is liver transplantation [53]. LSEC participate in the fibrotic events through activation of stellate cells which is characterised by an increase of α-smooth muscle actin and type I collagen [54]. DeLeve demonstrated that if stellate cells were cultured alone, they became activated, but if stellate cells were co-cultured with differentiated LSECs, the activation was reversed, and if stellate cells were co-cultured either with dedifferentiated LSECs or with hepatocytes, the activation persisted. This indicated that LSECs sustained a quiescent stellate cells phenotype under physiological conditions and that dedifferentiated LSECs promoted stellate cell activation. LSEC-derived nitric oxide was a prerequisite to sustain stellate cell quiescence and was induced by VEGF from hepatocytes or stellate cells which emphasize the tightly regulated signalling events in the hepatic vascular niche.

The final fate of chronic liver disease is in some cases hepatocellular carcinoma (HCC) and loss of the LSEC marker profile correlated with the disease outcome [55]. In mouse models of HCC, loss of LSEC marker was observed in liver tumours and the extent of marker reduction correlates with the size of tumour nodules. Similarly, in liver samples from HCC patients LSEC markers were lost in the tumours. Analysis of the peritumoural tissue identified Stab2 to be less expressed and loss of peritumoural Stab2 was associated with an increase of the overall survival rate. The authors concluded that loss of specific marker expression in the progression of HCC could provide a tool to identify subsets of HCC and facilitate the prognosis and treatment of this severe cancer.

1.1.4. Targeting liver sinusoidal endothelial cells by transgenic mouse models

Genetic manipulation of protein functions *in vivo* has considerable benefits compared to the investigation of protein functions *in vitro*. The discovery of new methods over the past decades facilitated the targeted depletion, modification or overexpression of genes and ribonucleic acid (RNA) molecules. In 1992, Orban *et al.* described a method that would allow the tissue- and/or site-specific DNA recombination [56]. The Cre/loxP system utilizes the ability of the bacteriophage P1 derived Cre recombinase to recognize the loxP site, a 34 base pairs (bp) long DNA sequence and to recombine two loxP sites. Depending on the orientation of the loxP sites, either as direct or as inverted repeats, the Cre recombinase is able to excise or to invert a DNA fragment, respectively. Flanking of promoter regions, exon fragments or whole coding sequences with loxP sites enables the targeted manipulation of proteins by a precise excision of gene fragments. The expression of the Cre recombinase does not have to be ubiquitous but can be restricted or targeted by promoters of proteins with known spatial or temporal activity.

With a growing interest in the macro- and microvascular system, the number of available transgenic mice increases that allow for an endothelial specific activity of the Cre recombinase. Until today, three transgenic mouse models are accessible that are frequently used to target the sinusoidal endothelium of the liver. First, the Tek-cre transgenic mouse, published by Kisanuki *et al.* [57] that utilizes the promoter of the angiopoietin receptor Tie2 to drive the expression of the Cre recombinase in ECs. Second, the Cdh5-cre transgenic mouse, which was published by Alva *et al.* [58], that uses the promoter of the junctional molecule cadherin-5. Third, the flk-1-cre transgenic mouse, which was published by Licht *et al.* [59] that utilizes the promoter of the VEGF receptor 2, which fulfils a variety of functions in ECs.

All three transgenic mouse models show an activity of the Cre recombinase in ECs from early fetal development onwards and target the complete macro- and microvasculature in all organs of the adult mouse. Therefore, a transgenic mouse model with activity selectively in the liver sinusoids has not been generated yet.

1.2. Liver organogenesis

The liver is the largest internal organ with functions in metabolism as well as secretion from endocrine and exocrine glands. The hepatoblasts and biliary epithelium develop from the endodermal-derived foregut whereas sinusoidal ECs, Kupffer cells and stellate cells are rather mesodermal-derived cell types. In the following section, hepatic specification, liver growth and postnatal liver development will be described (Figure 3).

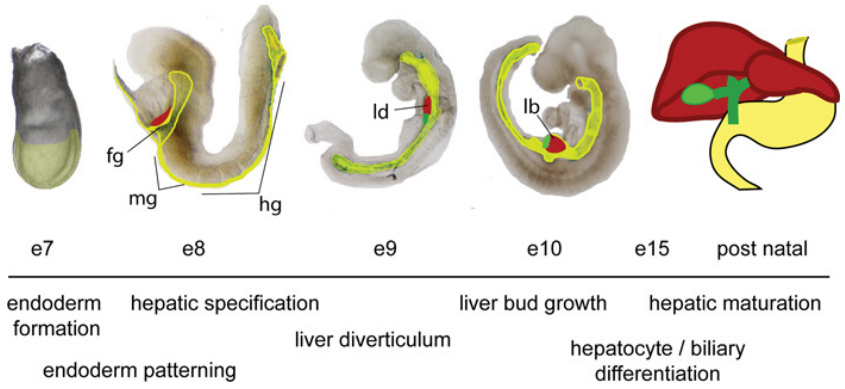

Figure 3: Time line of mouse liver development.
The three germ layers are formed during gastrulation between embryonic day (E)6.5 and E7.5 The endoderm is patterned along the anterior-posterior axis which results in the separation of foregut (fg), midgut (mg), and hindgut (hg) around E8. The liver diverticulum (ld) emerges from the ventral foregut adjacent to the heart and expands to the liver bud (lb) at E9. From E10 onwards the liver growth and maturation proceeds into the postnatal stage. From Zorn [60]

1.2.1. Initiation of liver development

During gastrulation, between embryonic day (E)6.5 and E7.5, the three germ layers (ectoderm, mesoderm, and endoderm) are formed from the inner cell mass and generate subsequently the definitive endoderm. Surrounded by the mesoderm and further anterior-to-posterior patterning subspecialize the now ventral definitive endoderm into foregut, midgut, and hindgut [61]. The closure of the foregut and morphogenetic movements of mesodermal layers at E8.5 positions the hepatic rudiment distant to cardiac mesoderm and close to the surrounding mesenchyme of the septum transversum [62]. During this process important inductive cues derive from GATA4, Bone morphogenetic protein (BMP)4 and FGFs. Further signalling from the heart and mesenchyme initiate a transition from unspecified cells of the liver diverticulum into cells with a columnar morphology that start to express typical hepatocyte genes like Albumin or hepatocyte nuclear factor (HNF)4α. Approximately at E9, the liver diverticulum has transitioned into a pseudostratified epithelium that starts to delaminate and invade the surrounding stroma [63]. BMP signalling from the septum transversum mesenchyme (STM) plays a pivotal role during this process. The septum transversum mesenchymal cells, which contribute to the epicardium and diaphragm, promote outgrowth of the liver bud into the septum transversum. After colonization by hepatoblasts, cells from the STM and liver bud move toward the midgut and caudal to the developing heart [4]. A research published by

Matsumoto *et al.* investigated the role of ECs on liver organogenesis prior to liver bud formation [65]. They detected single ECs between the pseudostratified hepatic epithelium and the STM around E8.5. From E9.0 to E9.5, during delamination and invasion of the hepatic cord into the STM, single ECs started to organize into vascular structures and lined the nascent sinusoids from E9.5 onwards. Depletion of ECs from the embryos induced the formation of the liver diverticulum but the invasion in the STM was missing. By using explants experiments the authors could show that ECs are crucial for the growth of the hepatic mass. Consequently, Matsumoto *et al.* postulated a critical role for the nascent endothelium by providing angiocrine factors to stimulate proliferation of the hepatoblasts.

1.2.2. Fetal liver haematopoiesis

Immediately after formation of the liver bud the FL becomes the primary haematopoietic organ until birth when haematopoiesis shifts to the BM. Several haematopoietic waves take place during embryogenesis switching thereby anatomical locations in the embryo and ensuring by that the generation of a large number of haematopoietic cells with different pronounced differentiation states. In the first wave the FL is seeded by myeloerythroid progenitors that arose in the YS around E7.5 and entered circulation with the initiation of the heartbeat. The terminal differentiation takes place in the FL because the YS does not provide a proper niche for the final maturation. During the second wave definitive haematopoietic stem cells (HSCs) immigrate into the FL from the aorta-gonad-mesonephros (AGM) region and the placenta. The AGM region consists of the ventral wall of the dorsal aorta, the genital ridges and the mesonephros and is the first intraembryonic site of haematopoiesis. Here, the definitive HSCs are sought to develop around E10.5. After E12.5 the FL becomes the only haematopoietic organ where HSCs proliferate and differentiate, however, the FL is not able to generate HSC *de novo* [66]. The rapid expansion of the FL from E10.5 to E11.5 is primarily a consequence of the increase of haematopoietic activity. The relative amount of the haematopoietic cells increases from one third to three quarter of the total FL mass from E11.5 to E13.5 [67]. In order to gain a better understanding of the events that happen during initiation, peak, decline, and disappearance of the FL haematopoiesis Guo *et al.* investigated the FL at E11.5, E14.5, E15.5 and 3 days postpartum (dpp), respectively [68]. The authors discovered more transcriptomic and proteomic differences between E14.5 and E15.5 than between E11.5 and E14.5 suggesting for a key step from E14.5 to E15.5. Between E11.5 and E14.5 genes involved in proliferation, maintenance or differentiation of haematopoietic cells were increased and genes involved in several metabolic functions were suppressed. From E14.5 to E15.5, haematopoietic activity was rapidly decreased and the FL displayed an increase of genes typical for the adult liver function including upregulation of genes associated with metabolism of carbohydrates, protein and fatty acids. This key point during maturation of the FL was characterized by a decreasing number of HSCs and a gain of transcriptional activity for metabolism-associated genes. The metabolic liver functions were restricted during the proliferation and differentiation phase of HSC and were subsequently expanded from E15.5 onwards which was accompanied by the differentiation from hepatoblasts to hepatocytes. Guo *et al.* hypothesized that both, the FL stromal cells and undifferentiated

hepatocytes, support and stimulate haematopoiesis by releasing cytokines or creating a hypoxic milieu.
Since the haematopoietic progenitor cells (HPCs) from the YS or AGM region have to encounter first the endothelium before migrating into the FL the role of fetal LSECs during this process was investigated. In 2014, Dartsch *et al.* published a study about the effect of increased junctional stability of FL sinusoids on haematopoiesis [69]. Junctional stability was manipulated by covalently linking vascular endothelial (VE-) cadherin to α-catenin which resulted in embryonic lethality during mid-gestation, a reduced FL size as well as an aberrant haematopoietic-to-hepatoblast ratio. Investigation of HSPCs revealed proper formation in the AGM region but an accumulation in the fetal blood. The authors observed a low number of HSPCs in the liver that were still able to differentiate into various haematopoietic lineages. Thus, the increased junctional stability of LSECs caused an impaired entry of HSPCs into the FL.

1.2.3.Perinatal liver zonation

During mid-gestation hepatoblasts are still bi-potent and are able to differentiate into hepatocytes or biliary epithelial cells. Around E13, FL cells that are in contact with the PV start to increase cytokeratin-19 expression and decrease hepatic genes. From E17 onwards, the cells are surrounded by the portal mesenchyme and further formation of the intrahepatic bile ducts takes place until the perinatal period. Cells that are not in contact with the PV start to differentiate into hepatocytes which is triggered by signalling molecules secreted from haematopoietic cells. Around E17, hepatocytes adopt their characteristic morphology and are arranged in hepatic chords [60]. During the prenatal phase the foetus is provided with nutrients from the maternal liver but after birth the hepatocytes perform metabolic functions. The organization of hepatocytes within the liver acini is thereby not uniform but rather are the hepatocytes distributed heterogeneously and are divided in zones according to their vicinity to the PV. Liver zonation is fully established at 10 dpp and is controlled by Wnt/β-catenin signalling which demonstrated the highest activity around the CV. Since Rspondins (Rspo) were reported to regulate Wnt signalling activity, Rocha *et al.* studied the role of Rspo signalling on the formation of liver zonation [70]. Expression of Rspo-3 was observed in liver ECs of the CV at E17 and remained until adulthood. Induced deletion of Rspo-3 during at E16.5 or after 8 weeks resulted in defects of the formation of the liver zonation with a characteristic abrogation of the periportal zonation pattern. Vice versa, ectopic expression of Rspo-1 reverses the effect of the Rspo-3 knockout and established an expansion of the pericentral zone. The authors concluded that the loss of Rspo signalling prevents pericentral differentiation which indicates a periportal gene expression profile in the hepatocytes as a default state.

1.3. The transcription factor GATA4

Control of gene expression is a key element in different cell types and during development to adapt the repertoire of proteins and respond to external stimuli. Gene activity is regulated by TFs that bind to proximal or distant regulatory DNA elements and thereby activate or repress transcription. Classification of TFs into specific families and subfamilies is dependent on their DNA-binding domain which is mostly comprised of an α-helix that interacts with the major groove of the DNA. The zinc finger proteins are one of the major families of TFs and are named after the central Zn^{2+} ion in their conserved DNA binding motif [16]. In the following section the GATA-binding TF family of zinc finger proteins are described more in detail with a main focus on GATA4.

1.3.1. The family of GATA-binding transcription factors

The first member of the mammalian family of GATA-binding TFs was described in 1988 by Evans *et al.* by the identification of GATA1 as an enhancer for the β-globin gene expression [71]. Over the years five additional homologues (GATA2/3/4/5/6) were discovered and grouped into two subfamilies based on their functional implications. GATA1/2/3 play a central role during differentiation of the haematopoietic system and GATA4/5/6 are involved in formation endodermal-derived organs. The GATA TFs are named after the consensus DNA sequence (A/T)GATA(A/G) which they recognise with a class IV zinc finger. In proteins with two zinc finger domains the C-terminal zinc finger binds the DNA whereas the N-terminal zinc finger regulates the DNA binding through interaction with co-factors. The C-terminal zinc finger and basic domain are highly conserved throughout evolution in vertebrates, insects, Nematode, fungi, slime mould, and plant [72].

1.3.2. Expression of GATA4 in the mouse

The TF GATA4 was identified by Arceci *et al.* by using oligonucleotides that map the conserved region in the zinc finger domain in order to screen a complementary DNA (cDNA) library of murine embryo at E6.5 [73]. GATA4 differs from the GATA1/2/3 group through low sequence homology outside the zinc finger domain and the absence of binding to other GATA TFs. Northern Blot analysis revealed GATA4 messenger (m)RNA expression in the heart, ovary and testis and to a weaker extent in the lung, liver, and small intestine. By in situ hybridization, GATA4 transcripts were detected, among other things, in the fetal heart and primitive endoderm. In order to deepen the knowledge about GATA4 expression during murine development a transgenic mouse was generated that harbours a knockin allele containing a DsRed2-IRES-cre expression cassette instead of the GATA4 exon 2 to monitor endogenous GATA4 transcriptional activity [74]. The initiation of reporter expression at E5.5 indicates a transcriptional start of GATA4 at the blastocyst stage. The authors could detect GATA4 messenger RNA (mRNA) by whole mount in situ hybridization in the inner cell mass at E4.5 indicating that GATA4 is involved in primitive endoderm differentiation. Application of several transgenic mouse lines demonstrated a

GATA4 expression in migratory neural crest cells and in subpopulations of neural crest stem cells.
These studies show that GATA4 is expressed during pre-implantation period and is involved in cell fate decision in embryonic germ lines. Observation of GATA4 transcripts in heart, liver, lungs, gonads, and intestine inspired many researchers to study the function of GATA4 in those organs. Highlights of these studies are summarized in the following section.

1.3.3. Critical role of GATA4 during development

1.3.3.1. Cardiac development

Two studies were published characterising the global GATA4 knockout. First, Kuo *et al.* generated a GATA4 genetic inactivation by replacing the first coding exon [75]. The mutant embryos were characterised by an embryonic lethality around E8.5, absence of the heart tube, malformations of the gut and yolk sac (YS). No delay in development was observed. They concluded that GATA4 was not required for differentiation of cardiac myocytes or endocardial cells but instead for embryonic folding which is a prerequisite to generate the pericardial cavity, the heart tube, and the foregut. In a slightly different approach Molkentin *et al.* generated the global GATA4 knockout in the mouse [76]. The replacement of exons encoding the zinc finger domains with a neomycin cassette resulted in a loss of functional GATA4 mRNA. Similar to Kuo *et al.*, the embryos died around E9.5 with prominent cardiac defects and arrested in development. The authors concluded that GATA4 controlled lateral to ventral folding by regulating the migration of mesodermal precursors along the endoderm. Notably, the only difference between these studies is the use of a GATA4 transgenic mouse on C57BL/6 and SV129 mixed background by Molkentin *et al.* [76] or on a C57BL/6 and CD1/Agouti mixed background by Kuo *et al.* [75].
Function of GATA4 on early heart specification was obvious but early embryonic lethality precluded the analysis during cardiac maturation. In order to elucidate the function of GATA4 in endocardial cells and endocardial-derived mesenchymal cells during cardiogenesis, Rivera-Feliciano *et al.* inactivated the GATA4 gene in ECs by using the Tek-cre transgenic mouse [77]. Functional GATA4 was absent in atrioventricular cushions at E11.5 which caused an embryonic lethality around E12.5 with peripheral haemorrhage and pericardial effusion in the mutant embryos (Figure 4). Notably, the mutant embryos showed a reduced FL size resulting either from the developmental defects of the heart or from Cre activity of the Tek-cre mouse in the FL. During formation the heart, the atrioventricular cushions develop into the atrioventricular valves which are essential for the proper separation of atrium and chamber. The decreased cellularity of the atrioventricular cushions in the mutant embryo was a result of an impaired transformation of the endocardium into an invasive mesenchyme which is a prerequisite for cushion formation. Explants and rescue experiments demonstrated a role of GATA4 on the regulation of Erbb3 expression in atrioventricular endothelium which induced the transformation of cardiac endothelium to mesenchymal cells.

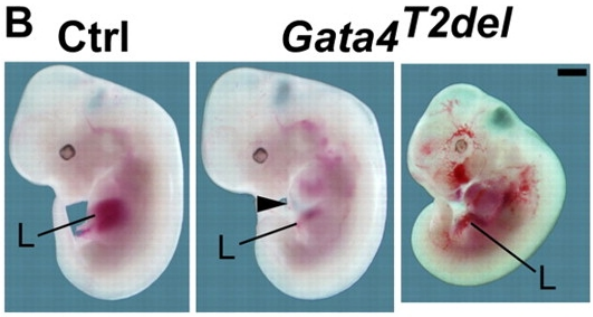

Figure 4: Phenotype of embryos with endothelial-restricted inactivation of GATA4 (Gata4^{T2del}). Gross appearance of E12.5 control and Gata4^{T2del} littermates. Mutants showed liver hypoplasia (L) and variable growth retardation, peripheral haemorrhage and pericardial effusion (arrowhead). From Rivera-Feliciano *et al.* [77]

The interaction of GATA-4 with Friend of GATA (FOG) cofactors was investigated by Crispino *et al.* [78]. The disrupted interaction of GATA4 with FOG-2 due to a single amino acid mutation caused an embryonic lethality around E12.5 and numerous defects in formation of the right ventricle and thicker endocardial cushions.
GATA4 fulfils regulatory functions either during initiation of cardiac development [75,76] or during separation of the heart chambers [77–79]. The studies give a small insight into the critical role of GATA4 during cardiogenesis but also highlight the influence of GATA4 as a main TF.

1.3.3.2. Liver organogenesis

One of the earliest studies that investigated the role of GATA4 on liver organogenesis was published by Rossi *et al.* in 2001 [64]. Apart from their main focus, the role of BMPs on induction of liver formation, the authors questioned, whether GATA4 expression in the nascent hepatic endoderm could be regulated by BMPs. Explants experiment with murine ventral foregut demonstrated that GATA4 mRNA was induced by BMPs. A GATA4 binding site at the enhancer of the albumin gene indicated a role for BMP4 and GATA4 in the endodermal liver induction.
The function and expression pattern of GATA4 in the nascent liver bud was then investigated by Watt *et al.* [62]. Detailed analysis of the GATA4 protein showed an expression in the extraembryonic visceral endoderm, ventral foregut endoderm and cardiac mesoderm around E8.0. At E8.5, GATA4 expression decreased within the liver bud whereas the expression level in the neighbouring STM and ECs surrounding the liver bud persisted. At E9.0, during commitment of primary liver bud cells into the hepatic lineage, GATA4 expression was lost in hepatocyte progenitor cells but remained in the STM. Following genetic inactivation of GATA4, the growth and development of the liver bud was arrested although hepatic lineage differentiation had occurred. As endogenous GATA4 expression was lost during expansion of the liver bud but was required for the growth of the liver bud in GATA4 knockout embryos the authors argued that GATA4 act in STM cells, cardiac mesodermal cells or ECs surrounding the liver bud. Since the STM was absent from the GATA4 knockout embryos, Watt *et al.* concluded that GATA4 plays a role in the

formation of the STM which was required for the subsequent expansion of the liver bud. This hypothesis was further investigated by the conditional inactivation of GATA4 in the STM [80]. An STM-specific transcriptional enhancer of the GATA4 gene produced a transgenic Cre driver mouse (G2-Cre). Conditional deletion of GATA4 by the G2-Cre mouse caused an embryonic lethality at E13.5 with multiple defects in the FL including dilated sinusoids, decreased number of haematopoietic cells and reduction of proliferation and an increase of apoptosis in the hepatocyte. An increase of perisinusoidal collagen fibres and Laminin was observed from E13.5 onwards. An increase of Desmin$^+$ and alpha smooth muscle actin$^+$ cells in the FL of GATA4 knockout embryos indicated an activation of hepatic stellate cells. Detailed analysis revealed a decrease of the TF LHX2 which contains conserved GATA binding sites in the promoter region. After promoter binding studies, it was concluded that GATA4 controls the transcription of LHX2. Since the genetic inactivation of LHX2 led to similar fibrotic phenotype [81], Delgado *et al.* argued that the loss of GATA4 alters the transcriptional level of LHX2 provoking an hepatic stellate activation and fibrotic phenotype which impairs all together proper growth and development of the FL.
The selected studies show a critical role of GATA4 during several steps of liver organogenesis. Rossi *et al.* [64] demonstrated a BMP4 dependent function of GATA4 in the stage of hepatic specification followed by Watt *et al.* [62] who postulated a direct role of GATA4 during growth of the liver bud and finally Delgado *et al.* [80] who emphasized a purpose GATA4 in the mesenchyme and mesenchymal-derived cells.

1.3.4.GATA4 dysfunction in pathological processes

GATA4 function during several stages of fetal development suggests a key role during initiation and progress of pathological conditions. There are several mutations of GATA4 described which were associated with congenital heart diseases which is currently one of the major birth defects [82–84]. Moreover, some researches have correlated loss or mutation of the GATA4 gene to HCC [85].

1.3.4.1. Liver fibrosis

Chronic damage to the liver and an accumulation of ECM proteins results in liver fibrosis which leads to cirrhosis and portal hypertension in case of a persisting injury [53]. Delgado *et al.* reported a liver fibrosis in the embryo with an increase of ECM and activation of hepatic stellate cells [80]. In the second part of their study, a role of GATA4 on fibrosis in a murine model of CCl_4 induced fibrosis and on progression of the disease in human cirrhotic livers was investigated. Short-term treatment of mice with CCl_4 induced a mild liver fibrosis in control mice that was more severe in mice heterozygous for GATA4. Examination of human liver samples with various stages of fibrosis or cirrhosis demonstrated a loss of GATA4 protein during the course of the disease progression. This showed a correlation of GATA4 levels in response to fibrotic injury and indicated that progression of fibrosis in human may be dependent on the GATA4 expression.

1.3.5.Function of GATA4 in non-mammals

Transcriptional activity of GATA4 was also reported for non-mammalian organism, such as the fruit fly *drosophila melanogaster*, the frog *Xenopus laevis*, and the nematode *Caenorhabditis elegans*.

Holtzinger and Evans investigated function of *gata4* during development of the zebrafish [86]. Treatment of fish embryos with *gata4* morpholinos resulted in an improper looped heart, delay in development and absence of blood circulation. Later in development, the mutant fish embryos fail to initiate organogenesis of the intestine, liver, pancreas. Analysis of the liver development revealed proper formation of the liver bud and generation of hepatocytes but the liver bud failed to expand. Torregroza *et al.* continued the work on the characterization of the phenotype of the *gata4* morphants and analysed the lack of blood circulation more in detail [87]. As *gata4* is not expressed in haematopoietic cells, the caudal haematopoietic tissue (CHT), a specialized region of the zebrafish that is necessary for initiation of the second haematopoietic wave, was investigated more in detail. Analysis of the vascularization of the CHT revealed a less branched vascular plexus and a reduced size. HPCs circulated in the *gata4* morphants but were not able to seed the CHT. Investigation of stromal factors known to be involved for seeding of HSC identified the chemokine ligand *sdf1a* to show increased transcript levels. Since *gata4* and *sdf1a* were both not expressed in the CHT, Torregroza *et al.* analysed at which time point *gata4* was decisive and showed that the transcriptional activity of *gata4* was needed during gastrulation to ensure proper CHT development and restrict levels of *sdf1a*. The authors proposed a role for *gata4* and *sdf1a* in the establishment of haematopoietic niches since *gata4* was linked to liver growth and *sdf1a* is a known chemoattractant for HPCs.

2. Aims of the thesis

LSECs are unique organ-specific ECs that constitute the largest sinusoidal vascular bed of the body. LSECs are characterized by a characteristic gene expression profile that comprises transcription and growth factors as well as surface proteins involved in adhesion and endocytosis. The functional investigation of such specific genes of LSEC will often require Cre-mice that mediate genetic recombination in specific subgroups of ECs only to prevent off-target effects in other organs and other cells. Therefore, Aim1 of this thesis will focus on the generation and characterisation of such mice. In Aim2 these mice will be used to analyse the function of the TF GATA4 in mice with deletion of GATA4 in LSECs. This investigation could so far not be carried out as global endothelial deletion of GATA4 is lethal before liver development takes place. Aim2 therefore builds on Aim1 and provides proof of principle that the transgenic mouse generated in Aim1 provides an advantage to investigate organ-specific endothelial functions in vivo.

Aim1

Targeting liver sinusoidal endothelial cells by cell type-specific Cre driver mice

The aim in this part of the PhD thesis is to characterise transgenic mouse lines with regard to their suitability to target LSECs and to critically evaluate their potential to generate a conditional knockout mouse. This will be achieved by the generation of the Stab2-cre and Clec4g-cre mice (1) and characterisation of the Cre activity by the respective reporter mice (2). The reporter will be analysed in LSECs of the fetal and adult mouse as well as in microvascular ECs of BM, LN and spleen and will be investigated in ECs and non-ECs of other organs.

Aim2

Function of GATA4 for the fetal development of liver sinusoidal endothelial cells

In this part of the PhD thesis the implications of the conditional deletion of GATA4 in LSECs on embryonic and liver development will be analysed. In order to achieve this overall and liver development of the mutant embryos will be characterised (1), LSEC marker expression and endothelial ultrastructure of the FL will be analysed (2) and the FL haematopoiesis will be assessed by quantitative and qualitative methods (3).

3. Results

3.1. Targeting liver sinusoidal endothelial cells – characterisation of LSEC-specific Cre driver mice

3.1.1. The Stab2-cre mouse

3.1.1.1. Generation of the transgenic Stab2-cre mice

LSECs express a unique set of marker proteins of which the promoter element of Stab2 was chosen to create an LSEC-specific Cre driver mouse strain (Stab2-cre). Strong protein expression of Stab2 was reported in endothelial sinuses of the liver [88–90], but as well in the spleen and the LN [27], and in the BM [91]. Three founder mice were obtained of which two were viable and fertile, Stab2-cre founder 2 (f2) and founder 3 (f3). The founder lines were characterised by reporter strains, the R26LacZ [92] (f2;LacZ and f3;LacZ) and the R26YFP [93] (f2;YFP and f3;YFP) mouse. The reporter activity was analysed in the fetal and adult mouse and results of the founder lines compared.

3.1.1.2. Reporter analysis during fetal development

3.1.1.2.1. Initiation of liver development

In order to determine the onset of Cre activity, the Stab2-cre mouse was analysed during embryogenesis. F2;LacZ and f3;LacZ embryos were investigated by whole-mount β-galactosidase assay during initiation of liver development, at E9.5 and at E10.5 (Figure 5). Cre expression induces the excision of a stop codon leading to the transcription of the β-galactosidase protein (LacZ) which reacts with the X-gal substrate (5-bromo-4-chloro-indolyl-β—D-galactopyranoside) in order to generate an insoluble blue precipitate (5,5'-dibromo-4,4'-dichloro-indigo) [94].

At E9.5, f2;LacZ embryos showed a LacZ expression in the FL and in the dorsal part of the embryo (Figure 5 A). At E10.5, reporter activity of f2;LacZ embryos was observed throughout the embryo with signals in the cranial region, dorsal aorta and somites. The FL demonstrated a strong LacZ expression (Figure 5 C). Additionally, a reporter signal was detected in the YS (not shown). In contrast to this, the f3;LacZ embryos showed neither a LacZ signal at E9.5 (Figure 5 B) nor at E10.5 (Figure 5 D).

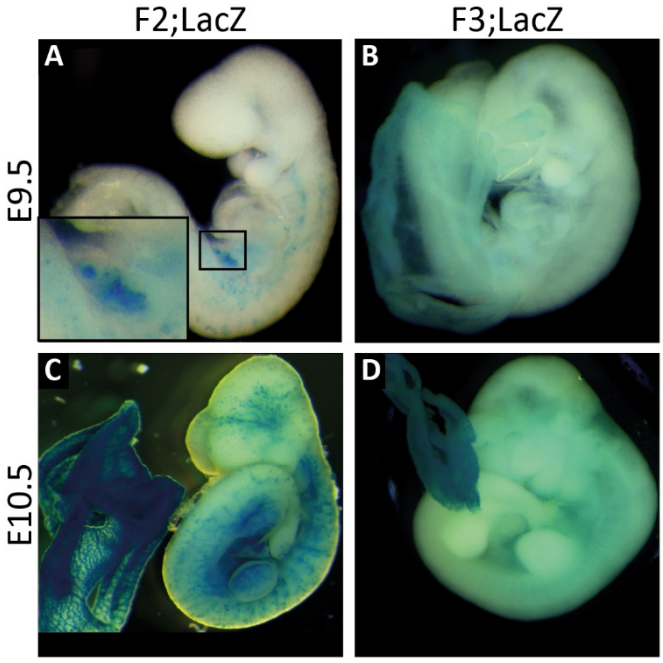

Figure 5: β-galactosidase assay of f2;LacZ and f3;LacZ at E9.5 and E10.5.
A – **D**, F2;LacZ (**A**, **C**) and f3;LacZ (**B**, **D**) embryos were dissected at E9.5 (**A**, **B**) or E10.5 (**C**, **D**), and subjected to whole-mount β-galactosidase assay. Embryos were photographed under a stereo microscope. The detail in **A** shows a magnification of the FL of f2;LacZ embryo at E9.5. Representative images from two independent experiments with at least three biological replicates.

Based on this, the embryos of Stab2-cre f2 were examined more in detail and analysed by the R26YFP reporter line. Here, Cre expression leads to the expression of the yellow fluorescent protein (YFP), instead of the LacZ protein, which was then detected by direct fluorescence or antibody staining. F2;YFP embryos were dissected at E10.5 and analysed by immunofluorescence (IF). The cranial region showed distinct $CD31^+$ cells with YFP expression (Figure 6 A) whereas in the AGM region multiple YFP^+ $CD31^+$ cells were detected (Figure 6 B). In the liver, endothelial reporter activity was observed in $CD31^+$ cells (Figure 6 C) and in $Stab2^+$ cells (Figure 6 D). The reporter activity was also detected in $CD31^-$ non-endothelial round cells. In order to analyse if these cells are of haematopoietic origin a co-staining with cKit for haematopoietic stem cells (HSC) [95] or with Ter119 for immature erythrocytes [95] was performed. YFP expression was observed in erythrocyte progenitor cells but not in HSC (Figure 6 E).

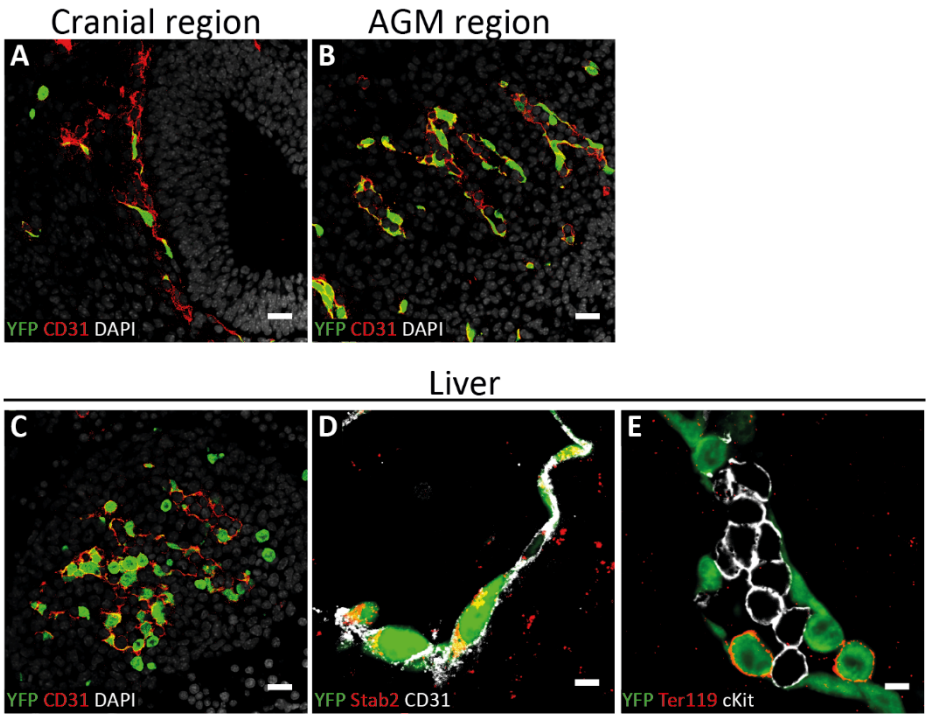

Figure 6: Immunofluorescent analysis of f2;YFP embryos at E10.5.
A – **E**, Immunofluorescence (IF) on cryosections of f2;YFP embryos at E10.5. Images from confocal microscopy shows YFP (green), endothelial marker CD31 (red), and DAPI (grey) in the cranial region (**A**), AGM region (**B**), and FL (**C**). Micrographs of the FL after IF of YFP (green) with Stab2 (red) and CD31 (grey) (**D**) or with Ter119 (red) and cKit (grey) (**E**). Scale bar 20µm (A - C) and 5µm (D, E). Representative images from two independent experiments with two three biological replicates.

3.1.1.2.2. Fetal liver maturation

Based on the previous results, reporter activity of f2;YFP embryos was investigated later during fetal development. During mid-gestation, at E12.5, organs, such as the liver, heart, the somites have been formed and intestinal anlagen have been separated into foregut, midgut, and hindgut [96]. Haematopoiesis shifts from AGM region and extraembryonic tissue to the liver [66]. YFP expression in f2;YFP embryos was investigated in CD146^{+} EC of the brain, heart, liver, midgut, and somites as well as in LYVE1^{+} FL EC of f3;YFP embryos (Figure 7). Furthermore, reporter activity was analysed in FL cells more in detail (Figure 8).

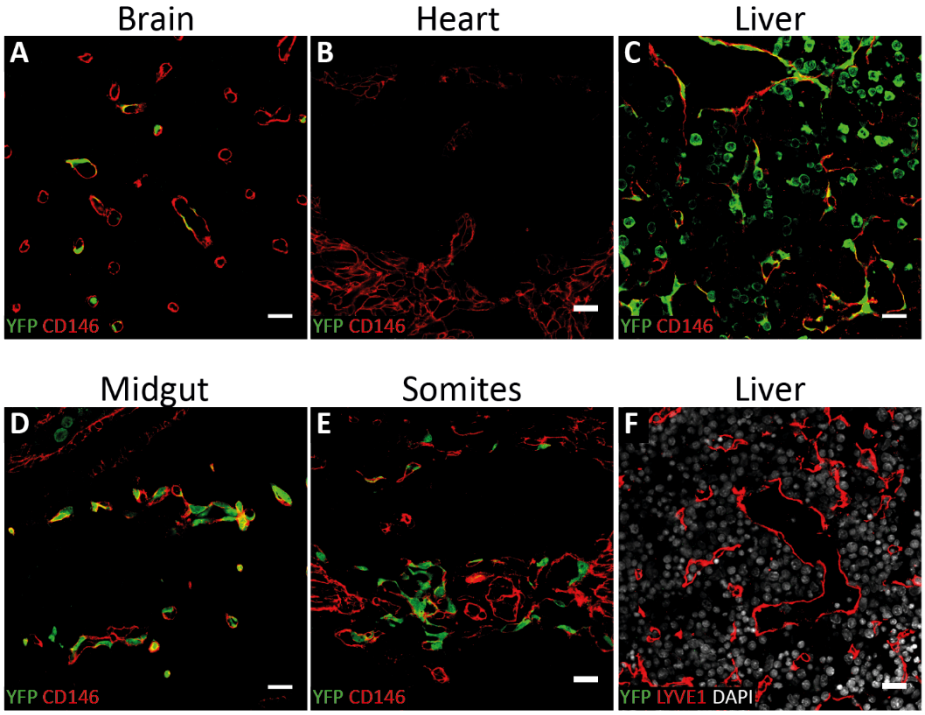

Figure 7: Immunofluorescent analysis of f2;YFP and f3;YFP embryos at E12.5.and E13.5.
A – **E**, IF was carried out on cryosections of f2;YFP embryos at E12.5. Images from confocal microscopy shows YFP (green) and CD146 (red) in the brain (**A**), heart (**B**), liver (**C**), midgut (**D**), and somites (**E**). **F**, IF was carried out on cryosections of f3;YFP embryos at E13.5. Confocal micrograph shows YFP (green) and LYVE1 (red) in the FL. Scale bar 20µm. Representative images from more than three independent experiments with at least three biological replicates.

YFP expression was observed in CD146$^+$ EC of the brain (Figure 7 A), midgut (Figure 7 D), and somites (Figure 7 E) whereas no YFP was seen in CD146$^+$ EC of the heart (Figure 7 B). F3;YFP embryos showed no reporter activity in the FL at E13.5 (Figure 7 F). In the liver of f2;YFP embryos (Figure 7 C), YFP expression was observed in two cell types, CD146$^+$ EC and in CD146$^-$ non-endothelial round cells. A comprehensive analysis of the reporter activity in the FL cells demonstrated a YFP expression in Stab2$^+$ LSECs (Figure 8 A) but not in Liv2$^+$ immature hepatocytes (Figure 8 B). Interestingly, reporter activity was observed in Cre$^+$ cells and in non Cre expressing cells (Figure 8 C) indicating a reporter activity in cells without active Cre recombinase. Furthermore, reporter activity was detected in cKit$^+$ haematopoietic stem cells (Figure 8 D), in Ter119$^+$ erythroblasts (Figure 8 E), and in F4/80$^+$ FL macrophages (Figure 8 F). This prompted us to investigate the YFP reporter expression in haematopoietic cells of the FL by fluorescent activated cell sorting (FACS). YFP expression was detected in 15.7% of Sca1$^+$ and cKit$^+$ haematopoietic stem cells (Figure 8 G) as well as in 5.7% CD45$^+$ CD146$^-$ Sca1$^-$ cKit$^-$ differentiated haematopoietic stem cells (Figure 8 H).

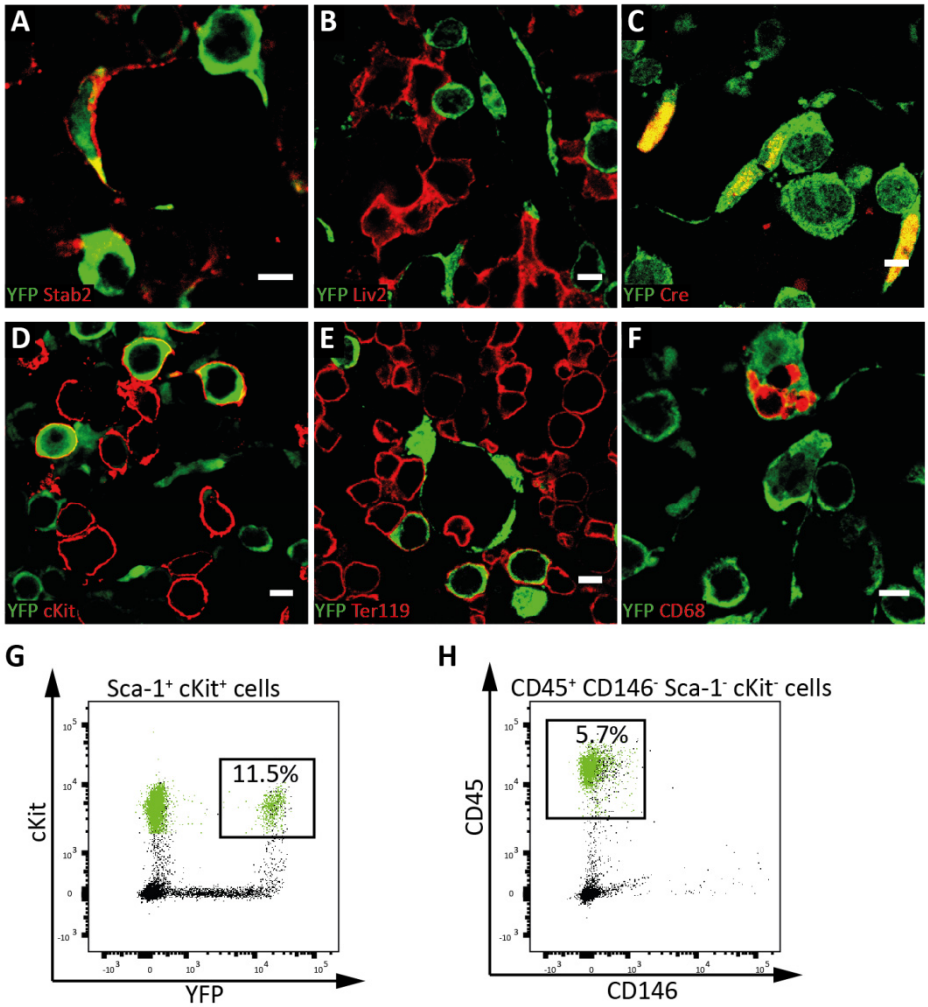

Figure 8: Immunofluorescent analysis of fetal livers of f2;YFP embryos at E12.5 and at E13.25.
A – **F**, IF on cryosections of f2;YFP embryos at E12.5. Images from confocal microscopy shows the FL with co-staining of YFP (green) and Stab2 (**A**), Liv2 (**B**), Cre (**C**), cKit (**D**), Ter119 (**E**), or F4/80 (**F**). Scale bar 5µm. Representative images from more than three independent experiments with at least three biological replicates. **G** – **H**, FL cells of f2;YFP embryos at E13.25 were subjected to fluorescent activated cell sorting (FACS) and analysed for YFP expression in $Sca1^+$ $cKit^+$ cells (**G**) and in $CD45^+$ $CD146^-$ $Sca1^-$ $cKit^-$ cells (**H**). Representative FACS plots from one experiment with five biological replicates.

In summary, the analysis from E9.5 to E13.5 demonstrated a reporter activity in Stab2-cre f2 but not in Stab2-cre f3. F2 showed a reporter activity in the FL from E9.5 onwards, in the head and AGM region at E10.5 and in the brain, somites, and midgut but not in the heart at E12.5. Reporter activity was also observed in liver ECs and in subpopulations of haematopoietic stem and differentiated cells.

3.1.1.3. Reporter analysis in the adult mouse

3.1.1.3.1. Analysis of liver, bone marrow, lymph node, and spleen

Next, the reporter activity was analysed in the adult mouse. Liver, tibia and femur, mesenteric LNs, and spleen from f2;YFP and f3;YFP mice were harvested and YFP expression was investigated.

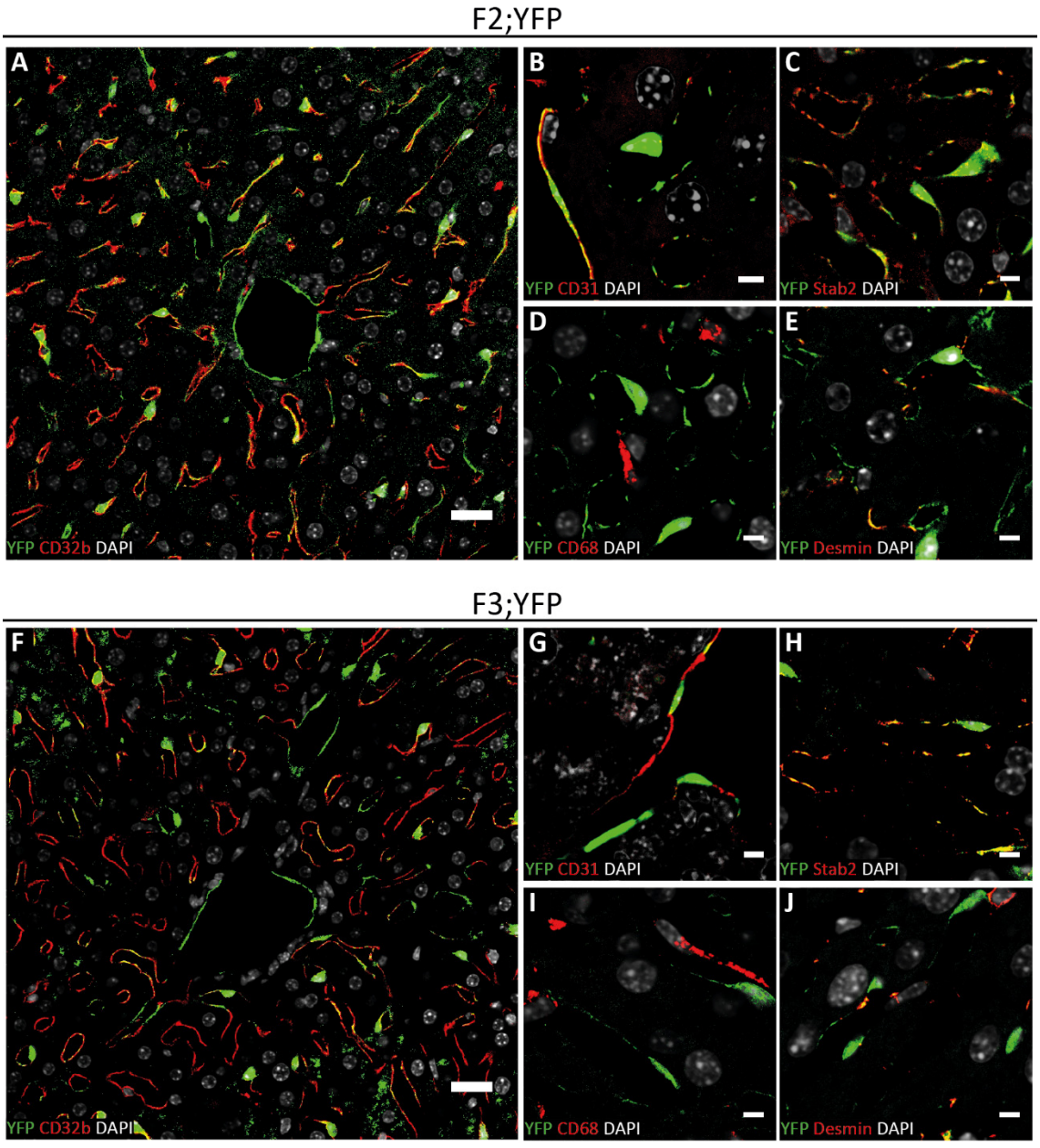

Figure 9: Immunofluorescent analysis of livers from f2;YFP and f3;YFP mice.
A – J, IF was carried out on liver cryosections of f2;YFP and f3;YFP mouse followed by confocal microscopy. Livers of f2;YFP (**A – E**) and f3;YFP (**F – J**) were stained for YFP (green) and CD32b (red) (**A**, **J**), CD31 (red) (**B**, **G**), Stab2 (red) (**C**, **H**), CD68 (red) (**D**, **I**), or Desmin (red) (**E**, **J**). DAPI (grey) stains the cell nuclei. Scale bar 20 µm (**A**, **F**) or 5µm. Representative images from more than five independent experiments with more than five biological replicates.

Livers of the f2;YFP (Figure 9 A - E) and the f3;YFP (Figure 9 F - J) mice showed a YFP expression. CD32b$^+$ LSECs of f2;YFP and f3;YFP expressed YFP. F2;YFP demonstrated a broader and more intense YFP expression pattern in the liver than f3;YFP (Figure 9 A, F). In both founder lines, we observed YFP expression in CD31$^+$ venous and arterial ECs (Figure 9 B, G) and in Stab2$^+$ LSECs (Figure 9 C, H). Hepatocytes represent the major cell type in the liver but the explicit sinusoidal expression pattern of the reporter excluded a hepatocellular reporter activity. Co-staining of YFP with Kupffer cell marker CD68 in livers of f2;YFP and f3;YFP (Figure 9 D, I) mice showed the absence of reporter activity in these cells. Stellate cells are resident liver cells in the perisinusoidal space and can be identified as Desmin$^+$ cells [97]. Due to their close contact with sinusoidal ECs an incidental co-localisation of Desmin and YFP was observed (Figure 9 E, J) although the signal derived from different cells.

In summary, the reporter analysis in the liver showed Cre activity in endothelial sinuses of Stab2-cre f2 and f3. F2 displayed a YFP expression in a larger number of LSECs. Both founder lines show reporter activity in arterial and venous EC but not in hepatocytes, Kupffer or stellate cells.

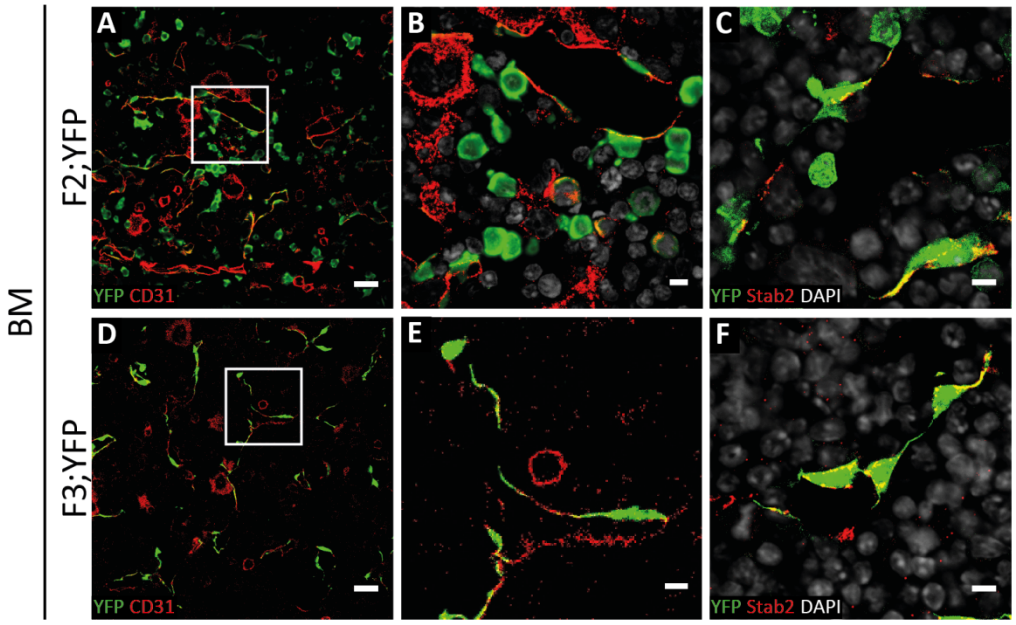

Figure 10 (continued on the next page)

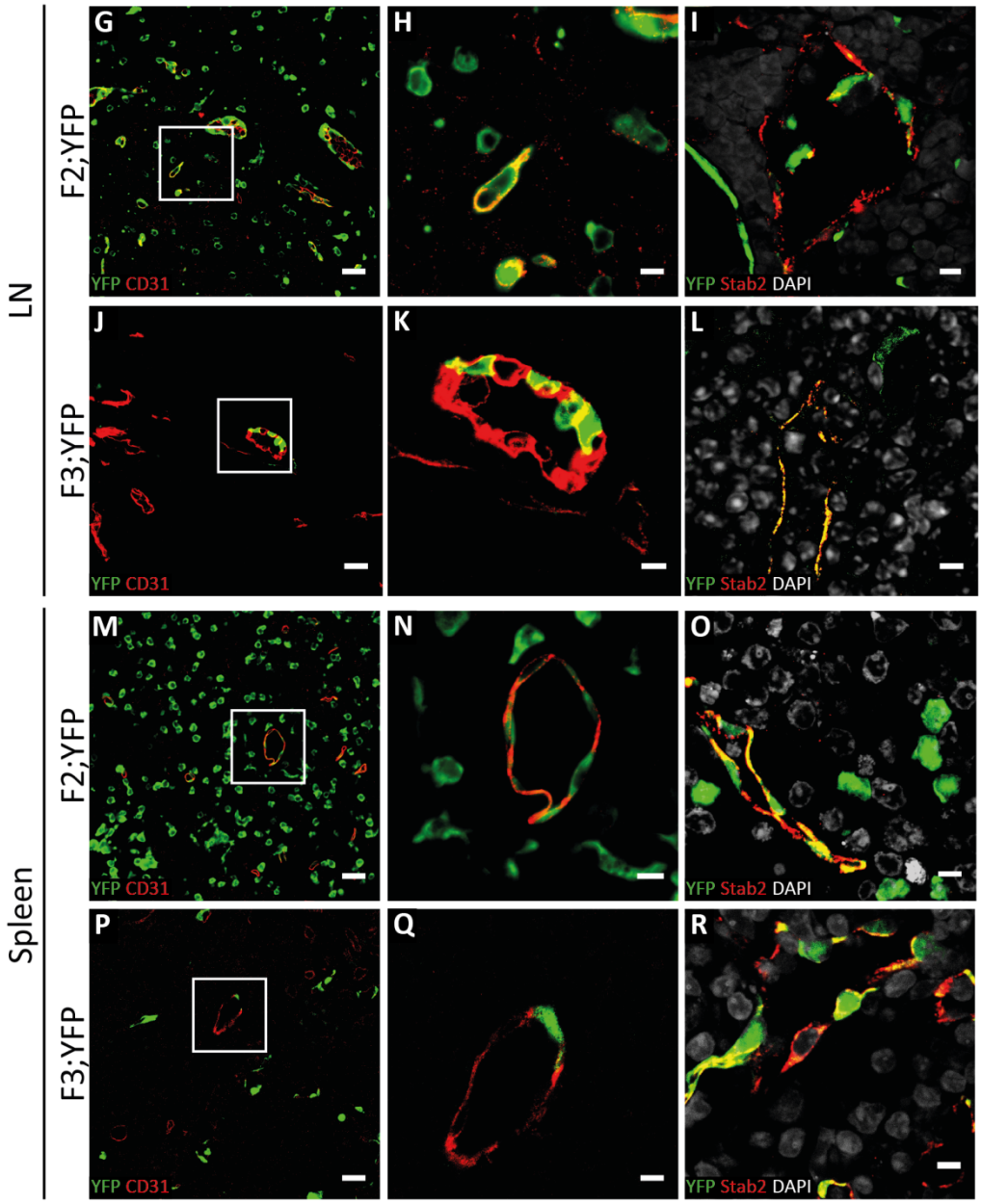

Figure 10 (continued): Immunofluorescent analysis of BM, LN, and spleen from f2;YFP and f3;YFP mice.
A – R, Cryosections show the BM, mesenteric LNs, and spleen of f2;YFP (**A – C**, **G – I**, **M – O**) and f3;YFP (D – **F**, **J – L**, **P – R**). Organs were subjected to IF of YFP (green) with CD31 (red) or Stab2 (red) in the BM (**A - F**), LN (**H – L**), and spleen (**M – R**). **B**, **E**, **H**, **K**, **N**, or **Q** is a magnification of the selected area in **A**, **D**, **G**, **J**, **M**, or **P**, respectively. Scale bar 20 µm (**A**, **D**, **G**, **J**, **M**, and **P**) or 5µm. Representative images from at least three independent experiments with more than three biological replicates.

In the BM, YFP expression was detected in f2;YFP (Figure 10 A - C) and f3;YFP (Figure 10 D - F). $CD31^+$ EC in f2;YFP and f3;YFP and $Stab2^+$ cells in f2;YFP and f3;YFP expressed YFP. Furthermore, the BM of f2;YFP showed YFP expression in $CD31^-$ and $Stab2^-$ cells which was not observed in the BM of f3;YFP. This will be analysed more in detail in section 3.1.1.3.2. Analysis of the LN showed a YFP expression in f2;YFP (Figure 10 G - I) and f3;YFP (Figure 10 J - L) . $CD31^+$ EC lining HEVs and trabeculae expressed YFP in LNs of f2;YFP and

f3;YFP. Co-staining with Stab2 demonstrated a YFP expression in Stab2$^+$ cells of f2;YFP and f3;YFP. Furthermore, YFP was detected in CD31$^-$ and Stab2$^-$ cells of the LN of f2;YFP but not of the LN of f3;YFP. The spleen demonstrated a reporter activity in f2;YFP (Figure 10 M - O) and f3;YFP (Figure 10 P - R). Reporter YFP expression was observed in CD31$^+$ EC and Stab2$^+$ cells. Similar to the BM and LN, YFP expression was also seen in CD31$^-$ and Stab2$^-$ splenic cells of f2;YFP but not in f3;YFP.

In summary, Stab2$^+$ microvascular EC of BM, LN, and spleen of f2;YFP and f3;YFP showed YFP expression. Both founder lines demonstrated a reporter activity in arterial and venous ECs of BM, LN, and spleen. Different observations were made with regard to non-endothelial reporter activity in the founder lines since f2;YFP showed YFP expression in CD31$^-$ Stab2$^-$ non-EC which was not observed in f3;YFP.

3.1.1.3.2. FACS analysis of the peripheral blood mononuclear cells, bone marrow, and spleen

In previous sections, reporter YFP expression of f2;YFP was detected in non-ECs of BM, LN and spleen. Since reporter activity was also observed in FL haematopoietic cells during development we applied FACS analysis to characterise the reporter activity in peripheral blood mononuclear cells (pBMCs), BM and splenic cells of f2;YFP and f3;YFP more in detail. Due to technical difficulties, the LNs were not be examined by FACS analysis.
Reporter YFP expression was detected in 11.5% of pBMCs in f2;YFP (Figure 11 A) and in less than 0.01% (6.2×10^{-3}) of pBMCs in f3;YFP (Figure 11 D). Detailed analysis of the reporter activity in the blood of f2;YFP showed that 7.7% of b-cells, 6.4% of t-cells, 8.0% of granulocytes, and 7.4% of macrophages (Figure 11 B) expressed YFP. In the BM, 3.9% YFP$^+$ cells were found in all BM cells of f2;YFP (Figure 11 D) which is in contrast to a YFP expression in less than 0.1% (1.6×10^{-2}) BM cells of f3;YFP (Figure 11 F). Investigation of BM cells from f2;YFP demonstrated that 9.6% of long term (lt)-HSC, 8.1% of short term (st)-HSC, and 7.2% of multipotent progenitor cells (MPP) expressed YFP (Figure 11 E). Reporter activity was investigated in splenic cells and resulted in a YFP expression in 3.6% of total spleen cells in f2;YFP (Figure 11 G) and in 0.1% YFP$^+$ splenic cells in f3;YFP (Figure 11 I). Splenic cells of f2;YFP were investigated more in detail and showed that 7.3% of b-cells, 6.1% of t-cells, 6.7% of granulocytes, and 6.7% of macrophages (Figure 11 H) expressed YFP.

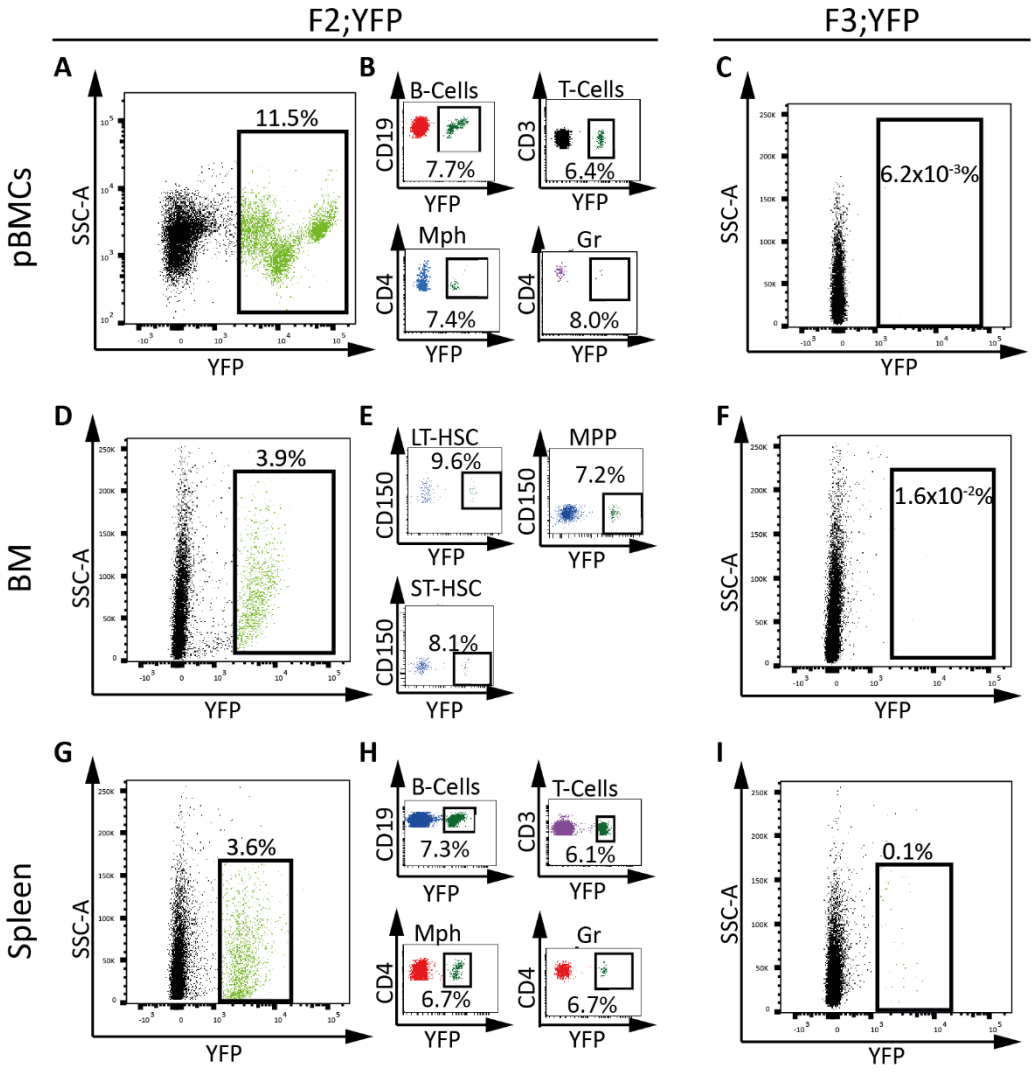

Figure 11: FACS analysis of pBMCs, BM, and spleen from f2;YFP and f3;YFP mice.
A – **I**, FACS analysis of YFP expression in the pBMCs, BM, and spleen. YFP expression was analysed in pBMCs of f2;YFP (**A**) and in f3;YFP (**C**), BM cells of f2;YFP (**D**) and f3;YFP (**F**), and splenic cells of f2;YFP (**G**) and in f3;YFP (**I**). The percentage of the YFP$^+$ population in FSC/SSC gated pBMCs, BM or splenic cells is illustrated by an YFP/SSC FACS plot. YFP expression was analysed in CD19$^+$ CD3$^-$ b-cells, CD3$^+$ CD19$^-$ t-cells, CD4$^+$ Gr1$^-$ CD3$^-$ CD19$^-$ macrophages (Mph), or CD4$^+$ Gr1$^+$ CD3$^-$ CD19$^-$ granulocytes (Gr) of the pBMCs (**B**) or spleen (**H**) as well as was YFP expression analysed in Lineage$^-$ Sca1$^+$ cKit$^+$ (LSK) CD48$^-$ CD150$^+$ long term (lt)-, LSK CD48$^-$C D150$^-$ short term (st)-HSC, or LSK CD48$^-$ CD150$^-$ multipotent progenitor cells (MPP) of the BM of f2;YFP (**E**). Representative FACS plots from one (**B**, **H**), two (**E**), or more than three experiments with at least three biological replicates.

In summary, reporter activity was observed in a variable fraction (3% - 12%) of pBMCs, BM and spleen of f2;YFP and in less than 0.1% of pBMCs, BM and spleen of f3;YFP. 6% to 8% of macrophages, granulocytes, b- and t-cells in the blood and spleen as well as 7% to 10% of lt-HSC, st-HSC and MPP in the BM demonstrated YFP expression.

3.1.1.3.3. Investigation of kidney, pancreas, small intestine, and thymus

As reporter activity of both founder lines was not strictly confined to Stab2+ microvascular EC, the analysis was extended to organs harbouring fenestrated EC. Kidney, intestine, pancreas, and thymus of f2;YFP and f3;YFP were harvested and subjected to immunofluorescent staining of YFP.

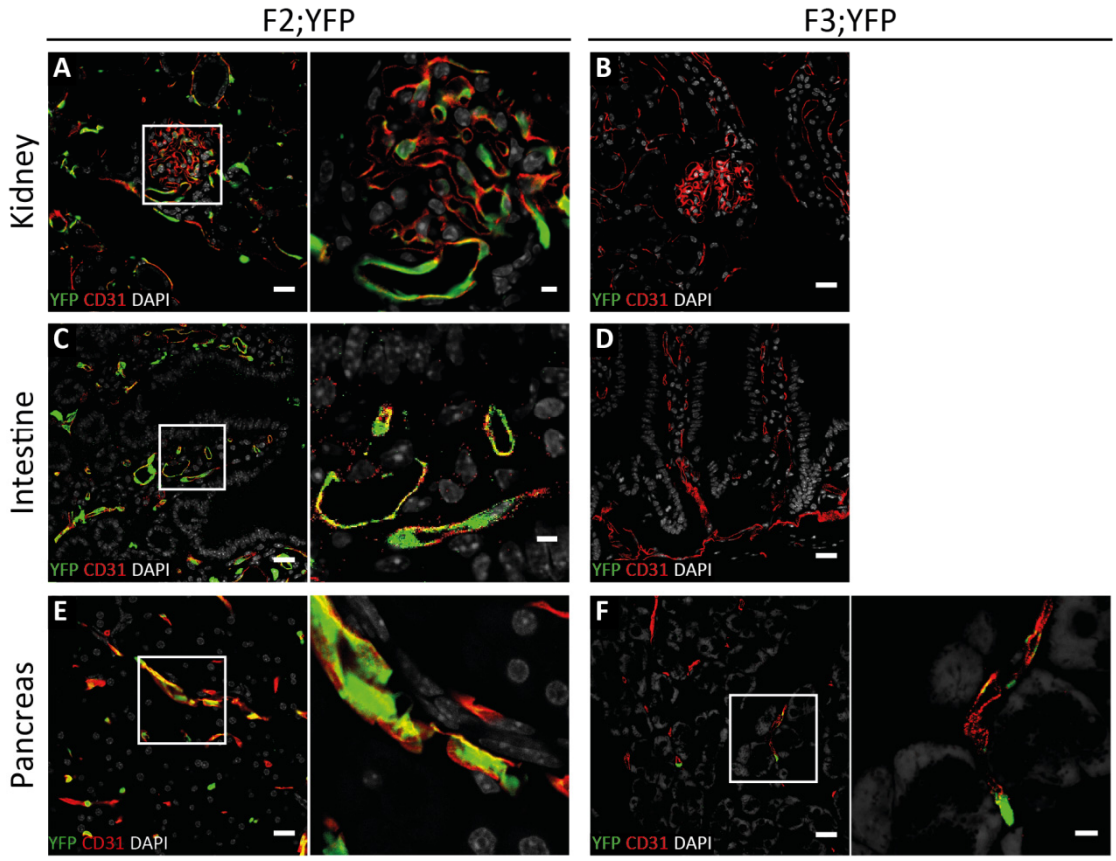

Figure 12 (continued on the next page)

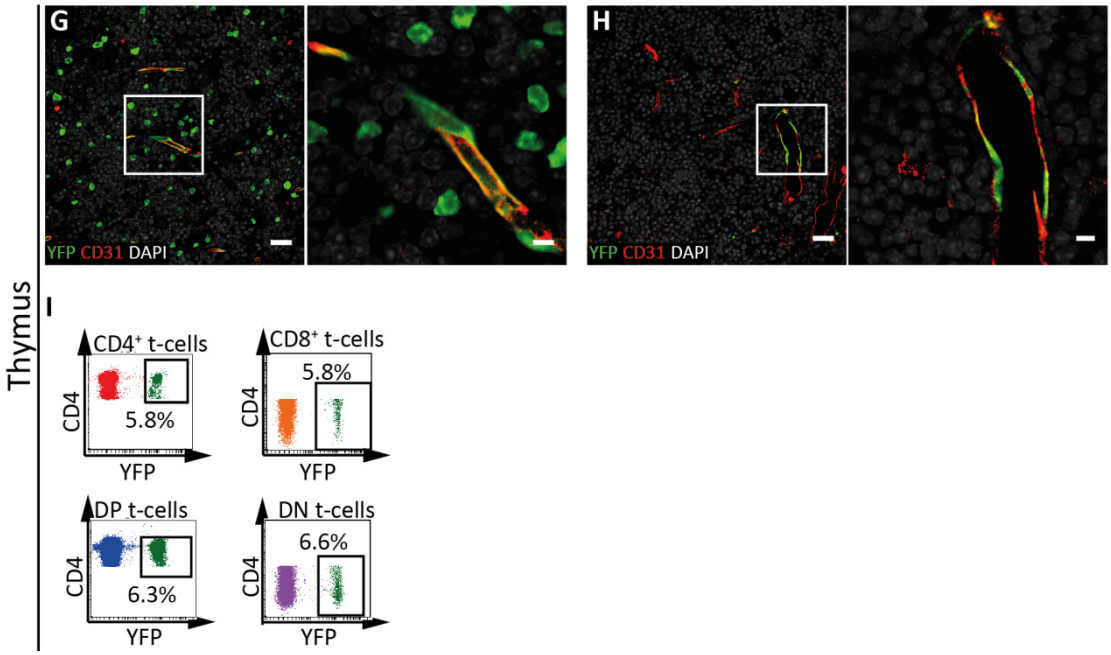

Figure 12 (continued): Immunofluorescent analysis of kidney, small intestine, pancreas and thymus from f2;YFP and f3;YFP mice.
A – **H**, IF was carried out on cryosections from kidney (**A**, **B**), small intestine (**C**, **D**), pancreas (**E**, **F**), and thymus (**G**, **H**) of the f2;YFP (**A**, **C**, **E**, **G**) and f3;YFP (**B**, **D**, **F**, **H**) mouse. Images from confocal microscopy show staining of YFP (green), CD31 (red), and DAPI (grey). Selected areas in **A**, **C**, **E**, **F**, **G**, or **H** are magnified in the right image next to it. Scale bar 20 µm or 5 µm (magnification). Representative images from at least two independent experiments with more than three biological replicates. **I**, FACS plots show YFP expression in $CD4^+$ $CD8^-$ or $CD4^-$ $CD8^+$ t-cells as well as in $CD4^+$ $CD8^+$ double positive (DP) or $CD4^-$ $CD8^-$ double negative (DN) t-cells of the f2;YFP mouse. Representative FACS plots from one experiment with five biological replicates.

In the kidney, YFP expression was observed in f2;YFP; namely in $CD31^+$ EC lining the glomerular capillaries and the arteries and vein of the renal medulla (Figure 12 A). No reporter activity was detected in the kidney of f3;YFP (Figure 12 B). In the intestine of f2;YFP, YFP expression was detected in $CD31^+$ EC of the villi (Figure 12 C) whereas no YFP expression was observed in the small intestine of f3;YFP (Figure 12 D). In the pancreas of f2;YFP, YFP expression was observed in $CD31^+$ EC (Figure 12 E). In some f3;YFP mice (3 of 8 mice) we detected YFP in $CD31^+$ EC (Figure 12 F). In the thymus of f2;YFP, YFP expression was seen in $CD31^+$ EC and in $CD31^-$ non-EC (Figure 12 G). FACS analysis was carried out in order to examine the YFP^+ population more in detail (Figure 12 I). We discovered that 5.8% of $CD4^+$ t-cells, 5.8% of $CD8^+$ t-cells, 6.3% of $CD4^+$ $CD8^+$ t-cells, and 6.6% of $CD4^-$ $CD8^-$ t-cells expressed YFP. The thymus of f3;YFP showed reporter activity in $CD31^+$ EC (Figure 12 H).
In summary, analysis of the f2;YFP mouse showed reporter activity in ECs of the kidney and intestine, whereas f3;YFP did not show a YFP expression in those organs. F2;YFP and f3;YFP displayed endothelial reporter activity in the pancreas and thymus, and in addition, t-cells expressed the YFP reporter in the thymus of f2;YFP.

3.1.1.3.4. Analysis of aorta, brain, eye, heart, lung, and skin

Next, we were interested whether aorta, brain, eye, heart, lung, and skin demonstrated reporter activity. For this purpose, organs were dissected from f2;YFP and f3;YFP and the reporter activity investigated by IF of YFP.

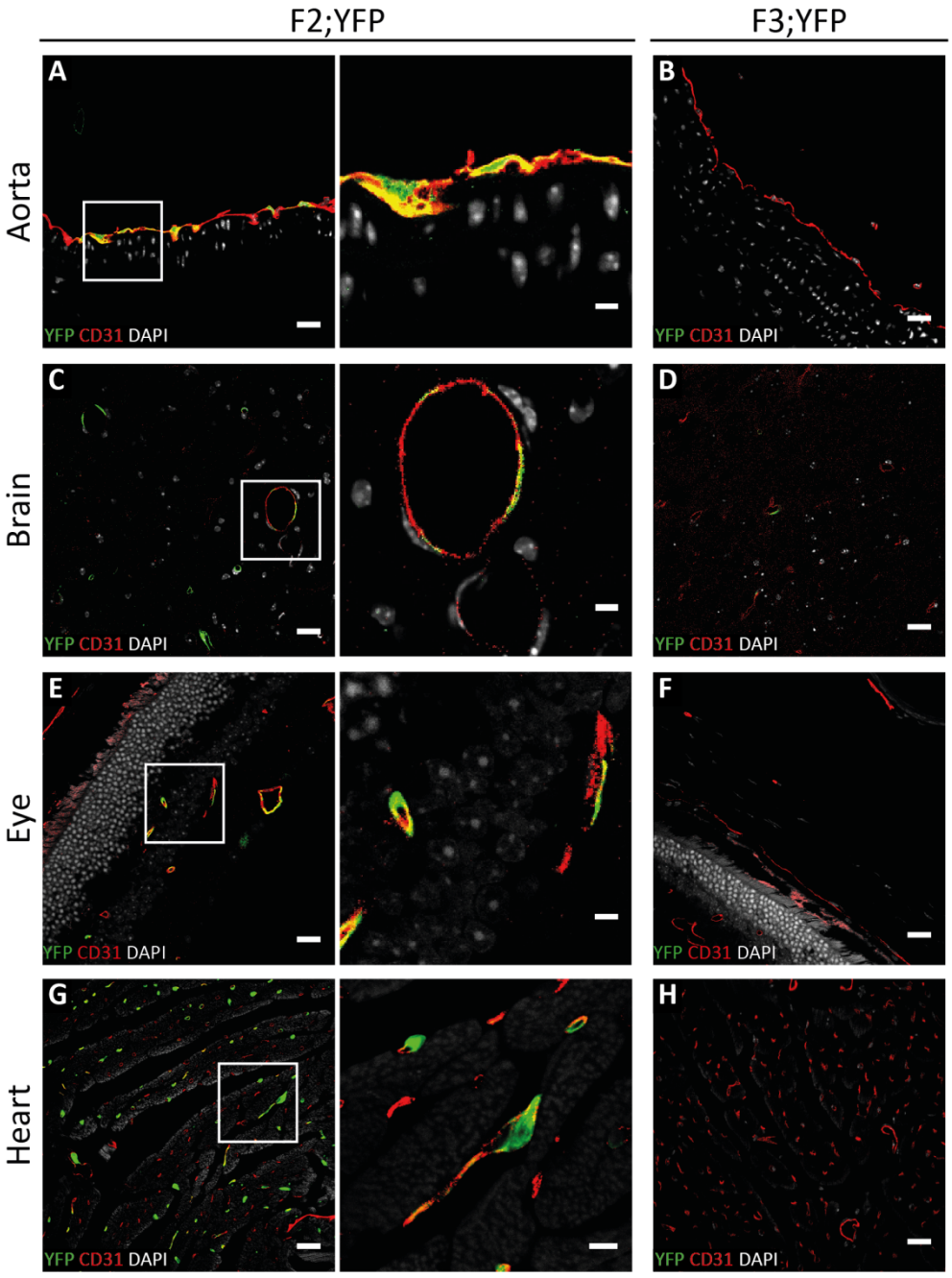

Figure 13 (continued on the next page)

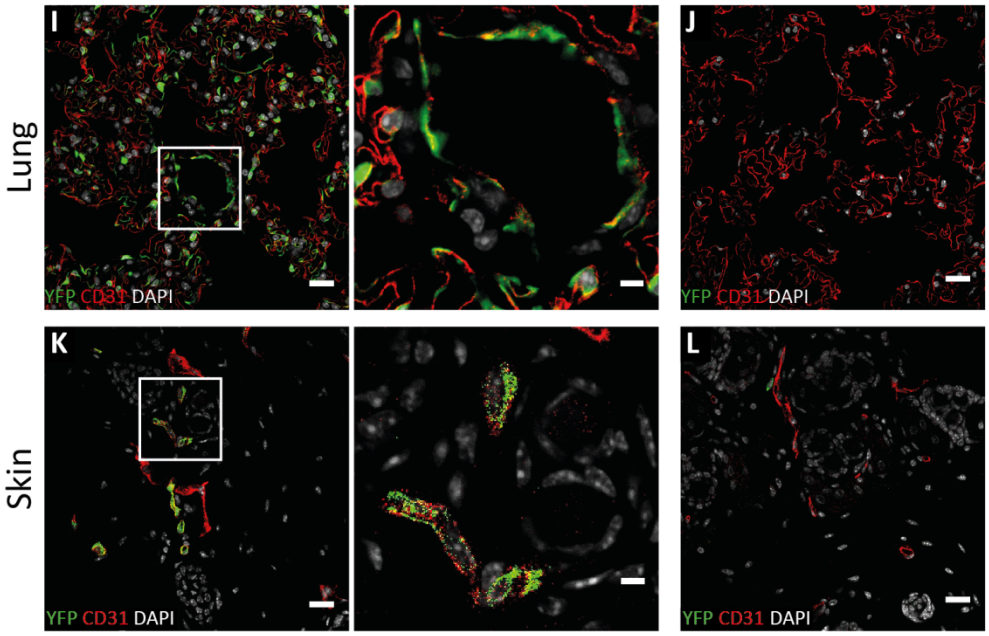

Figure 13 (continued): Immunofluorescent analysis of aorta, cerebral cortex, eye, heart, lung, and skin from f2;YFP and f3;YFP mice.
A – L, IF was carried out on cryosections from aorta (**A**, **B**), brain (**C**, **D**), eye (**E**, **F**), heart (**G**, **H**), lung (**I**, **J**), and skin (**K**, **L**) of the f2;YFP (**A**, **C**, **E**, **G**, **I**, **K**) and f3;YFP (**B**, **D**, **F**, **H**, **J**, **K**) mouse. Images from confocal microscopy show staining of YFP (green), CD31 (red), and DAPI (grey). Selected areas in **A**, **C**, **E**, **G**, **I**, or **K** are magnified in the right image next to it. Scale bar 20 µm or 5 µm (magnification). Representative images from one (**A**, **B**) or more than two independent experiments with at least three biological replicates.

YFP expression was observed in the aorta of f2;YFP (Figure 13 A), namely in CD31⁺ ECs, but not in the aorta of f3;YFP (Figure 13 b). Few CD31⁺ EC of the cerebral cortex (Figure 13 C) and most CD31⁺ EC in the choroid of the eye (Figure 13 E) of f2;YFP expressed YFP. Reporter YFP expression was neither observed in the brain (Figure 13 D) nor eye of f3;YFP (Figure 13 F). Cardiac CD31⁺ EC showed a YFP expression in f2;YFP (Figure 13 G) but not in f3;YFP (Figure 13 H). In the pulmonary endothelium, a strong reporter YFP expression (Figure 13 I) was observed in f2;YFP that was absent in the lung of f3;YFP (Figure 13 J). CD31⁺ EC of the skin in f2;YFP showed a YFP expression (Figure 13 K) that was not observed in the skin of f3;YFP (Figure 13 L).

3.1.1.4. Summary

Reporter activity was investigated in two founder lines of the Stab2-cre mouse. Both transgenic lines showed Cre activity in LSECs and Stab2⁺ microvascular ECs of BM, LN, and spleen. In f2, YFP expression was detected in haematopoietic cell populations of the FL, BM, pBMCs, spleen, and thymus which was not observed in f3. Broad reporter activity of f2 was detected in vascular beds of most organs whereas the reporter activity of f3 in arterial and venous ECs was restricted to the BM, LN, spleen, and thymus.

3.1.2.The Clec4g-cre mouse

3.1.2.1. The generation of the transgenic Clec4g-cre mice

CLEC4G is a member of the lectin family that recognizes a variety of carbohydrate structure such as mannose and fucose as ligands on cell surfaces. The tissue expression of murine CLEC4G is largely unknown due to the lack of proper antibodies but function and expression pattern of the human Clec4g has been investigated intensively. It is expressed by endothelial sinuses of liver and LN and is also found in Kupffer cells. The human CLEC4G shares about 65% homology to the murine CLEC4G and both show similar binding properties [98–103].

Since the human CLEC4G protein is widely recognized as a LSEC marker, we generated a transgenic Cre mouse whose Cre activity is driven by the murine CLEC4G promoter to create an LSEC-specific Cre mouse (Clec4g-cre). After initial screening of three founder lines (12.5, f18.3 and f20.1), founder 12.5 (f12.5) was chosen for broad analysis of Cre activity with the R26YFP [93] (f12.5;YFP) reporter mouse.

3.1.2.2. Reporter analysis in the liver

3.1.2.2.1. Mid- and late-gestation of fetal liver development

In order to determine the onset of Cre activity, embryos from f12.5;YFP were analysed during fetal development. Expression of *Clec4g* mRNA was described in the FL from E15.5 onwards [104] and timed matings were prepared for f12.5;YFP embryo dissection at E13.5, E15.5 and E17.5.

Reporter activity was detected in the FL at E13.5 (Figure 14 A). Expression of YFP was observed in two distinct cell types, in a low number of $LYVE1^+$ EC and in a great majority of $LYVE1^-$ non-endothelial round cells. Additionally, YFP expression was found in some $CD68^+$ FL myeloid cells (Figure 14 B) and in a few $cKit^+$ HSCs (Figure 14 C). At E15.5, similar YFP expression pattern was seen in the FL, namely in $LYVE1^+$ ECs and $LYVE1^-$ round cells, but we observed a broader endothelial reporter YFP expression than at E13.5 (Figure 14 D). Reporter expression was also found in $CD68^+$ FL myeloid cells (Figure 14 E). The FL at E17.5 showed reporter YFP expression predominantly in $LYVE1^+$ EC and almost no YFP^+ $LYVE1^-$ round cells were detected in the FL (Figure 14 F). Besides this, $CD31^+$ FL arterial and venous EC displayed reporter YFP expression (Figure 14 G).

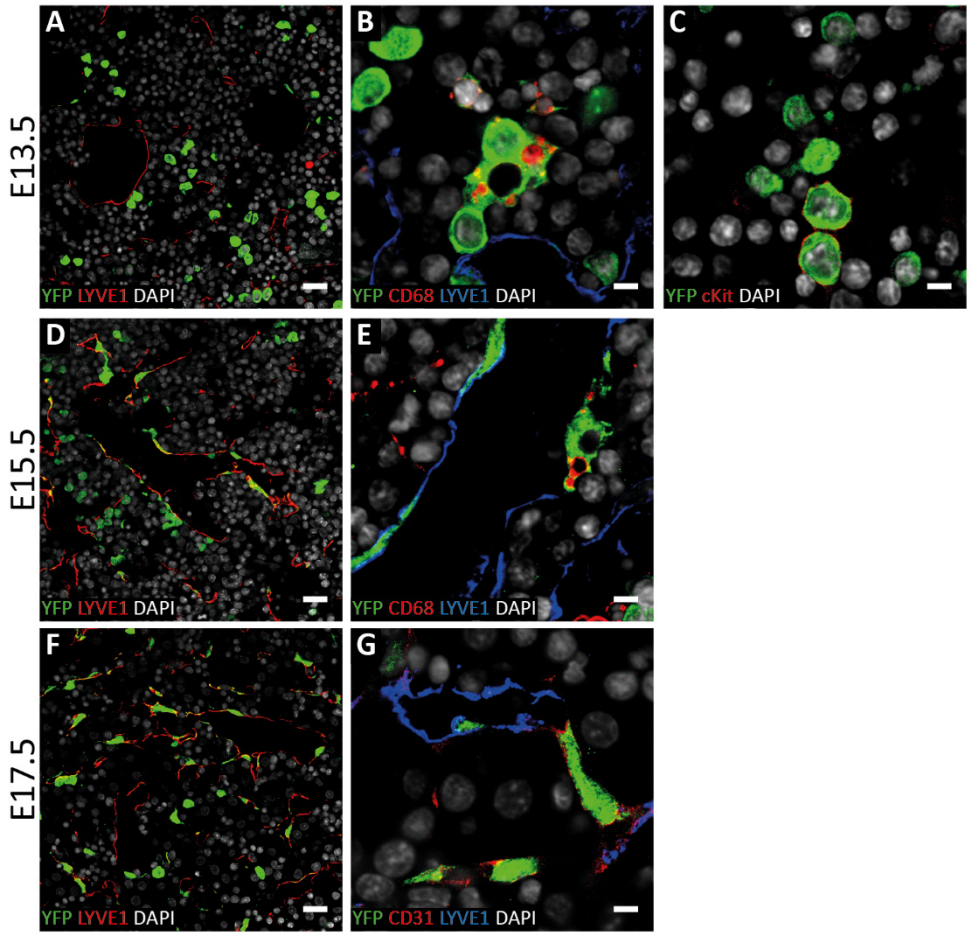

Figure 14: Immunofluorescent analysis of f12.5;YFP embryos at E13.5, E15.5, 17.5.
A - **G**, IF was carried out on cryosections from f12.5;YFP embryos at E13.5 (**A**) and at E15.5 (**B**) or on dissected livers from f12.5;YFP embryos at E17.5 (**C**). Images from confocal microscopy show the FL with co-staining of YFP (green), DAPI (grey) and LYVE1 (red) (**A**, **D**, **F**), CD68 (red) and LYVE1 (blue) (**B**, **E**, **G**), or cKit (red) (**C**). Scale bar 20 µm (**A**, **D**, **F**) or 5 µm. Representative images from two experiments with at least two biological replicates.

3.1.2.2.2. Immunofluorescent staining of the adult liver

In order to analyse the suitability of the Clec4g-cre mouse to target LSECs, reporter activity of f12.5;YFP was analysed in the adult mouse. Livers of were harvested and subjected to immunofluorescent analysis.

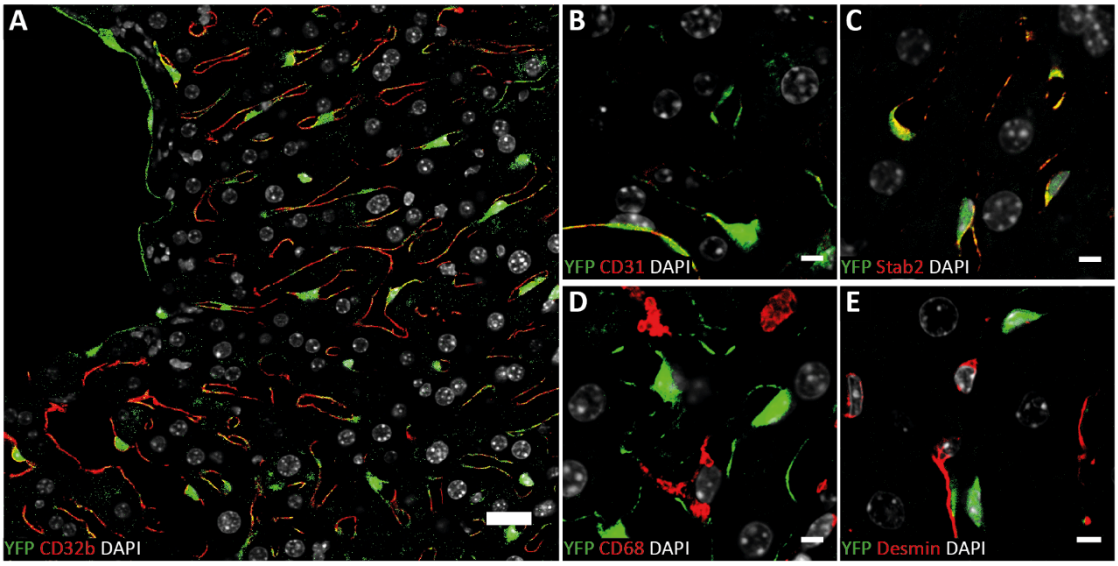

Figure 15: Immunofluorescent analysis of livers from f12.5;YFP mouse.
A - E, Liver cryosections of the f12.5;YFP mouse were subjected to IF and analysed by confocal microscopy. Micrographs show staining of YFP (green), DAPI (grey) and CD32b (red) (**A**), CD31 (red) (**B**), Stab2 (red) (**C**), CD68 (red) (**D**), or Desmin (red) (**E**). Scale bar 20 µm (A) or 5 µm. Representative images from at least three experiments with more than five biological replicates.

The liver of f12.5;YFP displayed a YFP expression with a strong sinusoidal expression pattern (Figure 15). YFP was detected in CD32b$^+$ and Stab2$^+$ microvascular ECs (Figure 15 A, C) as well as in CD31$^+$ ECs lining the CV and portal vessels (Figure 15 B). In order to differentiate the YFP staining of ECs lining the sinusoids from Kupffer cells and stellate cells, co-staining of YFP with CD68 and Desmin were carried out. Neither CD68$^+$ Kupffer cells (Figure 15 D) nor Desmin$^+$ stellate cells (Figure 15 E) demonstrated reporter activity.

In summary, reporter activity was observed in the liver of the f12.5;YFP mouse from E13.5 onwards. The number of YFP$^+$ liver ECs was low during mid-gestation and increases then until in the adult liver all Stab2$^+$ and CD32b$^+$ LSECs as well as CD31$^+$ EC showed reporter YFP expression. During fetal development a fraction of haematopoietic cells displayed reporter activity.

3.1.2.3. Reporter analysis in non-hepatic organs

3.1.2.3.1. Investigation of peripheral blood mononuclear cells, bone marrow, lymph node, and spleen

Next, reporter activity was analysed in other Stab2+ microvascular beds. BM, LN and spleen were dissected from f12.5;YFP mice and YFP expression examined by IF.

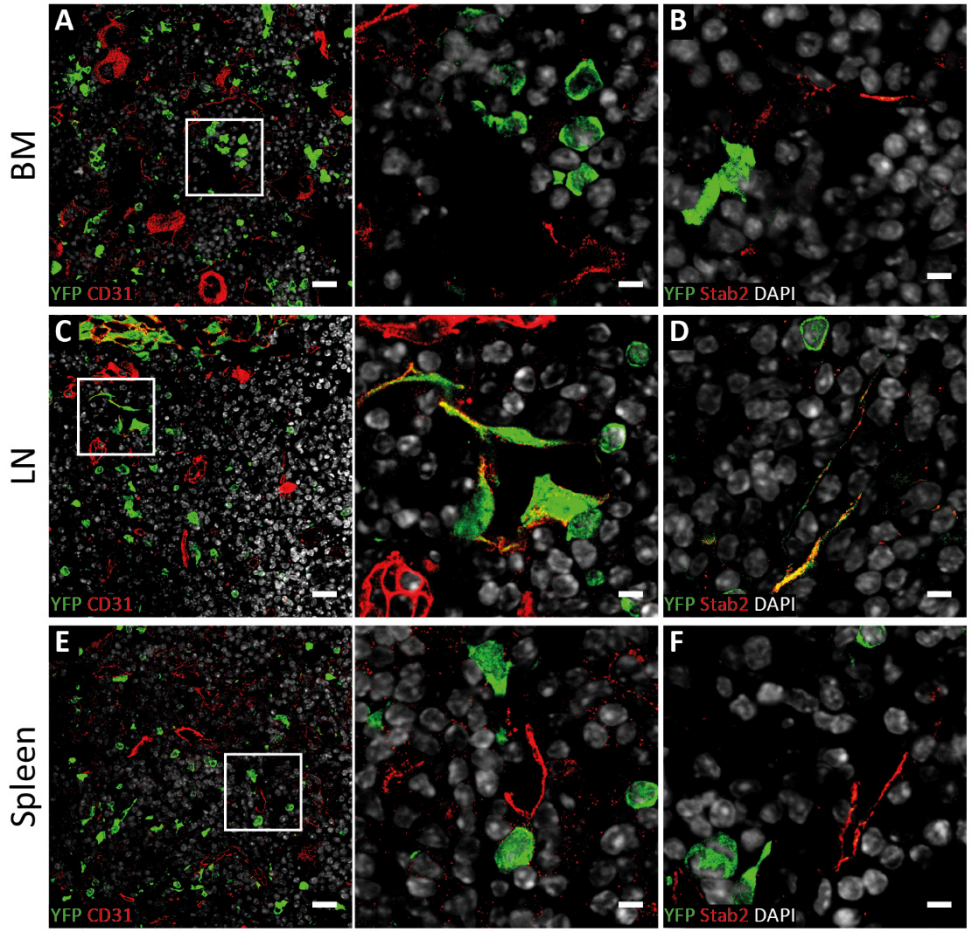

Figure 16: Immunofluorescent analysis of BM, LN, and spleen from f12.5;YFP mouse.
A – **F**, Cryosections show the BM (**A**, **B**), mesenteric LNs (**C**, **D**), and spleen (**E**, **F**) of the f12.5;YFP mouse. Images from confocal microscopy after IF show YFP (green) with CD31 (red) or Stab2 (red). Selected areas in **A**, **C**, or **E** are magnified in the right image next to it. Scale bar 20 µm or 5 µm (magnification, **B**, **D**, **F**). Representative images from at least two independent experiments with more than three biological replicates.

Reporter YFP expression was observed in the BM (Figure 16 A, B), LN (Figure 16 C, D) and spleen (Figure 16 E, F) of the f12.5;YFP mouse. In the BM, reporter YFP expression was neither observed in CD31+ EC (Figure 16 A) nor in Stab2+ cells (Figure 16 B). In the LN, CD31+ EC lining the blood vessel but not the HEV (Figure 16 C) displayed YFP expression. YFP was also observed in Stab2+ cells (Figure 16 D). In the spleen, YFP expression was neither detected in CD31+ EC (Figure 16 E) nor in Stab2+ cells (Figure 16 F).

In order to characterise the YFP$^+$ but CD31$^-$ Stab2$^-$ cell population more in detail, FACS analyses were performed. Cells from pBMCs, BM and spleen were harvested and analysed for reporter activity in haematopoietic cells.

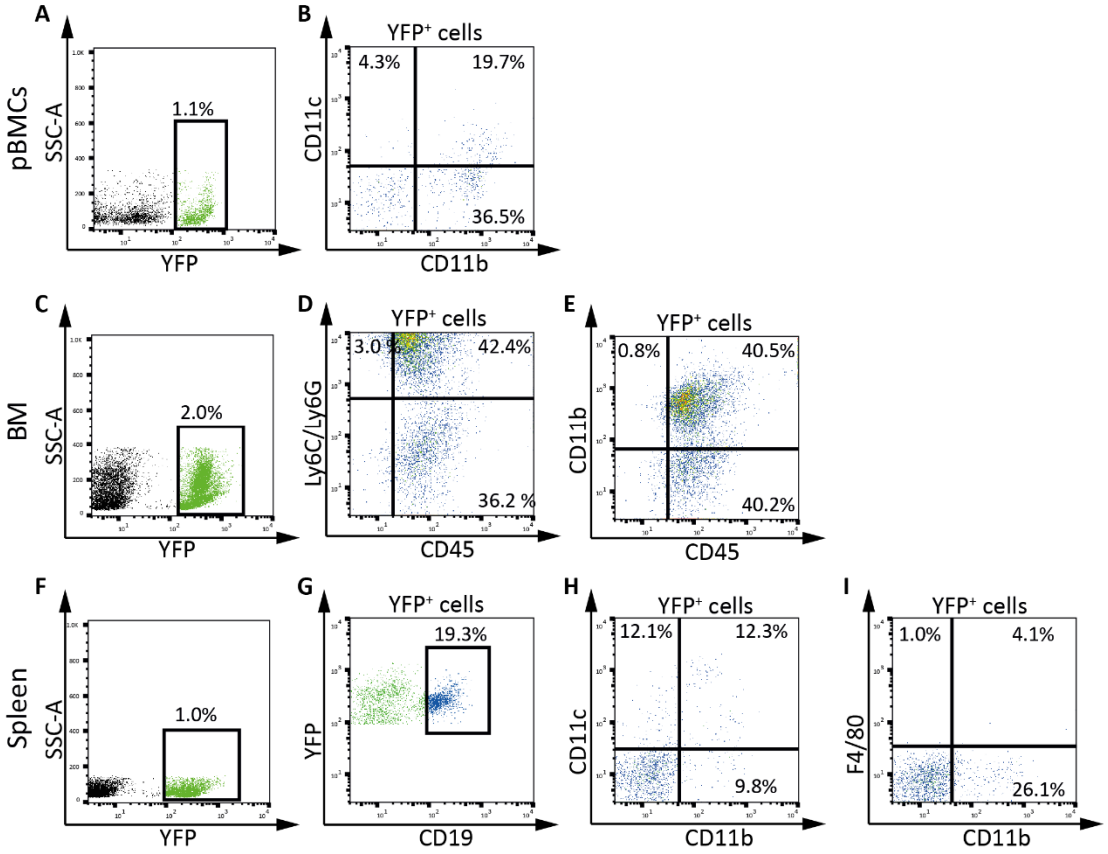

Figure 17: F12.5;YFP shows reporter activity in haematopoietic cells of the pBMCs, BM, and spleen. **A – I**, YFP expression was analysed by FACS in pBMCs (**A - B**), the BM (**C - E**) or spleen (**F - I**) from 12.5;YFP. The percentage of the YFP$^+$ population in FSC/SSC gated pBMCs (**A**), BM (**C**) or splenic cells (**F**) is illustrated by an YFP/SSC FACS plot. YFP$^+$ cells were then gated for CD11b and CD11c (**B**, **H**), CD45 and Ly6C/Ly5G (Gr-1) (**D**), CD45 and CD11b (**E**), or CD11b and F4/80 (**I**) expression. The cell number of the respective population is illustrated in relation to the total cell number of YFP-expressing cells. YFP$^+$ splenic cells were gated for CD19 expression (**G**) and the number of CD19$^+$ cells is depicted in relation to the total cell number of YFP$^+$ cells in the FACS plot. Representative FACS plots of two independent experiments with more four biological replicates.

YFP expression was detected in 1.1% of pBMCs (Figure 17 A). Cells were gated for YFP$^+$ and analysed for reporter activity in CD11b$^+$ CD11c$^+$ monocytes, CD11b$^+$ CD11b$^-$ macrophages and CD11b$^-$ CD11c$^+$ dendritic cells [105,106]. 4.3% were CD11b$^-$ CD11c$^+$ cells, 19.7% were CD11b$^+$ CD11c$^+$ cells and 36.5% were CD11b$^+$ CD11c$^-$ cells. In the BM, 2.0% of cells expressed YFP (Figure 17 B). The YFP$^+$ cells were identified and gated by CD45 and CD11b expression in order to identify CD45$^+$ CD11b$^-$ immature monocytes and CD45$^+$ CD11b$^+$ neutrophils and macrophages [107] as well as by CD45 and Gr-1 expression to identify CD45$^+$ Gr-1^{low} monocytes and CD45$^+$ Gr-1^{high} neutrophils [108]. 40.5% were CD45$^+$ CD11b$^+$, 40.2% were CD45$^+$ CD11b$^-$ and 0.8% were CD45$^-$ CD11b$^+$ as well as 42.4% were CD45$^+$ Gr-1$^+$, 36.2% were CD45$^+$ Gr-1$^-$ and 3.0% were CD45$^-$ Gr-1$^+$ cells. In the spleen, reporter YFP expression was detected in 1.0% of the total splenic cells (Figure 17 C). The

YFP$^+$ cells were gated by the expression of CD19 to identify b-cells [109] and showed that 19.3% of YFP$^+$ cells were also CD19$^+$ b-cells. Additionally, cells were gated for YFP-positivity and CD11b and CD11c splenic dendritic cells or CD11b and F4/80 splenic macrophages were identified [110,111]. A fraction of the YFP$^+$ cells were CD11b$^-$ CD11c$^+$ (12.1%), CD11b$^+$ CD11c$^+$ (12.3%), CD11b$^+$ CD11c$^-$ (9.8%) cells or CD11b$^-$ F4/80$^+$ (1.0%), CD11b$^+$ F4/80$^+$ (4.1%), CD11b$^+$ F4/80$^-$ (26.1%) cells.

Taken together, the f12.5;YFP mouse showed reporter activity in Stab2$^+$ microvascular and CD31$^+$ EC in the LN. FACS analysis demonstrated that only a small percentage of the cells in the pBMCs, BM and spleen expressed YFP. Of those cells a variable fraction of monocytes and myeloid cells as well as splenocytes displayed YFP expression.

3.1.2.3.2. Analysis of the intestine, kidney, pancreas, and thymus

F12.5;YFP mice were investigated in the intestine, kidney, pancreas, and thymus to provide a comprehensive analysis. Organs were collected and YFP expression investigated by IF.

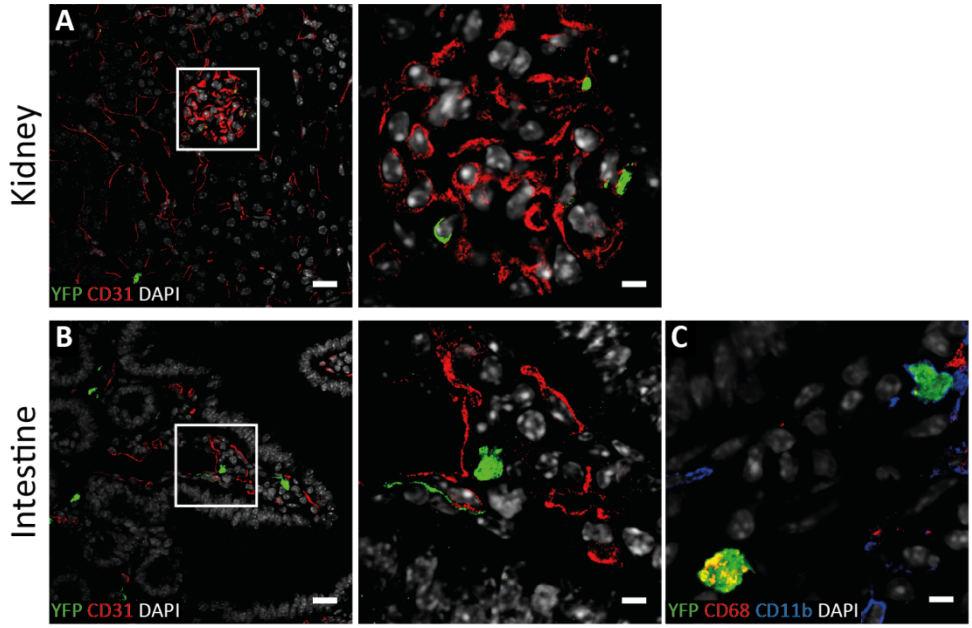

Figure 18 (continued on the next page)

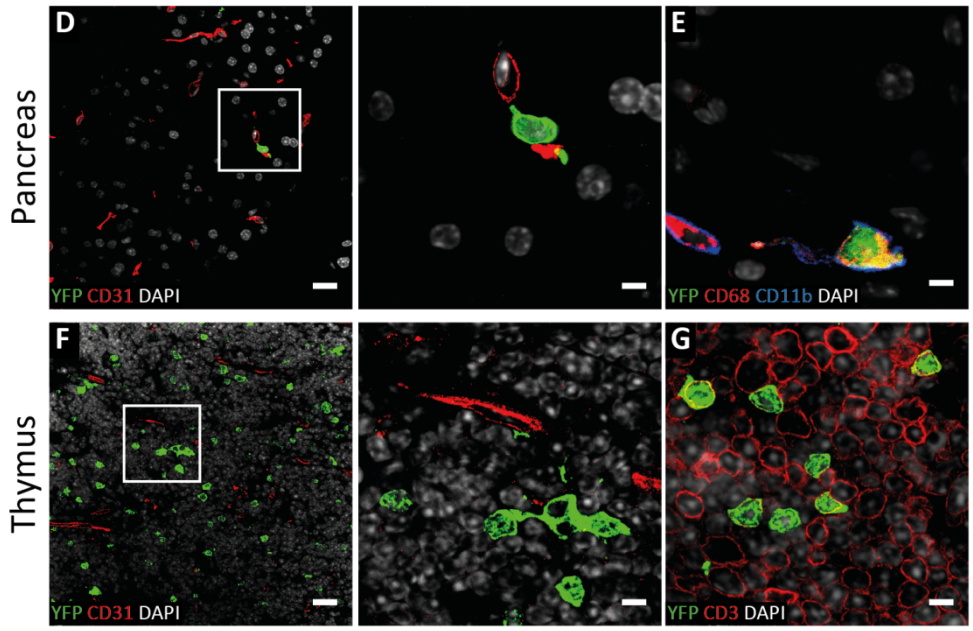

Figure 18 (continued): Immunofluorescent analysis of kidney, small intestine, pancreas, and thymus from f12.5;YFP mouse.
A – G, IF was carried out on cryosections of kidney (**A**), intestine (**B**, **C**), pancreas (**D**, **E**), and thymus (**F**, **G**). Images from confocal microscopy show YFP (green), DAPI (grey) with CD31 (red) (**A**, **B**, **D**, **F**), CD68 (red) and CD11b (blue) (**C**, **E**), or CD3 (red) (**G**). Selected areas in **A**, **B**, **D** or **F** are magnified in the right image next to it. Scale bar 20 µm or 5 µm (magnification, **C**, **E**, and **G**). Representative images from at least three independent experiments with more than three biological replicates.

Reporter activity was detected in a few cells of the kidney (Figure 18 A) that were identified as $CD31^-$ cells. In the small intestine, YFP expression was observed in distinct $CD31^-$ cells of the villi (Figure 18 B). CD68 and CD11b were reported to stain different sub-types of myeloid cells of the intestinal mucosa [112,113]. Co-staining of YFP with CD68 and CD11b revealed a reporter activity in intestinal macrophages and intestinal dendritic cells of the f12.5;YFP mouse, respectively (Figure 18 C). In the pancreas, few YFP^+ cells were observed (Figure 18 D). These cells were $CD31^-$ non-EC and co-expressed CD68 and CD11b (Figure 18 E) demonstrating a reporter activity in pancreatic myeloid cells. In the thymus, YFP expression was detected in $CD31^-$ non-ECs (Figure 18 F) which were defined as $CD3^+$ t-cells expressing YFP (Figure 18 G).

3.1.2.3.3. Characterisation of the brain, heart, lung, and skin

Next, reporter activity was investigated in EC lining the vascular beds of brain, heart, lung, and skin. Organs were harvested from the f12.5;YFP mice and expression of YFP was analysed.

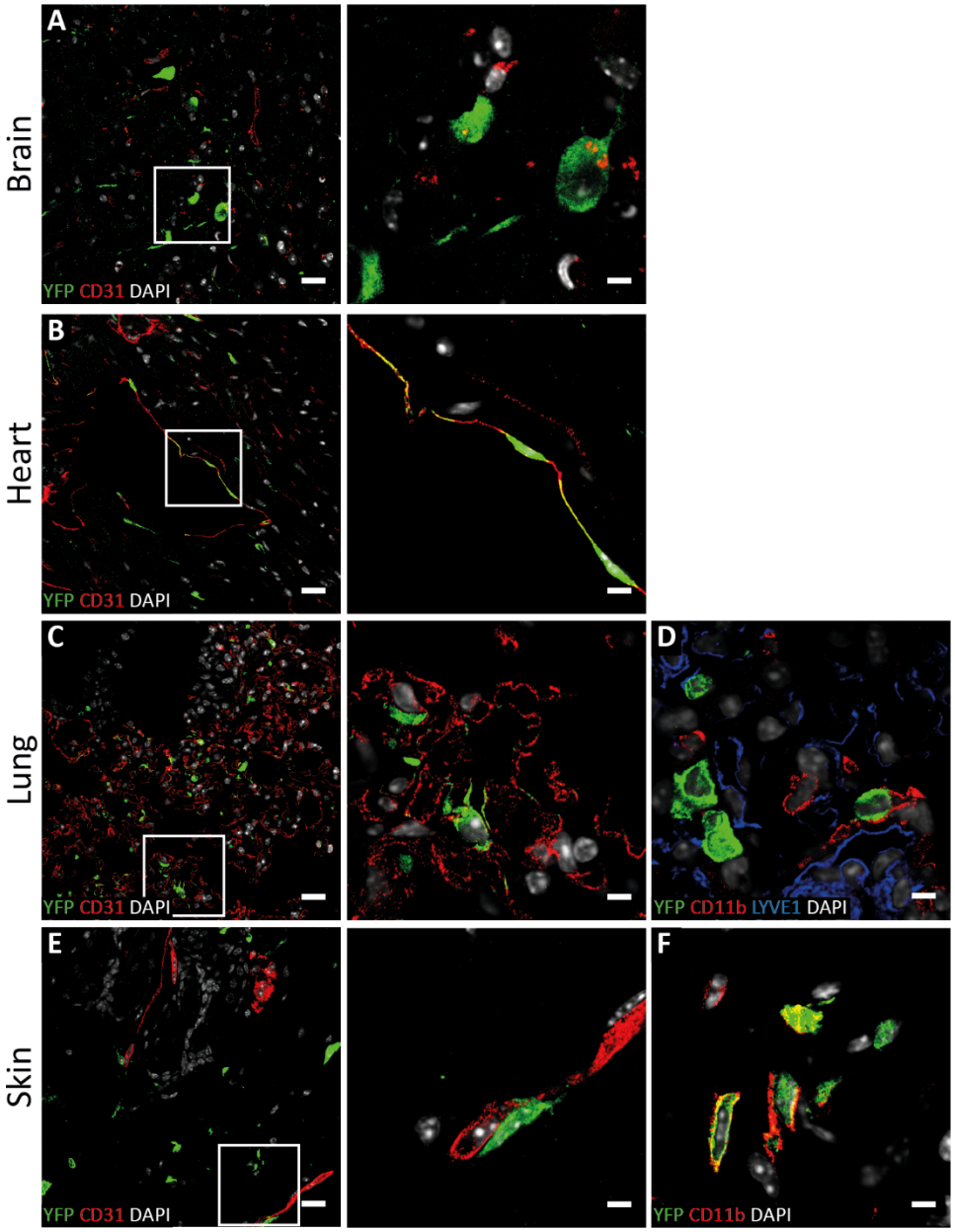

Figure 19: Immunofluorescent analysis of brain, heart, lung, and skin from f12.5;YFP mouse.
A – **F**, IF was carried out on cryosections of brain (**A**), heart (**B**), lung (**C**, **D**), and skin (**E**, **F**). Images from confocal microscopy show YFP (green), DAPI (grey) and CD31 (red) (**A**, **B**, **C**, **E**), CD11b (red) and LYVE1 (blue) (**D**), or CD11b (red) (**F**). Selected areas in **A**, **B**, **C**, or **E** are magnified in the right image next to it. Scale bar 20 µm or 5 µm (magnification, **D**, **F**). Representative images from at least two independent experiments with at least three biological replicates.

The brain of the f12.5;YFP mouse showed reporter activity in CD31$^-$ non-ECs of the pre-frontal cortex (Figure 19 A), no YFP expression was detected in other cerebral regions such as the hippocampus or cerebellum. In the heart, broad reporter YFP expression was observed in CD31$^+$ EC of the myocardium and endocardium (Figure 19 B). Reporter activity was detected in the lung but neither was it observed in CD31$^+$ EC (Figure 19 C) nor in LYVE1$^+$ lymphatic endothelium. CD11b$^+$ cells of the lung were reported as alveolar dendritic cells [114] and co-staining of YFP with CD11b in the lung demonstrated a reporter activity in those cells (Figure 19 D). Similar to the lung, the skin of the f12.5;YFP mouse did not show reporter YFP expression in CD31$^+$ EC (Figure 19 E) but in CD11b$^+$ dermal cells (Figure 19 F).

3.1.2.4. Summary

Reporter activity was investigated in the Clec4g-cre mouse model. In the adult liver, YFP expression was observed in ECs lining the sinusoids and the vascular bed of the periportal and pericentral vessel. In the LN, endothelial reporter activity was detected in the sinuses whereas the HEV did not show a YFP expression. Furthermore, endothelial reporter activity was only found in the heart. The Clec4g-cre mouse displayed reporter activity in a small percentage of haematopoietic cells in BM, pBMCs, intestine, kidney, pancreas, and spleen as well as in t-cells. Analysis of the liver during embryonic development revealed strong endothelial reporter YFP expression from E15.5 onwards, at earlier time points transient reporter activity was also observed in CD68$^+$ haematopoietic cells.

3.2. Differentiation of liver sinusoidal endothelial cells

3.2.1. Function of GATA4 during LSEC development

Transcriptional regulators that control maturation and differentiation of organotypic microvascular EC have not been established. The LSEC-specific differentiation programme was investigated by gene expression profiling [24] and identified GATA4 in a set of TFs by comparing rat LSEC with rat lung microvascular EC. During embryogenesis GATA4 is one of the earliest TFs expressed in cardiac progenitor cells [75] but study of the molecular function in LSECs was compromised by the early embryonic lethality resulting from cardiac defects from the general [75,76] and pan-endothelial knockout [77]. In order to investigate the function of GATA4 in LSECs a Cre driver mouse was required that would induce GATA4 deficiency in microvascular EC of the liver but not in ECs of the developing heart.
Screening of the LSEC-Cre driver mouse lines demonstrated Cre activity of Stab2-cre f2 in fetal LSEC but not in the fetal heart (Figure 5 - Figure 8). Stab2-cre f3 did not show reporter activity during fetal development (Figure 7). Endothelial reporter activity in livers of Clec4g-cre embryos was observed from E15.5 onwards (Figure 14), however, endothelial YFP expression was not as strong as for Stab2-cre f2. Therefore, Stab2-cre f2 was examined for suitability to generate GATA4 specific knockout in fetal LSECs.

3.2.1.1. Stab2-cre driven GATA4 deficiency in the fetal liver endothelium

Double immunofluorescent labelling of GATA4 with Stab2 showed a co-expression in the FL (Figure 20 A) but not in the fetal heart (Figure 20 C). This is in contrast to CD31 and GATA4 double labelling in hepatic (Figure 20 B) and cardiac ECs (Figure 20 D) suggesting the Stab2 promotor driven Stab2-cre mouse as a suitable Cre driver. Besides the reporter activity of the f2;YFP mouse in fetal (Figure 6 D, Figure 8 A) and adult LSECs (Figure 9 A, C), co-expression of the reporter with GATA4 was observed in ECs of the FL (Figure 20 E). This established Stab2-cre f2 as an ideal Cre driver mouse to study GATA4 function in LSECs.

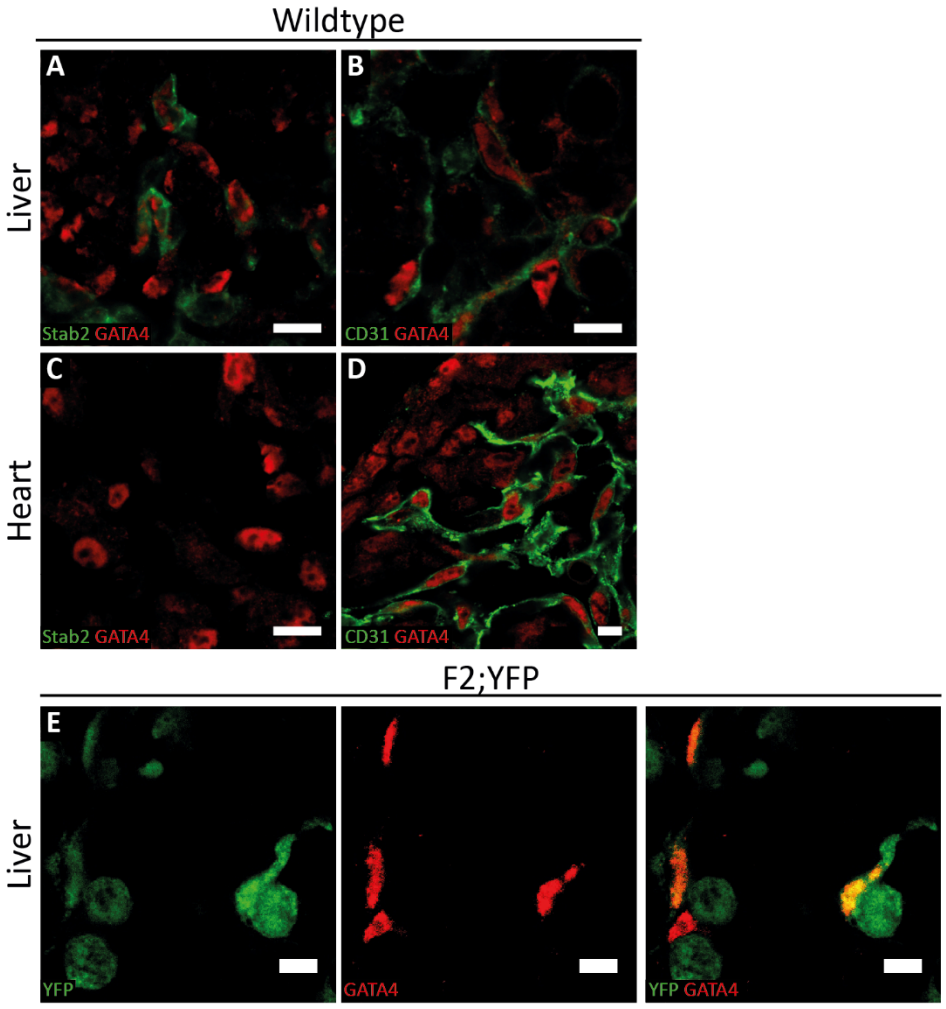

Figure 20: Stab2-cre f2 mouse is suitable to analyse GATA4 function in LSECs during fetal development.
A – **D**, IF was carried out on cryosections of wildtype embryos at E10.5. Images from confocal microscopy show the FL or the fetal heart with co-staining of GATA4 (red) with Stab2 (green) or CD31 (green). **E**, IF was carried out on cryosections of f2;YFP embryos at E12.5. Single channel images and composite image after confocal microscopy show the FL with co-staining of YFP (green) and GATA4 (red). Scale bar 5 µm. Representative images from at least two independent experiments with more than three biological replicates.

3.2.1.2. Basic analysis

3.2.1.2.1. Stab2-cre driven GATA4 deficiency causes embryonic lethality

Mice homozygous for the Gata4^{loxP} allele were bred with Stab2-cre f2 mouse to generate a heterozygous GATA4 knockout which was then again mated with homozygous Gata4^{loxP} mouse to receive a homozygous GATA4 knockout (Gata4$^{\Delta LSEC}$) (Figure 21 A).

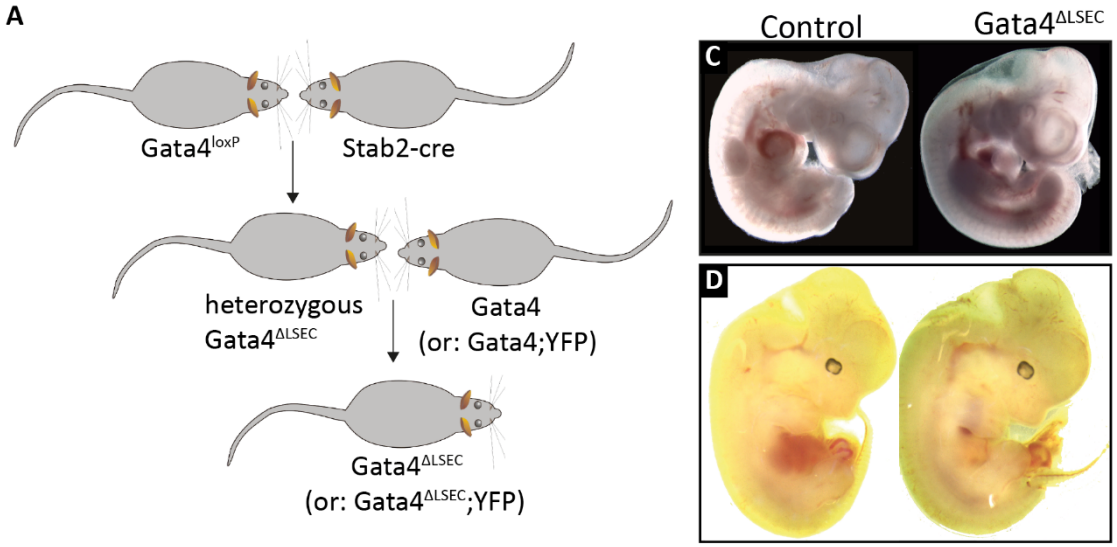

B

Age	Total	Viable Knockout	Mendelian ratio /expected ratio
E9.5 - E10.5	101	27	27% /25%
E11.5 - E12.5	536	131	24% / 25%
E13.5 - E14.5	163	46	28% / 25%
E17.5	11	0*	0% / 25%
P28	242	-	-/ 25%

Figure 21: Embryonic lethality of Gata4$^{\Delta LSEC}$ knockout.
A, Scheme to illustrate the generation of Gata4$^{\Delta LSEC}$ or Gata4$^{\Delta LSEC}$;YFP knockout mouse. **B**, Results from genotyping of Gata4$^{\Delta LSEC}$ knockout and control embryos at indicated time points. Viable embryos were identified by beating heart. *, at E17.5, two knockout embryos were found in the uterus but did not show a heartbeat and had a pale appearance. **C** – **E**, Macroscopic images of control (left) and Gata4$^{\Delta LSEC}$ (right) knockout embryos at E10.5 (**C**), E11.5 (**D**), and E13.5 (**E**). Representative images from at least three independent experiments with more than three biological replicates.

Distribution of the genotypes showed a normal Mendelian ratio from E9.5 to E14.5 (Figure 21 B). At E17.5, no viable knockout embryos were found. No knockout was detected among the pubs of 4 weeks of age indicating an embryonic lethality between E14.5 and E17.5. Knockout embryos were analysed macroscopically (Figure 21 C - E), no differences were observed between control and knockout embryos at E10.5. At E11.5 and E13.5 growth of knockout and control embryos was unaltered but FL was heavily reduced in size.

3.2.1.2.2. GATA4 knockout in LSEC causes fetal liver growth arrest

Next, Gata4$^{\Delta LSEC}$ and control embryos were investigated more in detail by haematoxylin & eosin (H&E) staining and the fetal liver and heart were dissected for gross comparison.

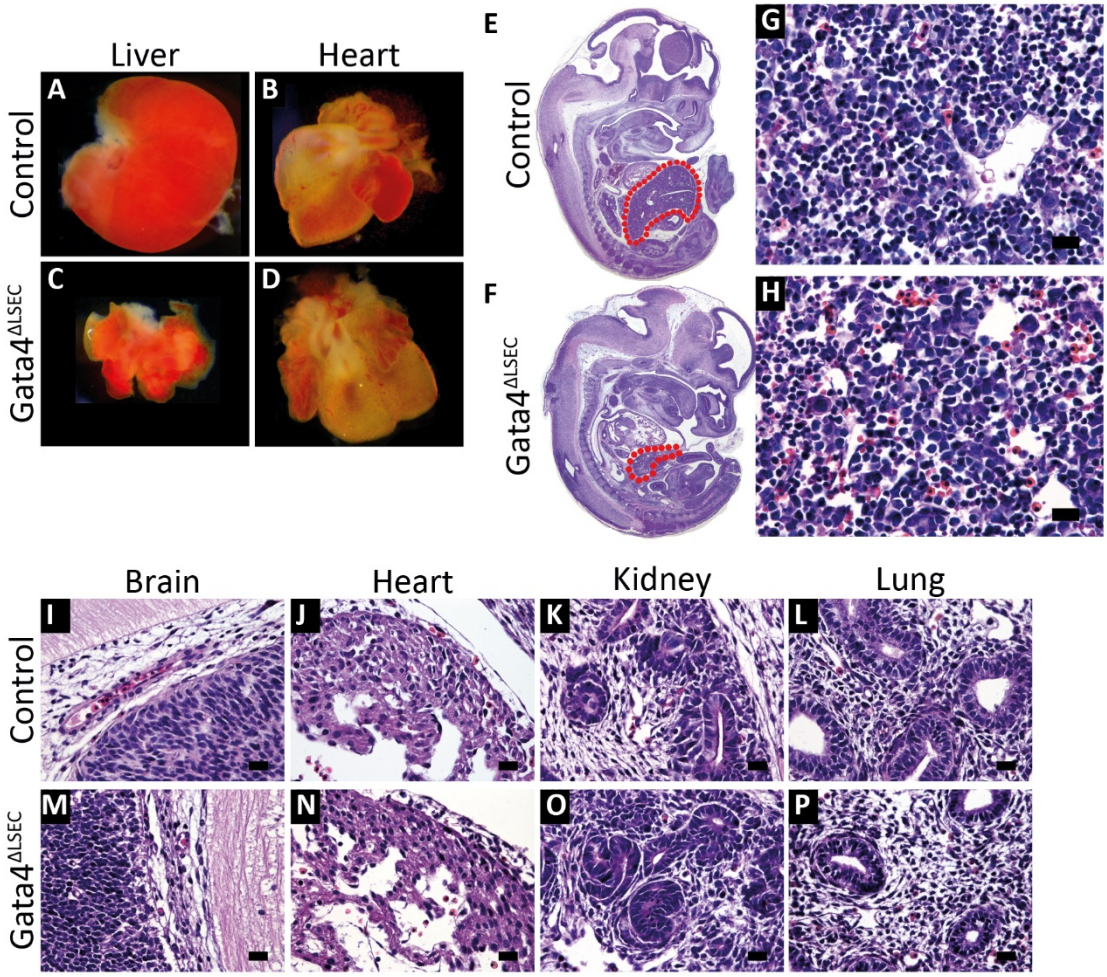

Figure 22: Reduced size and distorted structure of livers from Gata4$^{\Delta LSEC}$ knockout embryos.
A – **D**, Photomicrographs of the FL and fetal heart of control (**A**, **B**) and Gata4$^{\Delta LSEC}$ knockout (**C**, **D**) embryos at E13.5. **E** – **P**, H&E staining of control (**E**, **G**, **I**, **K**, **M**, **O**) and Gata4$^{\Delta LSEC}$ knockout (**F**, **H**, **J**, **L**, **N**, **P**) embryos at E13.5. Red dotted lines indicate the FL in the cross-section of the embryos (**E**, **F**). H&E staining of the liver (**G**, **H**) brain (**I**, **J**), heart (**K**, **L**), lung (**M**, **N**), and kidney (**O**, **P**). Scale bar 20 µm. Representative images from one experiment with at least two replicates.

The dissected FL from Gata4$^{\Delta LSEC}$ embryos displayed a reduced size compared to control embryos (Figure 22 A, C) whereas the heart did not show any gross abnormalities (Figure 22 B, D). H&E staining showed a severely hypoplastic liver (Figure 22 E, F), an impaired vascular organisation and an increase of red blood cells in the knockout liver (Figure 22 G, H). Growth and development of vascular structures in brain, lung, and kidney were not affected in Gata4$^{\Delta LSEC}$ embryos (Figure 22 I - P).

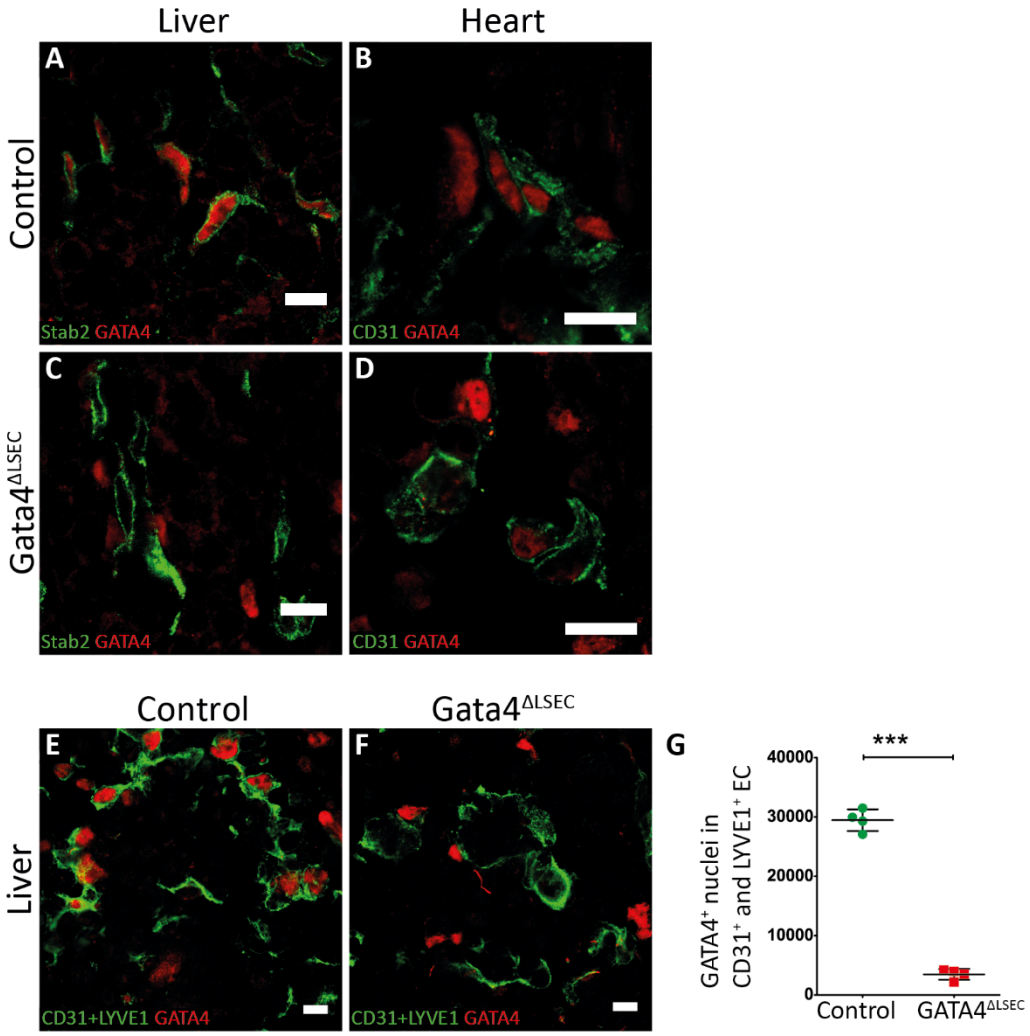

Figure 23: Immunofluorescent analysis of GATA4 in liver and heart from Gata4$^{\Delta LSEC}$ knockout and control embryos
A – **D**, IF was carried out on cryosections of control (**A**, **B**) and Gata4$^{\Delta LSEC}$ knockout (**C**, **D**) embryos at E10.5. Images from confocal microscopy show the co-staining of GATA4 (red) with Stab2 (green) or CD31 (green) in the FL (**A**, **C**) or the fetal heart (**B**, **D**). **E** – **F**, IF was carried out on cryosections of control (**E**) and Gata4$^{\Delta LSEC}$ knockout (**F**) embryos at E11.5. Images from confocal microscopy show the co-staining of CD31 and LYVE1 (both in green) and GATA4 (red) in the FL. Scale bar 10 µm. **G**, Quantification of GATA4$^+$ nuclei in CD31$^+$ and LYVE1$^+$ vessels. Scale bar 10 µm. Representative images from at least one experiment with at least three replicates. Student's t test: ***, $p < 0.001$.

GATA4 deficiency was then assessed by immunofluorescent staining of liver and heart at E10.5 (Figure 23 A - D) and E11.5 (Figure 23 E - G). Stab2$^+$ GATA4$^+$ LSECs were not observed in livers of Gata4$^{\Delta LSEC}$ embryos (Figure 23 C) only in livers of control embryos (Figure 23 A). GATA4 expression in cardiac EC was not affected in control or in Gata4$^{\Delta LSEC}$ mutant embryos (Figure 23 B, D). The number of GATA4$^+$ nuclei in the liver vasculature was quantified using double labelling of the hepatic EC by LYVE1 and CD31 (Figure 23 E - G). GATA4$^+$ nuclei were significantly reduced and showed GATA4 expression in less than 10% of liver EC in the Gata4$^{\Delta LSEC}$ embryos. This shows the efficient reduction of GATA4 protein expression in the hepatic microvasculature by the Stab2-cre f2 mouse.

3.2.1.3. Investigation of the fetal liver endothelium

3.2.1.3.1. Characteristics of the GATA4-deficient fetal liver micro-vasculature

As Gata4$^{\Delta LSEC}$ embryos displayed a reduced liver size and distorted hepatic vasculature, LSEC markers were investigated that characterise the adult liver sinusoids.

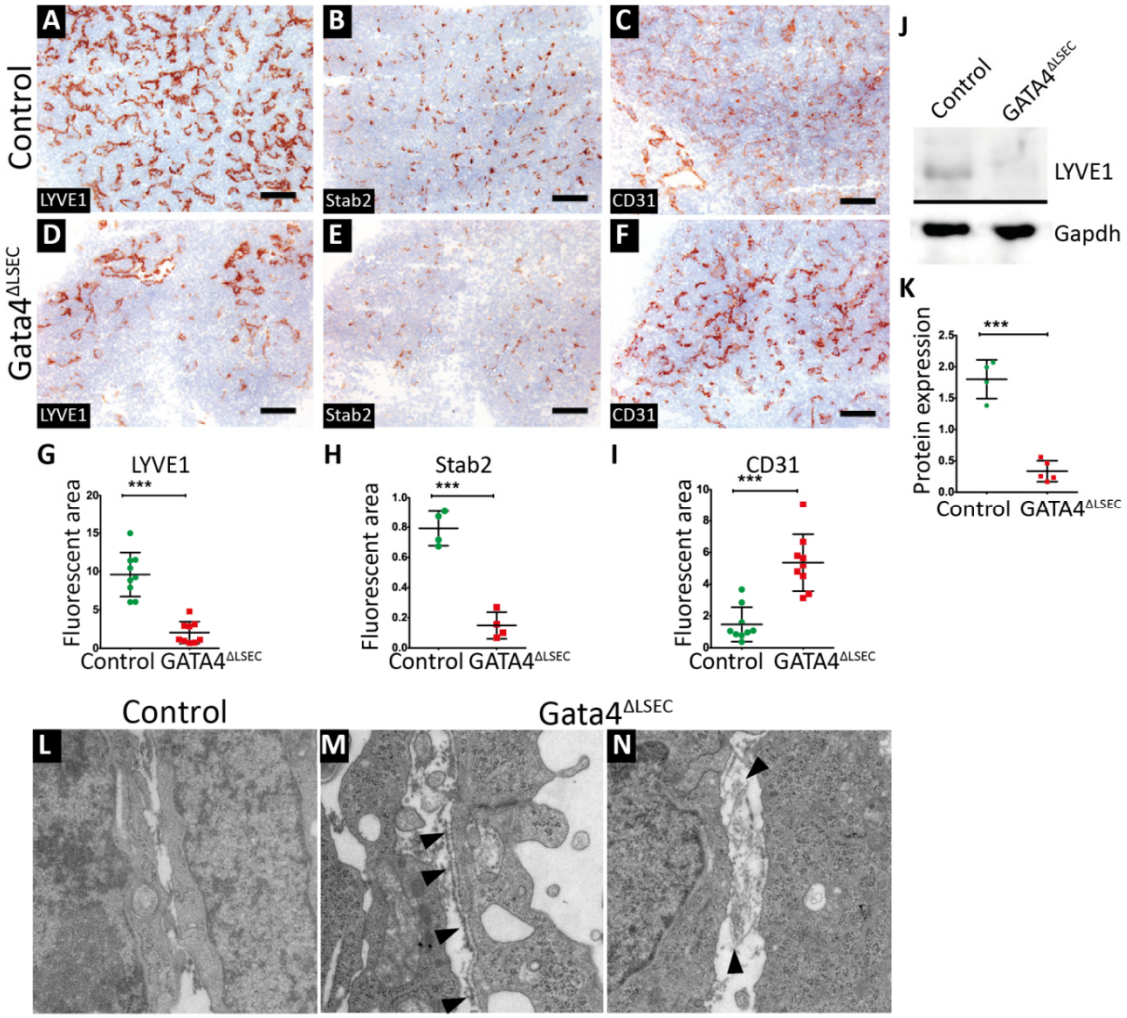

Figure 24 (continued on the next page)

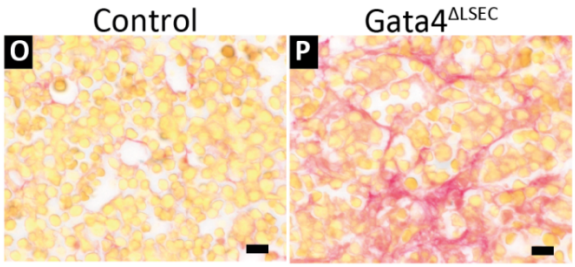

Figure 24 (continued): GATA4 expression in LSECs controls sinusoidal and continuous marker expression.
A – **F**, Immunohistochemistry was carried out on cryosections of control (**A** - **C**) and Gata4$^{\Delta LSEC}$ knockout (**D** - **F**) embryos at E11.5 to visualize LYVE1 (**A**, **D**), Stab2 (**B**, **E**), and CD31 (**C**, **F**) expression in the FL. **G** – **I**, Quantification of LYVE1 (**G**), Stab2 (**H**), or CD31 (**I**) staining in the FL of Gata4$^{\Delta LSEC}$ embryos at E11.5. IF was carried out on cryosections of Gata4$^{\Delta LSEC}$ embryos at E11.5 and the fluorescent area was quantified in relation to the total FL size. **J** - **K**, Western Blot and quantification shows expression of LYVE1 in the FL of control and Gata4$^{\Delta LSEC}$ knockout embryos at E11.5. Protein lysates of FL were separated by SDS-PAGE, blotted and incubated with antibodies detecting LYVE1 and Gapdh protein (**J**). Densitometric analysis and graphic illustration from Western Blot results (**K**). **L** – **N**, FLs of control (**N**) and Gata4$^{\Delta LSEC}$ knockout (**M**, **N**) embryos at E11.25 were subjected to electron microscopic analysis. **O** – **P,** Sirius Red staining of control (**O**) and Gata4$^{\Delta LSEC}$ knockout (**P**) embryos shows the FL at E13.5. Scale bar 100 µm (**A** - **F**) and 10 µm (**O**, **P**). Representative images one (**L** – **N**) or more than two experiments with at least three replicates. Student's *t* test: ***, $p < 0.001$.

LYVE1 and Stab2, both expressed by adult LSECs and in control FLs (Figure 24 A, B), showed a decreased expression in the FL of Gata4$^{\Delta LSEC}$ embryos at E11.5 (Figure 24 D, E). On the contrary CD31, which is low expressed by adult LSECs and in control FLs (Figure 24 C), displayed an increased expression in the FL of Gata4$^{\Delta LSEC}$ embryos at E11.5 (Figure 24 F). The difference in protein expression of control and Gata4$^{\Delta LSEC}$ mutant FLs was quantified using immunofluorescent micrographs and calculated as fluorescent area in relation to hepatic area. The percentage of LYVE1+ fluorescent area was reduced from 9.6% to 2.0% (Figure 24 G), the percentage of Stab2^{+} fluorescent area was reduced from 0.8% to 0.1% (Figure 24 H), and the percentage of CD31^{+} fluorescent area was increased from 1.5% to 5.4% (Figure 24 I). In addition, FL lysates were assessed for LYVE1 protein expression (Figure 24 J). We detected a significant lower protein amount of LYVE1 in Gata4$^{\Delta LSEC}$ FL at E11.5 (1.8% vs. 0.3%) (Figure 24 K) indicating a shift from sinusoidal to continuous endothelial marker expression in Gata4$^{\Delta LSEC}$ mutant livers. Sirius Red staining visualises collagen fibres and showed a deposition of collagenous proteins in the extracellular space in Gata4$^{\Delta LSEC}$ FLs at E13.5 (Figure 24 P) which was not observed in the control FLs (Figure 24 O). Since these changes were very profound, Gata4$^{\Delta LSEC}$ mutant livers were analysed on an ultrastructural level. Electron microscopy showed a formation of basement membrane (Figure 24 M) and deposition of ECM (Figure 24 N) in the FL of Gata4$^{\Delta LSEC}$ embryos at E11.5 which was not observed in the FL of control embryos (Figure 24 L).

In summary, the FL of Gata4$^{\Delta LSEC}$ transgenic embryos lost the special characteristics of liver sinusoidal endothelium. The switch of endothelial marker expression, the increase of ECM and formation of a basement membrane were striking in the Gata4$^{\Delta LSEC}$ mutant embryos and can be described as capillarization of the FL endothelium [115,116].

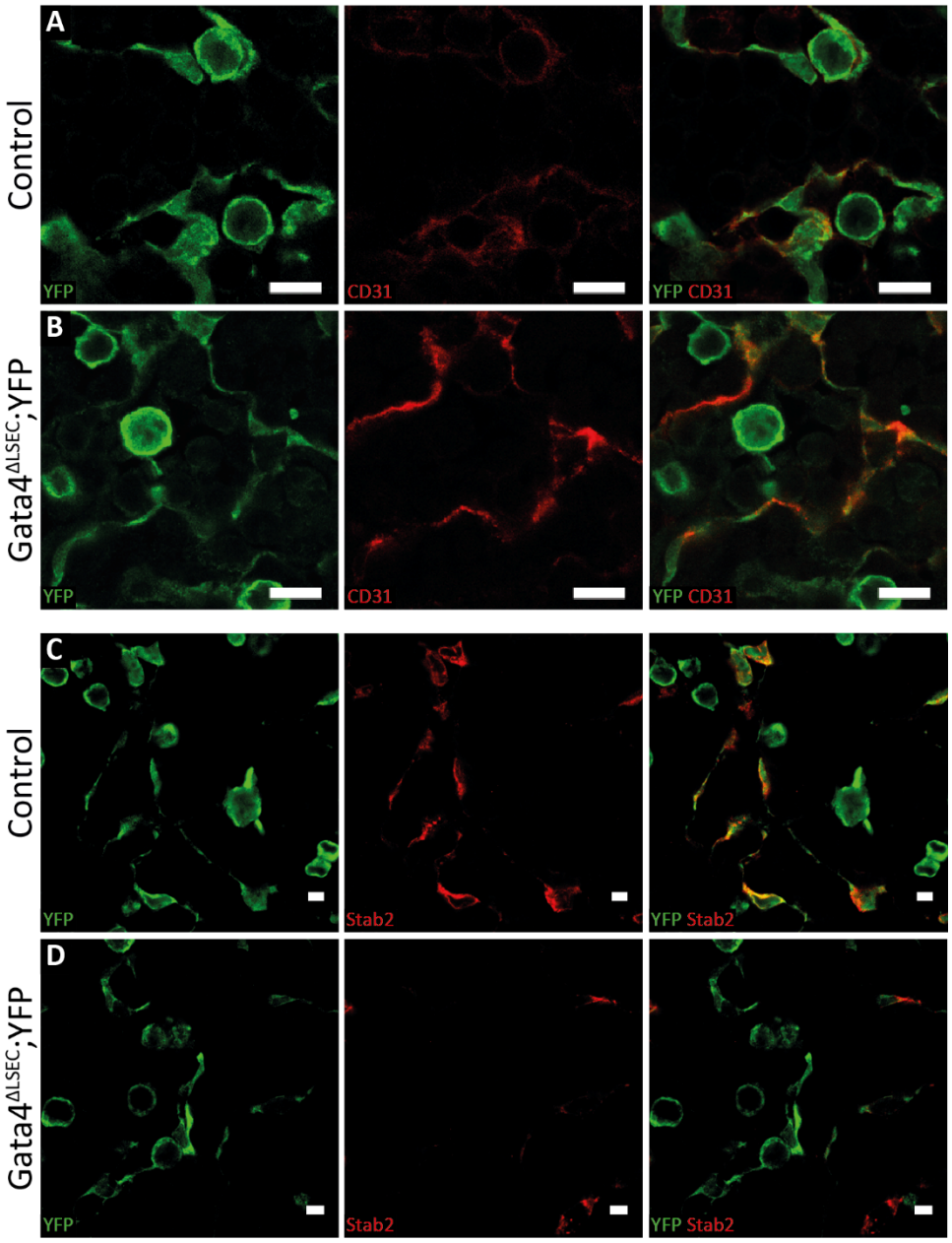

Figure 25: GATA4 deficient hepatic endothelium undergoes dedifferentiation.
A – **D**, IF was carried out on cryosections of control (**A**, **C**) and Gata4$^{\Delta LSEC}$;YFP knockout (**B**, **D**) embryos at E11.5. Images from confocal microscopy show the FL with single channels and composite image after IF of YFP (green) with CD31 (red) (**A**, **B**) or Stab2 (red) (**C**, **D**). Scale bar 5 µm. Representative images two experiments with at least three replicates.

In order to confirm that the capillarized endothelium results from transdifferentiation of the GATA4 deficient transgenic EC rather than from angiogenic processes of Stab2^{-} EC without Cre activity, we generated a YFP reporter Gata4$^{\Delta LSEC}$ mouse (Figure 21 A: Gata4$^{\Delta LSEC}$;YFP). This mouse model showed YFP expression and GATA4 deficiency upon Cre mediated recombination and allowed for visualisation of recombined ECs. In the FL of control embryos at E11.5 (here: GATA4 heterozygous deficiency) the YFP^{+} transgenic ECs showed a low CD31 expression (Figure 25 A) whereas in GATA4 homozygous deficient embryos the YFP^{+} transgenic endothelium was characterized by high CD31 expression

(Figure 25 B). Furthermore, the YFP+ transgenic endothelium in control livers showed a high Stab2 expression (Figure 25 C) in contrast to the YFP+ transgenic EC in Gata4$^{\Delta LSEC}$ livers in which Stab2 expression is almost absent (Figure 25 D). This demonstrated that the Stab2-cre driven GATA4 deficiency resulted in a capillarization of the transgenic microvasculature.

3.2.1.4. Examination of the fetal liver haematopoiesis

3.2.1.4.1. Haematopoietic defects upon GATA4 deficiency in fetal LSECs

So far, Gata4$^{\Delta LSEC}$ embryos displayed a reduced FL size with an increase of ECM. The GATA4 transgenic hepatic endothelium started to transdifferentiate which means loss of LSEC marker expression and formation of a basement membrane. Unlike adulthood, the FL is essential for seeding and differentiation of haematopoietic stem and progenitor cells. In order to evaluate potential defects on haematopoietic events due to hepatic maldevelopment, HPCs were quantified at E11.25 as well as the number of HSC was investigated at E13.25.

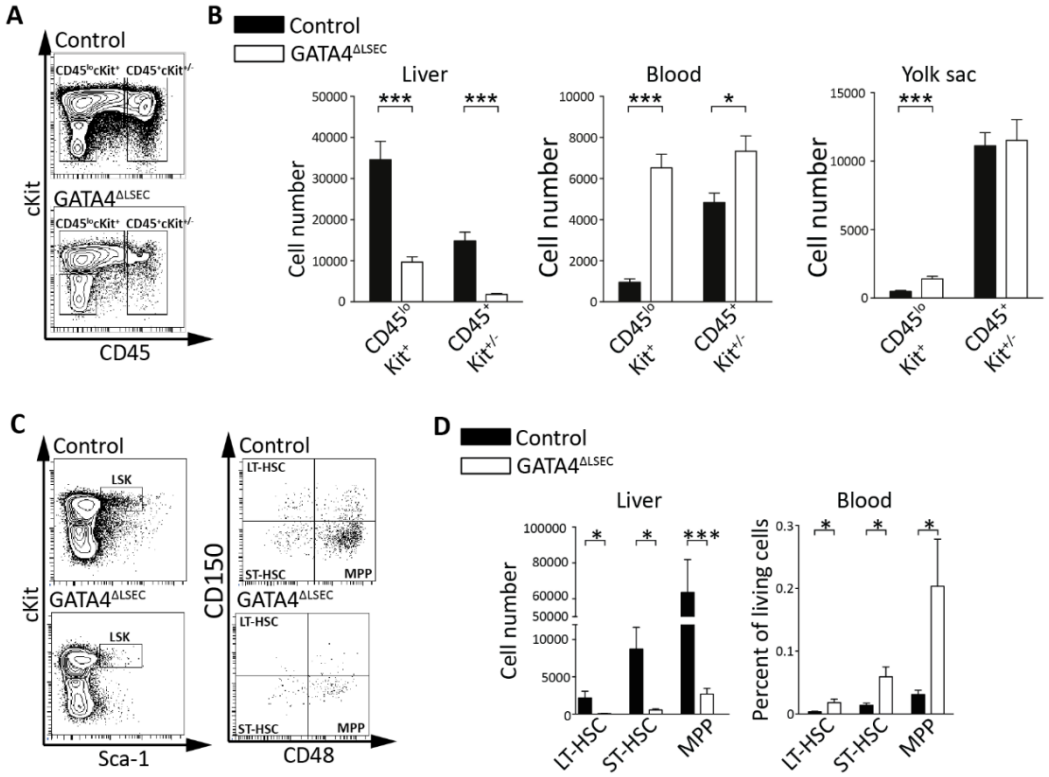

Figure 26: Defective haematopoiesis in the Gata4$^{\Delta LSEC}$ embryos.
A – **B**, FACS plot (**A**) and quantification (**B**) of CD45^{lo} Kit^{+} and CD45^{+} Kit$^{+/-}$ HPCs in the liver, blood and yolk sac (YS) of Gata4$^{\Delta LSEC}$ embryos at E11.25 [liver: n = 14 mutants and 10 controls; blood: n = 15 mutants and 10 controls; YS: n = 8 mutants and 16 controls (YS controls: *Stab2-cre$^{tg/wt}$;Gata4$^{fl/wt}$*, *Stab2-cre$^{wt/wt}$*;Gata4$^{fl/fl}$, *Stab2-cre$^{wt/wt}$*;Gata4$^{fl/wt}$)]. **C** – **D**, FACS plots (**C**) and quantification (**D**) of LT-HSC, ST-HSC, and MPP in liver and blood of Gata4$^{\Delta LSEC}$ embryos at E13.25. LT-HSC (LSK CD150^{+} CD48^{-}), ST-HSC (LSK CD150^{-} CD48^{-}) and MPP (LSK CD150^{-} CD48^{+}) (liver: n = 8; peripheral blood: n = 7 mutants and 8 controls). Representative FACS plots from at two independent experiments with more than five biological replicates. Student's *t* test: **p* < 0.05; ****p* < 0.001.

FL cells of Gata4$^{\Delta LSEC}$ embryos and littermate controls were isolated at E11.25 and single cell suspensions were examined by FACS (Figure 26 A, B). FACS blots of erythroid myeloid progenitor (EMP) marker CD45 and cKit showed a reduction of CD45^{lo} cKit^{+} and CD45^{+} cKit$^{+/-}$ populations in the FL of Gata4$^{\Delta LSEC}$ embryos (Figure 26 A). Quantification of total cell numbers of CD45^{lo} cKit^{+} and CD45^{+} cKit$^{+/-}$ cells confirmed a significant reduction in the FL of Gata4$^{\Delta LSEC}$ embryos in contrast to the increase of total cell numbers of EMPs in the peripheral blood of Gata4$^{\Delta LSEC}$ embryos (Figure 26 B). In the YS of Gata4$^{\Delta LSEC}$ embryos, the total cell numbers of CD45^{lo} cKit^{+} cells were increased whereas the cell numbers of CD45^{+} cKit$^{+/-}$ cells did not show any differences (Figure 26 B). Next, liver cells of Gata4$^{\Delta LSEC}$ embryos and littermate controls were isolated at E13.25 and analysed by FACS for indicated HSC populations (Figure 26 C, D). FACS blots of Lineage^{-} Sca-1^{+} cKit^{+} (LSK) stem cells, lt-HSC and st-HSC as well as of MPP showed a reduction in the FL of Gata4$^{\Delta LSEC}$ embryos (Figure 26 C). Quantification of the total cell number of lt-HSC, st-HSC and MPP revealed a significant decrease in the FL of Gata4$^{\Delta LSEC}$ embryos and a significant increase in the peripheral blood of Gata4$^{\Delta LSEC}$ embryos (Figure 26 D).
Thus, at E11.25 and E13.25, the FL of Gata4$^{\Delta LSEC}$ embryos displayed a strong reduction of HSPCs that were vice versa increased in the peripheral blood of Gata4$^{\Delta LSEC}$ embryos.

3.2.1.4.2. Transplantation of fetal liver HSCs

The reporter activity of the Stab2-cre f2 mouse in haematopoietic cells at E12.5 and E13.25 (section 3.1.1.2) as well as the low number of HSPCs in the FL of Gata4$^{\Delta LSEC}$ embryos at E11.25 and E13.25 (section 3.2.1.4.1) prompted us to investigate the multilineage differentiation potential from Gata4$^{\Delta LSEC}$ embryos.

FL donor cells of E13.25 Gata4$^{\Delta LSEC}$ embryos and littermate controls were harvested, sorted by FACS for LSK^{+} cells and transplanted into Rag2$^{-/-}$γc$^{-/-}$Kit$^{W/Wv}$ recipient mice [117] (Figure 27 A, B). Blood was collected from recipient mice after 4, 10 and 15 weeks and analysed for b-cells, t-cells and granulocytes. After 15 weeks, recipient blood from Gata4$^{\Delta LSEC}$ and control donor fetal cells showed formation of b-cells, t-cells and granulocytes (Figure 27 C) indicating proper lineage differentiation potential of FL haematopoietic cells from Gata4$^{\Delta LSEC}$ embryos.

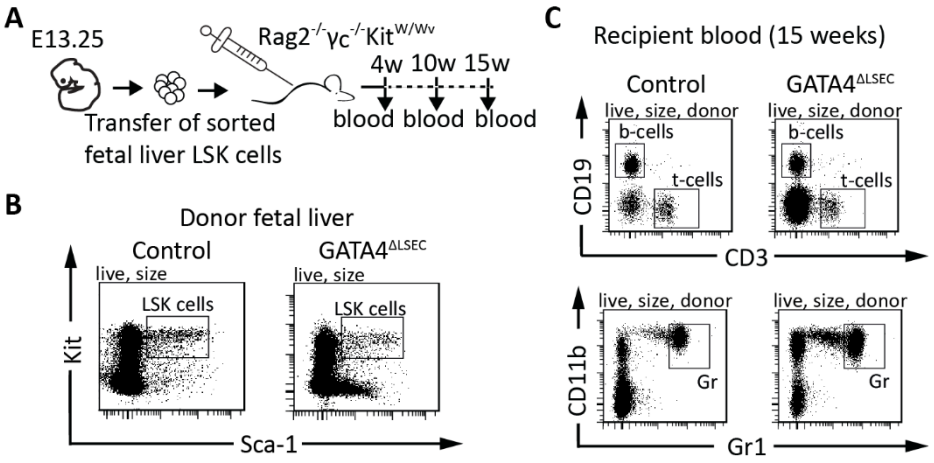

Figure 27: Analyses of lineage potential of fetal liver haematopoietic cells from Gata4$^{\Delta LSEC}$ embryos. **A – C**, Transplantation of isolated LSK cells from control and Gata4$^{\Delta LSEC}$ knockout embryos into adult immunodeficient mice. Schematic summary of the analysis: FACS sorting of FL donor LSK cells from Gata4$^{\Delta LSEC}$ (n = 3) or control (n = 5) embryos at E13.25. Cells were injected into Rag2$^{-/-}$γc$^{-/-}$Kit$^{W/Wv}$ mice and peripheral blood was analysed for donor-derived lymphoid (CD3^{+} t-cells, CD19^{+} b-cells) and myeloid (CD11b^{+} Gr1^{+} granulocytes) cells after 4, 10, and 15 weeks (**A**). FACS blots of donor FL cells are shown from control and Gata4$^{\Delta LSEC}$ embryos (**B**) as well as FACS blots of peripheral blood analysis of the corresponding recipient mouse (**C**).

3.2.1.5. Summary

Function of GATA4 for LSEC formation and development was investigated. The Stab2-cre f2 mouse was a suitable Cre driver line due to the Cre activity in fetal LSECs but not in fetal cardiac EC. The Stab2-cre driven GATA4 knockout caused an embryonic lethality and a severe liver hypoplasia. The defects of the knockout embryos were completely restricted to the FL, other developing organs, such as the heart did not show any malformations. Livers of the knockout embryos were characterised by a distorted vascular organisation, a switch from sinusoidal to continuous endothelial marker expression and a formation of a basement membrane. Moreover, we observed an increased expression of VE-Cadherin and Laminin α-4 in the GATA4 deficient FL endothelium [118]. Transcriptome profiling of the FL of Gata4$^{\Delta LSEC}$ and control embryos demonstrated that loss of GATA4 induced transcription of continuous EC-associated genes and that GATA4 protein expression promotes an LSEC-associated gene expression [118]. Finally, Gata4$^{\Delta LSEC}$ embryos showed severe haematopoietic defects which were most likely caused by migratory defects due to proper multilineage differentiation potential of the HSC from Gata4$^{\Delta LSEC}$ FLs.

4. Discussion

4.1. Genetic manipulation of liver sinusoidal endothelial cells in vivo

LSECs form the microvascular bed of the liver and secrete angiocrine factors that are critical for organ regeneration and hepatic homeostasis. The unique phenotype is represented by the lack of a continuous basement membrane and the presence of open pores. However, the investigation of LSEC specific characteristics *in vitro* is complicated due to their dedifferentiation in culture. Analysis of LSEC function *in vivo* by genetic knockout models is often compromised by an early embryonic lethality [119] or function of the protein of interest in other tissues and organs [120] and thereby preventing an LSEC specific investigation. Therefore, transgenic mouse models were generated that allow for a conditional genetic inactivation in the target cell type.
Targeted knockouts can be facilitated by the Cre/loxP system or the Tet-off/on system [121,122]. The Cre/loxP system utilises the bacteriophage derived protein Cre to fuse, invert or excise specific DNA fragments depending on the orientation of the loxP sites [56,123]. Promoter elements of interest can control the activity of *cre* in the desired cell type and further advances were achieved by fusing *cre* with sequences encoding a modified form of the oestrogen receptor ligand-binding domain (ER^{T2}) to control Cre expression by tamoxifen administration [124,125].

4.1.1. Endothelial-specific transgenic Cre driver lines

Due to the lack of LSEC specific mouse models, transgenic mouse lines with Cre activity in ECs in general have been applied. A spectrum of different mouse models has been described so far (Table 1). Promoter elements of proteins with an endothelial expression drive the Cre recombinase and induce Cre activity in a wide array of the vascular beds. The *Cdh5*, *Kdr* and *Tek* genes were used by multiple investigators to generate transgenic mouse lines and investigate LSEC specific function of the proteins of interest.
The *Cdh5* gene encodes VE-Cadherin, a component of adherens junctions that is expressed in the endothelium of adult mice and during vascular development [126]. The Cdh5-cre mouse lines were generated by Alva *et al.* [10] and Chen *et al.* [11] through fusion a 2.5 kb promoter sequence of the *Cdh5* gene with the *cre* gene. Alva *et al.* observed a reporter activity in the FL at E14.5 and in the venous and sinusoidal vessels of the adult liver [58]. Conditional deletion of the chromodomain helicase DNA-binding 4 protein [127] or the Notch1 intracellular domain [128] in LSECs resulted in an embryonic lethality due to an off-target recombination in lymphatic cells or haematopoietic cells, respectively. Chen *et al.* described a β-gal reporter activity in the FL at E10.5 and in almost all FL haematopoietic cells at E15.5 [129] which led the majority of researches to use this mouse line for investigation of protein function in HSCs of the fetal and adult mice [130–135,129] rather than in ECs [136–139].

Table 1: Published mouse lines for conditional genetic inactivation in EC

Driver gene	Mouse line	Cre activity
Acvrl1	Tg(Alk1-cre)-B1	Pan-endothelial at E10.5 and in the newborn mouse [140,141]
	Tg(Alk1-cre)-L1	Pulmonary EC and mosaic pattern in other ECs in the newborn mouse [141]
Cdh5	Tg(Cdh5-cre)7Mlia	Starting at 7.5, in ECs of the macro- and microvasculature, also in lymphatic ECs and in the adult quiescent vasculature [58]
	Tg(Cdh5-cre)1Spe	Embryonic vasculature and haematopoietic cells [129]
Kdr	Tg(Kdr-cre)15962Brei	EC of all vascular beds in the embryo [59]
	$Kdr^{tm1(cre)Sato}$	Muscle, endothelial and haematopoietic cells [142]
Pecam1	Tg(Pecam-cre)1Roml	Ubiquitous active [143]
Tek	Tg(Tek-cre)2352Rwng	ECs and blood cells from E11.5 onwards [144]
	Tg(Tek-cre)1Xyfu	EC of brain, heart and liver as well as in BM cells and splenocytes [145]
	Tg(Tek-cre)1Ywa	Pan-endothelial [57]
	Tg(Tek-cre)12Flv	ECs of brain, kidney, LNs, spleen, and thymus [146]
	Tg(Tek-cre)5326Sato	Pan-endothelial [147]
	Tg(Tek-cre)1Arnd	Pan-endothelial, haematopoietic cells [148]
	Tg(Tek-cre)#Xya	Pan-endothelial[149]
Tie1	Tg(Tie1-cre)9Ref	Pan-endothelial in embryonic and extraembryonic tissues, haematopoietic cells, subregions of the adult brain [150]

The *Kdr* gene encodes the VEGF receptor-2 which is expressed in the vascular endothelium and haematopoietic cells in the embryo upon E10 and in the adult heart, lung, kidney, brain and skeletal muscle [151]. Generation of the transgenic mouse lines was either accomplished by fusing the 939 bp 5' promoter and 2.3 kb 3' enhancer of the *Kdr* gene with the *cre* gene [59] or by creating a knock-in mouse through replacing the first exon of the *Kdr* gene with the *cre* gene [142]. Reporter activity was observed in arterial and venous ECs and sinusoidal endothelium of the FL at E11.5 [59] but no data for adult liver Cre activity was demonstrated. So far, both transgenic mouse lines have not been utilised for LSEC specific investigation.

The *Tek* gene encodes the Angiopoietin-1 receptor which is expressed in vascular ECs during embryogenesis and in the lung, heart, brain, liver and kidney of the adult mouse [152]. Several strategies were developed to generate a transgenic mouse line. First of all, a sequence encoding *cre* under the control the *Tek* promoter was introduced into the

genome [57,144,148], second, the 2.1 kb promoter and 10 kb of the first intron of the *Tek* gene drive the *cre* expression [146,147], third, the 2.1 kb promoter and a 10.5 kb fragment of exon 1 of the *Tek* gene were ligated to the *cre* [153], and last, the promoter and first intron enhancer element of the *Tek* gene drive *cre* expression [145]. Inclusion of the first intron enhancer into the targeting strategy was sufficient to drive recombination in adult vascular ECs [154]. Cre activity in fetal LSEC was demonstrated by genetic inactivation of the IκB kinase β [155] and in the adult liver endothelium by expression of the YFP reporter protein [156]. The off-target recombination in HSPCs was useful to study the function of the DNA excision repair protein ERCC-1 [157] and the signal transducer and activator of transcription 5A/B [158] in haematopoietic cells.

Off-target recombination in haematopoietic cells [128,157,158] or lymphatic cells [127] was circumvented by the generation of inducible endothelial specific transgenic mouse models. Fusing the tamoxifen-inducible *cre* either to the 2.5 kb promoter of the *Cdh5* gene [159] or to the 200.3 kb promoter sequence of the *Cdh5* gene on a bacterial artificial chromosome (BAC) clone [160] or to the open reading frame of the *Cdh5* gene on a P1-derived artificial chromosome (PAC) construct [161] generated different Cdh5-creER^{T2} transgenic mouse lines. Cre activity was induced in venous and sinusoidal EC of the liver through several tamoxifen doses and caused a specific ablation of CXCR7 in LSECs [47]. Other strategies to generate inducible endothelial-specific Cre driver lines include the fusion of the tamoxifen-inducible *cre* downstream of the 2.1 kb promoter and 10.5 kb first intron sequences of the *Tek* gene [162], the introduction of the tamoxifen-inducible *cre* into the first exon of the *Tek* gene obtained from a BAC clone [163] or the homologous recombination of the tamoxifen-inducible *cre* into the open-reading frame of the *Pdgfb* gene on a PAC construct [164]. However, Cre activity of the resulting Tek-cre/ERT2 [162,163] or Pdgfb-icre/ERT2 [164] has not been described in the hepatic microvasculature, yet.

Endothelial-specific Cre driver mice are convenient to study the function of protein in ECs during embryogenesis and have proven Cre activity in ECs of almost all vascular beds. However, the off-target recombination in haematopoietic or lymphatic cells is disadvantageous if genetic inactivation is desired in LSECs. Development of inducible endothelial Cre driver lines avoided the off-target recombination resulting from early embryonic Cre recombination that is transmitted to the descendant cells. Nevertheless, problem can occur due to the toxic effects of the tamoxifen [165], mosaic Cre activity [166] or inadequate recombination [167]. Moreover, the development of a protocol for the tamoxifen treatment can be very time consuming. Consequently, if studying LSEC function *in vivo* Cre driver mouse lines are needed with an LSEC-restricted recombination.

4.1.2.LSEC-specific transgenic Cre driver lines

LSEC-specific Cre driver lines were generated by insertion of the *cre* gene into the first exon of the *Stab2* gene or of the *Clec4g* gene on a bacmid construct resulting in the Stab2-cre or Clec4g-cre mouse line, respectively. Expression of Stab2 was observed in ECs lining the sinusoids in the liver, LN, BM, and spleen [27]. Generation of the Stab2-cre transgenic mouse yielded two viable and fertile founder lines, the Stab2-cre f2 and Stab2-cre f3 mice. Clec4g is expressed by sinusoidal ECs of liver and LN among various species [100,168] and is also found in Kupffer cells [169]. Generation of the Clec4g-cre transgenic mouse produced three viable and fertile founder lines, of which f12.5 demonstrated the most homogenous reporter expression in the hepatic endothelium during initial analysis and was chosen for further analysis.

Table 2: Cre activity of the LSEC-specific transgenic Cre driver mouse lines by YFP or LacZ reporter expression

Organ	**Cell type**	**Stab2-cre f2**	**Stab2-cre f3**	**Clec4g-cre**
Liver	microvascular EC | arterial and venous EC	+ | +	+ | +	+ | +
	other cell types	-	-	-
BM	microvascular EC | arterial and venous EC	+ | +	+ | +	- | -
	haematopoietic cells	+	-	+
LN	microvascular EC | arterial and venous EC	+ | +	+ | +	+ | +
	haematopoietic cells	+	-	+
Spleen	microvascular EC | arterial and venous EC	+ | +	+ | +	- | -
	haematopoietic cells	+	-	+
Brain	EC	+	-	-
Heart	EC	+	-	+
Intestine	EC	+	-	-
Kidney	EC	+	-	-
Lung	EC	+	-	-
Pancreas	EC	+	+	-
Skin	EC	+	-	-
Thymus	EC	+	+	-
FL, E13.5	microvascular EC | arterial and venous EC	+ | +	- | -	- | -
	haematopoietic cells	+	-	+

The Stab2-cre f2 mouse line targets LSECs in the adult and fetal liver. Cre activity was further observed in microvascular ECs of the LN, spleen and BM (summarized in Table 2). Moreover, Cre recombination was detected in ECs of all analysed organs and was identified in subsets of haematopoietic cells in the blood, BM, spleen, thymus, and the FL.

Cre activity in adult liver EC was utilised to investigate function of the protein wntless homolog (Wls) on metabolic zonation [170]. Transcripts of Wls were 12.5-fold reduced in isolated liver ECs causing an altered liver to body weight ratio, loss of pericentral as well as expansion of periportal gene expression. Homogenous endothelial Cre activity in the Stab2-cre f2 mouse shows a clear benefit towards the inducible endothelial specific transgenic mouse models due to the mosaic genetic inactivation of Wls by Cdh5-cre/ERT2 [171]. Next, BMP2 was abolished from the hepatic endothelium by using the Stab2-cre f2 mouse [172]. Levels of BMP2 mRNA were strongly decreased in the liver leading to a massive hepatic iron overload and in the peripheral blood. Finally, selective genetic inactivation of GATA4 in FL EC enabled the investigation of the LSEC differentiation *in vivo* [118] and avoided the embryonic lethality derived from cardiac defects when using the Tek-cre mouse [77]. Here, the intersection of Stab2-cre f2 driven recombination and GATA4 expression in LSECs allowed for the analysis of the effect of LSEC capillarization on liver organogenesis. Notably, Cre activity of the Stab2-cre f2 mouse in LSEC but not in cardiac EC during fetal development offers an advantage towards conditional endothelial Cre driver. Moreover, deletion of Wls and BMP2 in liver EC demonstrated homogenous Cre activity. However, off-target recombination in haematopoietic cells during embryogenesis and adulthood must kept in mind when using the Stab2-cre f2 mouse.

The Stab2-cre f3 mouse line is a useful mouse model to target LSECs. Additionally, Cre activity was detected in microvascular EC of the LN, spleen and BM (summarized in Table 2). Moreover, Cre recombination was detected in ECs of BM, liver, LN, spleen, pancreas, and thymus which make this mouse line a useful tool to investigate organ-specific endothelial functions. Compared to conditional endothelial-specific Cre mouse lines, the Stab2-cre f3 has the advantage that haematopoietic cells are not targeted in knockout studies. However, it has to be noted that the onset of Cre activity could not be determined in my experiments and that recombination is not as homogenous in the liver as for the Stab2-cre f2 mouse. In comparison to the Stab2-cre f2 mouse, the Cre activity of the Stab2-cre f3 mouse resembles more closely the endogenous protein expression of Stab2. Differences in the Cre activity of founder lines were also observed for other transgenic Cre mice. The generation of the *Prph*-cre mouse produced four founder lines [173] and the differences between the transgene expression and endogenous protein expression derived either from the site of chromosomal insertion or local genomic effects on transgene expression [174]. Higher copy number of the transgene could also cause differences between the founder lines or between transgene expression and endogenous protein expression. This was observed for the generation of the *Myh11*-cre [175] and the *Prox1*-cre [176] mice. Notably, the lowest numbers of transgene copies resulted in the most uniform reporter expression and higher copy number disturbed the transgene transcription most likely because of repeat-induced silencing of the transgene [176]. Generation of transgenic mice with the help of BAC clones has the advantage that endogenous gene expression patterns are rather reflected due to the amount of genomic information that is transferred to the recipient genome [177] and the size of the BAC clone does not affect the transgenic efficiency. The more ectopic expression of the Stab2-cre f2 transgene compared with the Stab2-cre f3 transgene is therefore either a result of different transgene copy numbers or the integration into a more open chromatin region.

The Clec4g-cre mouse line drives the Cre expression in LSECs. Cre activity was further identified in microvascular EC of the LN (summarized in Table 2) which makes this mouse line particularly advantageous in comparison to the Stab2-cre f2 mouse and Stab2-cre f3 mouse in which Cre expression was also detected in sinusoidal EC of the spleen and the BM. In addition to that, Cre activity was observed in macrovascular EC of liver and LN as well as in the heart. This has to be kept in mind when studying proteins with a similar expression pattern like GATA4. Interestingly, Kupffer cells were not targeted by the Clec4g-cre mouse line but distinct subpopulations of myeloid cells in the BM, lung, pancreas, skin, and spleen displayed a reporter protein expression. Currently, there is no data available describing the CLEC4G protein expression in the mouse but gene expression data demonstrate transcript levels in liver, testis, spleen, and lung [104] which are in line with the observed reporter activity in those organs. Unfortunately, information regarding the cell type of expression is not available from this database [104]. In human, CLEC4G is expressed by sinusoidal EC of liver and LN [100,101], in Kupffer cells [169] as well as in peripheral blood and in monocyte-derived macrophages and dendritic cells [178]. Here, protein expression in human is only partly consistent with the transgene activity in the mouse which could be explained by different expression pattern across species. For example, porcine transcripts of CLEC4G were detected in the liver, LN and spleen [168] although expression of CLEC4G in the spleen was neither described in human nor in mouse [104].

4.1.3.Conclusion

The Stab2-cre f2, Stab2-cre f3 and Clec4gCre mouse lines target the microvascular capillaries of the liver. All three transgenic mouse lines demonstrated Cre activity in the arterial and venous EC but neither were hepatocytes, Kupffer cells nor stellate cells targeted. Analogous to the expression pattern of the promoter gene, Cre activity was observed in sinusoidal EC of other organs. Reporter expression occurred in a varying degree in EC of other vascular beds which is either a result of the transgene integration into the genome or a result of a recombination event early during development causing all progeny cells to express the reporter.

Transgenic mouse models have been developed to target selectively organ-specific ECs in organs apart from the liver. In contrast to the sinusoidal endothelium of the liver, the brain microvasculature constitutes a physical barrier that strictly regulates the entry of nutrients and substances into the brain. Due to its relevance for pharmacotherapy [179] or during neurological disorders [180] and because of the difficulties to model the blood-brain barrier *in vitro* [181] many researches aimed to target specifically brain ECs by the Cre/loxP system. Two promising mouse models were developed in the past that achieve a degree of brain endothelial specificity. The Tg(Sftpa1-cre)1Xya mouse line in which Cre expression is controlled by the surfactant protein A demonstrated Cre activity in blood vessels of brain, in distinct alveolar cells and epithelial cells of stomach [182]. Selective genetic inactivation of the mothers against decapentaplegic homolog 4 protein in brain ECs [183] and lineage tracing of cerebrovascular ECs [184] established this mouse lines as a useful tool for targeting the blood-brain barrier. Additionally the off-target recombination in the gastric

epithelium allowed for the investigation of the PTEN/Akt signalling during gastric tumorigenesis [185]. Second, the Tg(Slco1c1-icre/ERT2)1Mrks mouse line in which Cre activity is under the solute carrier organic anion transporter 1c1 promoter and is induced by tamoxifen [186]. Recombination in brain ECs allowed the investigation of fever responses [186–188] or amyloid β clearance during Alzheimer's disease [189].

4.1.4.Perspectives

Although the Cre/loxP system provides a powerful tool to study function of proteins or to track cell fate decision *in vivo*, a disadvantage of this technique is that it cannot be applied for the use in humans. Therefore, genetic tools were developed that can be translated into the clinics. Modification of gene expression in LSECs can be beneficial during endothelial dysfunction in hepatic cirrhosis [190,191] or in order to target the tumour endothelium during HCC progression [192,193]

Viral vectors were engineered to modify gene expression in the target cells. The efficient transduction of genes into the genomes without transferring viral proteins have proven them useful and safe [194]. Retroviral and lentiviral vectors as well as the recombinant adeno-associated virus, recombinant simian virus 40 and recombinant adenovirus are commonly used as viral tools [194]. The high endocytic capacity of LSECs is suitable but in order to avoid viral tropism, surface receptors on the target cells were used to direct viral transduction. The specific transduction of LSEC in mouse and human by a modified lentivirus has been investigated by Abel *et al.* [195]. Endoglin on LSECs was targeted by single-chain variable fragment fused to the measles virus haemagglutinin envelope protein. Systemic administration of the mouse Endoglin-specific lentiviral vector transduced 98% of all liver ECs, only a small fraction was found in F4/80$^+$ Kupffer cells. The human counterpart of the Endoglin-specific lentiviral vector was shown to specifically infect human LSECs while leaving murine LSECs unaffected.

Beyond viral approaches, other methods have been employed to manipulate gene expression in LSECs, which include transfection of DNA, RNA interference via small interfering RNA (siRNA) or clustered regularly interspaced short palindromic repeats (CRISPR)/CRISPR-associated protein 9 (Cas9) system. Nonviral transfer of nucleic acids into LSECs is either facilitated by lipid-based drug carrier systems [196] or by hydrodynamic injections [197]. With the help of hydrodynamic injections, "naked" DNA is injected into the tail vein and arrives in the liver via the CV which often led to a disruption of the sinusoids and enlargement of the fenestrae in the pericentral region [198]. This makes this method more applicable for drug delivery into hepatocytes than into LSECs. On the other hand, LSEC are not quite susceptible for the interaction or uptake of liposomes [196]. Therefore, modifications of the liposomal surface with substrates that are taken up by scavenger receptors are advantageous. Kamps *et al.* increased the liver uptake 17-fold by coupling the poly-aconitylated human serum albumin to liposomes without affected the spleen [199]. The liposomes are mainly taken up by LSECs and Kupffer cells dependent on the liposomal size. Marquez *et al.* developed chondroitin sulphate functionalized nanoparticles [200]. Incorporation of plasmid encoding for EGFP into the nanoparticles demonstrated a delivery into LSECs via Stab2 mediated endocytosis but not into Kupffer cells.

Recent advances in the field of genetic modification and editing were achieved through the discovery and engineering of the CRISPR/Cas9 system. In brief, this technique consists of the single guide RNA that directs the Cas9 encoded RNA-guided nuclease to a target sequence in order to induce a double strand break [201]. During the following DNA repair the homologous recombination in conjunction with an exogenous template DNA can insert foreign genetic material into the host genome or the nonhomologous end joining induces a frameshift mutation leading to a gene knockout. The usefulness for liver specific gene modification was demonstrated by few studies [202–205]. Although, the focus of these researches was on hepatocytes, these strategies could also be applied towards LSECs.

4.2. Differentiation of liver sinusoidal endothelial cells

The TF GATA4 was identified by our group in a set of TFs to be required for the LSEC specific differentiation programme *in vitro* [24]. As LSECs are difficult to manipulate *in vitro* and because *in vivo* studies of GATA4 demonstrated an indispensable role during heart development [75–78,86,206,207], investigation of GATA4 function in LSECs required a cell-type specific inactivation. We therefore screened Cre expressing transgenic mouse lines for suitability to induce an LSEC restricted knockout and mated this mouse with mice homozygous for the $Gata4^{loxP}$ allele to generate a conditional knockout mouse.

Expression of GATA4 in fetal LSECs was confirmed and the Stab2-cre f2 mouse line was applied to generate the LSEC restricted GATA4 inactivation ($Gata4^{\Delta LSEC}$) that resulted in an embryonic lethality and liver-restricted growth arrest as well as an endothelial dysplasia. Expression of GATA4 was lost in 90% of the FL ECs in $Gata4^{\Delta LSEC}$ knockout embryos. Upon GATA4 deficiency, the FL sinusoids underwent a phenotypical shift that was characterised by an adoption of continuous endothelial marker profile, formation a basement membrane and increase of perisinusoidal ECM. As a result, the capillarized FL endothelium prevented the seeding of embryonic haematopoietic progenitor and stem cells into the FL and caused a lethal anaemia.

4.2.1. Liver sinusoidal endothelial-derived GATA4 is vital for fetal liver growth

The conditional inactivation of GATA4 by the Stab2-cre f2 mouse resulted in a reduced FL size and embryonic lethality. Although GATA4 transcripts were observed in the adult liver [73,208], here, expression of GATA4 was demonstrated in fetal LSECs as early as E10.5. In order to study function of GATA4 on LSEC differentiation a proper selection of a suitable Cre driver line was important due to reported lethal phenotypes [75–77]. The Stab2-cre f2 mouse displayed the required reporter activity in LSECs but also in FL haematopoietic cells as well as in ECs of AGM region, brain, midgut, somites. Off-target effects due to an overlap of the Cre activity and GATA4 expression were excluded because, first, the described role of GATA4 in FL haematopoietic cells did not represent endogenous protein expression [209–211], second, function of GATA4 in somites or AGM region has not been described, yet, and, third, expression of GATA4 in the brain [212] or intestine [213] was only reported for non-endothelial compartments. Consequently, the only overlap of GATA4 expression and Cre activity of the Stab2-cre mouse occurs in the FL sinusoidal endothelium.

Loss of GATA4 in fetal LSEC upon E10.5 affects the expansion of the FL immediately. The liver primordium is formed around E9.5 and expands rapidly in the subsequent period [60]. GATA4 was reported to play a role for the growth of the FL either as a transcriptional regulator in mesenchymal cells originating from the STM before E9.0 [62], by compensating the loss of GATA6 [214] or through the interaction with FOG-2 [78]. Cre activity of the Stab2-cre f2 mouse in mesenchymal cells has not been observed and the compensatory function of GATA4 and GATA6 is lost after E9.5 [214]. FOG-2 is a transcriptional regulator of GATA4 [215] and genetic inactivation of FOG-2 caused an embryonic lethality due to multiple cardiac

abnormalities with secondary defects in lung and liver development [216]. Expression of FOG-2 in livers of Gata4$^{\Delta LSEC}$ embryos has not been investigated and an endothelial function of FOG-2 has not been published, yet. Therefore, a possible role of FOG-2 on the liver hypoplasia of the Gata4$^{\Delta LSEC}$ embryos cannot be excluded.

4.2.2. GATA4 is required for sinusoidal differentiation of the fetal liver microvasculature

Reduction of GATA4^{+} nuclei in Stab2-expressing fetal LSECs of Gata4$^{\Delta LSEC}$ embryos were clearly seen as early as E10.5. Before E10.5, the FL is characterised by a simple sinusoidal vascular network with high expression of CD31 that is progressively lost during development and by low expression of sinusoidal marker that gradually increase during hepatic maturation [28–30]. Loss of GATA4 expression during this period prevents the differentiation from the primitive FL vasculature towards sinusoidal microvascular ECs. Factors that drive sinusoidal differentiation and specification were described for the adult liver. Rspo-3 is an angiocrine factors which is secreted by EC from the CV and was essential for establishment and maintenance of liver zonation [70]. Hepatocyte growth factor (HGF) is secreted by LSECs and stimulated liver regeneration in a model of partial hepatectomy [217]. LSEC-derived Wnt-2 promoted LSEC proliferation and induced VEGF receptor-2 signalling in cultivated LSECs [51]. Moreover, Wnt-2 was identified in a comparative gene expression profiling to be specific for the LSEC differentiation programme *in vitro* [24]. Similar to Wnt-2, BMP2 was specifically expressed in LSECs compared to LMECs and was lost during dedifferentiation *ex vivo* [24]. Conditional genetic inactivation of the angiokines by Stab2-cre f2 did not results in dedifferentiation of the FL sinusoids or defects in liver development [118] indicating that LSEC-derived Rspo-3, HGF, Wnt-2, and BMP2 do not participate significantly in liver development.

Similar to GATA4, hypoxia-inducible transcription factor 1 subunit β (Hif-1β) was essential for liver organogenesis [218]. Loss of function in ECs caused partial an embryonic lethality during late-gestation with a distorted hepatic vascular architecture, severe hypoglycaemia and downregulation of genes involved in gluconeogenesis. Less than 10% of knockout mice survived until adulthood and suffered from weight loss as well as they developed a hepatic portal arteriolar hyperplasia and a portal fibrosis with collagen and iron deposition. In contrast to GATA4 that regulated sinusoidal differentiation during early stage of liver development leading to an embryonic lethality at mid-gestation, endothelial-derived Hif-1β was essential for maintenance of the mature liver microvasculature with secondary defects in glucose metabolism. Additional factors known to be involved sinusoidal specification are TF Rbpj which mediates all canonical Notch signalling [219]. Notch signalling from hepatic EC regulated sinusoidal diameter and controlled vascular shunting in the newborn and adult mice. Disruption of Rbpj transcriptional activity caused liver endothelial malformations most likely through VEGF receptor-3 dysfunction and is further aggravated by an aberrant ephrin-B2 signalling. Liver X receptor α was shown to be involved in LSECs capillarization in a model of CCl_4-induced fibrosis [220]. LSEC capillarization was regulated through Hedgehog signalling *in vitro* and *in vivo* and was further diminished by liver X receptor α agonist treatment. Although these signalling

pathways were critical during specification and maintenance of the mature hepatic microvasculature, GATA4 possess superordinate functions during liver sinusoidal development which were elaborated here.

4.2.3. Loss of liver endothelial-GATA4 induces a hepatic fibrosis in the embryo

The capillarization of the FL endothelium contributes to the increase of ECM. Similar to the FL of Gata4$^{\Delta LSEC}$ embryos, Delgado *et al.* observed a FL fibrosis by inactivating GATA4 in STM derived cells [80]. The utilised G2-Cre mouse recombined in hepatic mesothelial, stellate and ECs [80] in contrast to the Stab2-cre f2 mouse which inactivated GATA4 in FL EC. Comparison of both mice, Gata4$^{\Delta LSEC}$ and G2-Cre;GATA4, indicates that the increase of ECM derives either from the GATA4-deificent endothelium or from an impaired hepatic vascular niche. In ECs GATA4 could repress the synthesis of pro-collagens or activate the transcription of matrix metalloproteinases which would lead to an increase of collagen or a decrease of matrix metalloproteinases activity in the Gata4$^{\Delta LSEC}$ embryo, respectively. Indeed, binding sites of GATA4 were found in regulatory elements of the human COL1A2 gene. Binding of GATA4 to the promoter sequence was demonstrated to inhibit the expression of collagen α-2(I) chain [221,222]. Another possible explanation is that the capillarized endothelium attracts myofibroblasts similar to the adult liver fibrosis [223]. In response to VEGF, LSEC derived nitric oxide contributed to the activation of stellate cells [54], however, no expression of endothelial nitric oxide synthase was observed in the FL [224,225]. But it was shown that LX2 stellate cells preferred adhesion on Laminin α-4 which was increased in the FL of Gata4$^{\Delta LSEC}$ embryos [118]. The contribution of other LSEC-derived angiokines should be taken into consideration. Endothelial derived Kruppel-like factor 2 had an impact on liver regeneration [226] and contributed to stellate cell deactivation [227] and the transforming growth factor β acted in a pro-fibrotic manner and led to the transdifferentiation of hepatic stellate cells into myofibroblasts [228].

4.2.4. Proper sinusoidal differentiation is required for fetal liver haematopoiesis

HSPCs in FLs of Gata4$^{\Delta LSEC}$ embryos were functionally potent but demonstrated an inability to generate sufficient amounts of progeny in the FL. During fetal haematopoiesis HPCs are generated in the AGM region and migrate around E11 into the FL in order to proliferate and differentiate [66]. HPCs accumulation in the fetal blood and the increase of VE-Cadherin in the FL endothelium indicates that the capillarization in livers of Gata4$^{\Delta LSEC}$ embryos prevented seeding of HSPCs into the FL. It was demonstrated by Dartsch *et al.* that an increased tightness of the FL endothelium impaired the immigration of HPCs into the FL as well [69]. The covalent linking of VE-Cadherin to α-Catenin caused a liver hypoplasia and an increase of HPCs in the blood despite their potential to differentiate into the myeloid lineage. This indicates that a proper endothelial phenotype is needed for seeding of HPCs into the FL. Rantakari *et al.* observed an impaired exit of differentiated monocytes into the

fetal blood due to the lack of diaphragms in fetal LSECs [229]. Here, the authors argued that the PLVAP+ diaphragm in fetal LSECs provided a surface to interact with chemokines or monocytes. These studies show that the discontinuity and proper fenestrations of LSECs are crucial for seeding and exit of haematopoiesis cells. Additionally, Kajikhina *et al.* provided evidence that cytokines from FL EC contributed to the homing and lineage differentiation of progenitor cells [230]. The authors showed that LYVE1^{high} ECs and CD166^{high} mesenchymal cells produced cytokines for the transendothelial migration of progenitor cells into the liver emphasizing by that the role of the vascular niche on FL haematopoiesis.

4.2.5.Conclusion

The results presented here provide insight into the function of GATA4 in LSECs. Sinusoidal differentiation from the primitive hepatic capillaries was dependent on the transcriptional activity of GATA4. Loss of sinusoidal differentiation impaired seeding of HPSCs and prevented growth of the FL. The contribution of GATA4 co-factors, such as FOG-2, on sinusoidal differentiation remains elusive. There are still open questions on how GATA4 regulates sinusoidal differentiation maybe through activation of signalling pathway like the Erbb3-Erk pathway in cardiac-derived ECs [77] or by regulating the transcription of angiocrine factors.

Similar to GATA4, other TFs are known to drive cell fate decision of ECs during fetal development. The TF PROX-1 is a well-studied master regulator for specifying the lymphatic EC fate. Mice that were deficient for PROX-1 die during embryogenesis with severe defects of lymphangiogenesis and an inability to generate lymphatic ECs [231,232]. Overexpression of PROX-1 in blood vascular ECs induced typical marker for the adult lymphatic vasculature and, vice versa, repressed marker for vascular ECs [233,234]. The Notch pathway regulates the arterial cell fate decision through signalling between adjacent cells [235]. In the zebrafish, notch1 expression regulates the zebrafish orthologue Hey2 which induces the arterial marker ephrin-B2 and represses the venous marker EphB4 receptor [236,237] and in mice Notch ligand delta like ligand-4 controlled the arterial specification in a dosage dependent manner [238]. Conversely, the TF COUP-TF 2 was shown to regulate the venous identity by upregulating arterial marker and downregulating of venous marker [239].

4.2.6.Perspectives

Similar to GATA4, LIM-domain-only (Lmo) protein 3, TF EC (Tfec) and c-Maf were identified to be induced upon LSEC dedifferentiation and to be preferentially expressed in LSECs when comparing to lung microvascular ECs [24].

Lmo proteins act as scaffolding proteins in order to regulate transcription and Lmo3 was primarily associated with oncogenic functions during neurological disorders [240]. In LSECs, Lmo3 counter-regulated the GATA4-mediated activation of autocrine BMP2 signalling presumably via the BMPR1-SMAD1 axis and without affecting the GATA4 induced transcriptional programme [241]. Since Lmo3 knockout mice survived until adulthood and displayed no phenotypical abnormalities in the brain [242], functional implication on LSECs during challenging conditions like liver metastasis remains to be investigated.

Tfec acts as a transcriptional inhibitor and is transcribed at low levels during fetal development and in the adult liver as well as at high levels in the spleen, lung and kidney [243]. Although Tfec mutant mice did not show any gross abnormalities [244], the related TF Tfeb is involved in the extraembryonic vascularization by regulating VEGF expression in the placenta [245]. In the zebrafish, tfec is expressed in ECs of the CHT and regulated the secretion of cytokines from ECs and promoted directly HSC expansion in the CHT [246].

C-Maf belongs to a family of proto-oncogenes and demonstrated versatile functions by being involved in the development of the skin [247], of the cartilage [248] and eye [249,250]. The genetic inactivation of c-maf produced different phenotypes as either a viable knockout mouse was generated with a reduced cell size in the kidney and liver [251] or an embryonic lethality was observed with a liver hypoplasia and defects in FL erythropoiesis [252]. Here, the different genetic backgrounds of the mice resulted in different phenotypes since either Balb/c mice [251] or C57BL/6J mice on a 129/Sv background [252] were used for the experiments. Although the defective FL erythropoiesis of the c-maf knockout embryos emerged from a defect of the adhesive function of the macrophages [252] it would be quite intriguing to investigate c-maf function in LSECs.

5. Material and methods

5.1. Methods

5.1.1. Animal experiments

5.1.1.1. Generation of Stab2-cre and Clec4g-cre transgenic mouse lines

A BAC encoding the genomic *Stab2* (RPCIB731O23129Q) or *Clec4g* locus (RPCIB731A07239Q) was obtained from SourceBioscience. A cDNA containing a codon improved version of cre recombinase [253] followed by polyA signal sequence was fused into exon 1 of *Stab2* (Figure 28) or *Clec4g* via homologous recombination [254]. In frame recombination into *Stab2* or *Clec4g* was realized via PCR added homologous arms of 45 bp in length flanking the 5' and 3' region of the start codon. Correct *Stab2*-cre or *Clec4g*-cre recombinant BAC were confirmed by sequencing and linearized, purified with Sepharose CL4B (GE Life Science), and injected into the pronuclei of fertilized C57Bl/6NCRL oocytes. Three B6.Stab2$^{tg1.1\text{-}3cre}$ transgenic founder mice (f1, 2 and 3) or B6.Clec4G$^{tg1.1\text{-}3cre}$ transgenic founder mice (f12.5, 18.3 and 20.1) were identified by PCR.

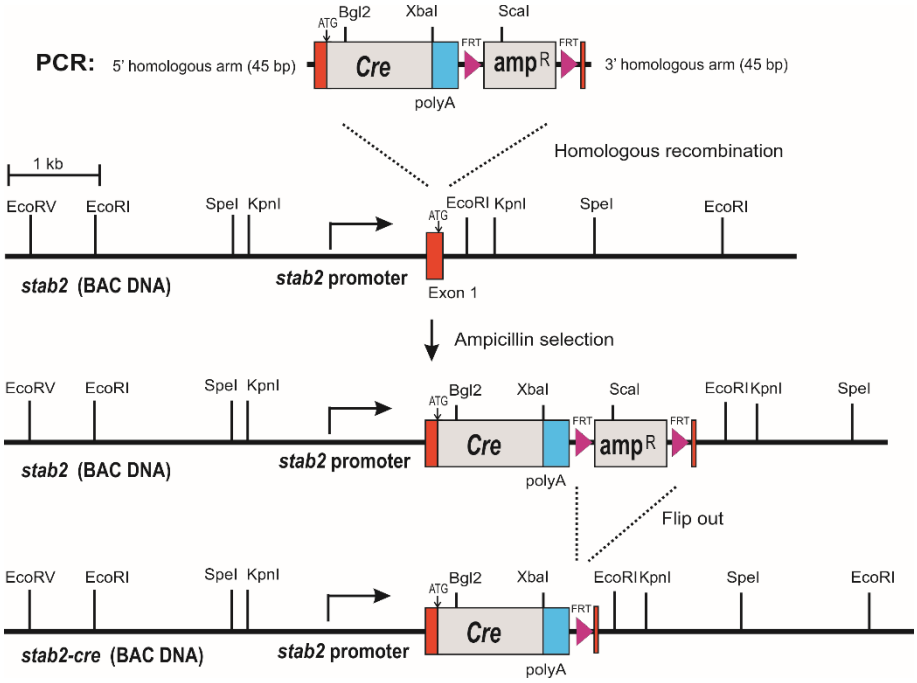

Figure 28 : Generation of the Stab2-cre transgenic construct.
The cDNA of the Cre recombinase was amplified by PCR and inserted into the exon 1 of *Stab2* on a bacmid by homologous recombination. Positive clones were selected by ampicillin resistance; flip mediated recombination of the ampicillin cassette generated the final Stab2-cre transgenic construct.

5.1.1.2. Animal housing and breeding

Animals were housed in a temperature- and humidity-controlled room with a 12 h/12 h light/dark cycle (lights on 6 am - 6 pm) and had access to food and water *ad libitum*. All animal experiments were approved by the Medical Ethics Committee II of the Medical Faculty Mannheim of the University of Heidelberg and filed with local authorities (Regierungspräsidium Karlsruhe). This research was performed on a mixed C57BL/6 and 129/Sv background.
Cre driver strains (Stab2-cre, Clec4g-cre) were characterized by R26LacZ [Gt(ROSA)26Sor^{tm1Sor}] reporter mouse [92] or R26YFP [Gt(ROSA)26Sor$^{tm1(EYFP)Cos}$] reporter mouse [93]. Homozygous floxed reporter mouse was bred with cre driver mouse resulting in the following cre;reporter mouse strains: f2;LacZ, f3;LacZ, f2;YFP, f3;YFP, and f12.5;YFP. The offspring of the F1 generation was analysed during embryogenesis or at the age of two month to one year.
Conditional deletion of GATA4 was achieved by breeding homozygous floxed *Gata4* mouse (Gata4$^{tm1.1Sad}$) [79] with cre driver mouse resulting in a heterozygous GATA4 knockout F1 generation. Mice from the F1 generation were bred with homozygous floxed *Gata4* mouse resulting in the Gata4$^{\Delta LSEC}$ knockout.
Triple mutant mice resulted from breeding homozygous floxed *Gata4*;YFP mouse with heterozygous GATA4 knockout F1 generation. The F2 generation was Stab2-cre driven GATA4 deficient and displayed reporter YFP expression (Gata4$^{\Delta LSEC}$;YFP).

5.1.1.3. Dissection of adult organs, embryos and fetal organs

Mice were killed by cervical dislocation and the organs of interests were dissected.
Aged-matched embryos were generated by timed mating. Females of at least 12 weeks were mated with males of at least 10 weeks. Two to three females were placed into the cage of the male over night, the noon of the day of the vaginal plug was considered as E0.5. Pregnant mice were sacrificed by cervical dislocation, tissues belonging to the mother, such as womb and fat, were removed. Then the placenta was removed, the yolk sac was cut gently and separated from embryo proper by tearing off the umbilical and vitelline vessels. Dissection was carried out under a transmitted light base microscope and YS were collected for genotyping.
For dissection of fetal heart and liver, embryos were placed in ice cold phosphate buffered saline (PBS) under a transmitted light base microscope and head was cut away. The chest and rip cage were opened and heart was dissected. The liver was identified as the largest peritoneal organ with its characteristic colour and shape. It was dissected by opening the fetal body laterally, removing the liver and eliminating gastrointestinal anlagen.

5.1.1.4. Transplantation

Experiments were performed in cooperation with the AG Rodewaldt from German Cancer Research Centre (Heidelberg).

FLs were mechanically dissociated and passed through a 100 µm cell strainer (BD). After incubation with purified mouse IgG (500 µg/ml, Jackson ImmunoResearch Laboratories) in 5% FCS/PBS the cells were stained with commercial antibodies in 5% FCS/PBS on ice for 30 min. LSK cells were isolated by electronic deposition into individual wells of a U-bottom 96-well plate containing 100 µl sterile 50% FCS using a FACS AriaIII (BD). The number of sorted cells ranged between 150 and 850 cells. Prior to injection, 100 µl sterile PBS was added to each well, and cells were injected intravenously into individual $Rag2^{-/-};\gamma_c^{-/-};Kit^{W/Wv}$ recipients [117]. Peripheral blood samples were collected 4, 10 and 15 weeks after transplantation from the submandibular vein into EDTA-containing microtubes (Sarstedt) to screen for progeny of donor cells (detected by the congenic marker CD45.1). Red blood cell lysis was performed by using RBC Lysis Buffer (BioLegend) to enrich for white blood cells. For FACS staining, the following antibodies were used: CD3e eFluor780 (clone 17A2, # 47-0032-80, eBioscience), CD11b PE-Cy7 (clone M1/70, # 25-0112, eBioscience), CD45.2 PE (clone 104, #12-0454, eBioscience), CD45.1-FITC (clone A20-1.7, #561871, BD), Gr-1 APC (RB6-8C5, # 553129, BD), CD19 QDot605 (clone 6D9, #Q10379, Invitrogen).

5.1.2. Histological techniques

5.1.2.1. Paraformaldehyde perfusion and pre-treatment

In order to analyse the fluorescent reporter protein of the cre;reporter mouse strains or triple mutant mice, adult animals were perfused or embryos were pre-fixed. For the adults, mice were anesthetized by intra-peritoneal injection of Ketamine/Xylazine anaesthesia with a dosage of 0.1 ml per 10 g of body weight. As soon as the mice were unresponsive, the abdomen was opened until the diaphragm was exposed. The diaphragm was cut through and the thoracic cavity was opened by cutting the ribs away. A 25 G butterfly needle was inserted into the left cardiac chamber and the animal was flushed with PBS at 1 ml per min. When blood has been cleared from body (after 10 -15 min), the perfusion switched from PBS to 4% paraformaldehyde (PFA) and the mice were perfused at 2 ml per min for 20 – 25 min. The perfusion was stopped; the organs of interest were excised and immersion-fixed over night at 4 °C. For the foetus, age-matched embryos were harvested as described, rinsed in PBS and fixed in 4% PFA over night at 4 °C.

5.1.2.2. Decalcification of tibia and femur

Bones were collected after perfusion and fixed in 4% PFA over night as described. The following day, bones were washed with PBS and decalcified in 10% EDTA / PBS at 4 °C on a tube roller up to two weeks while changing EDTA solution every three days.

5.1.2.3. Cryo-protection, -embedding and -sectioning

Pre-fixed organs and embryos were washed three times in PBS and cryoprotected in 30% sucrose over night at 4 °C. Next day, organs were placed in cryomolds, embedded within optimal cutting temperature (OCT) compound, slowly frozen in the gas phase of liquid nitrogen until the OCT becomes solid and finally frozen in liquid nitrogen for several minutes. Non-prefixed organs and embryos were embedded in OCT equally. Tissue was stored at -80 °C, transferred to the cryotome on dry ice and sections of 8 µm were melted on adhesion microscope slides.

5.1.2.4. Paraffin embedding and -sectioning

PFA fixed tissue was put into embedding cassettes dehydrated through a series of increasing concentration of ethanol and cleared in xylene. Paraffin wax infiltrated the tissue at 60 °C and the tissue was embedded into paraffin blocks. 1- 5 µm sections were cut at a microtome, flattened out in a water bath and melted on adhesion microscope slides.

5.1.3.Staining procedures

5.1.3.1. Beta-galactosidase assay

The f2;LacZ and f3;LacZ embryos ranging from E9.5 to E10.5 were assessed for whole mount β-galactosidase staining. For this purpose, freshly dissected f2;LacZ and f3;LacZ embryos were rinsed in ice cold PBS and incubated in β-galactosidase staining solution at 37 °C over night on a falcon tube roller to ensure even distribution of the staining solution. Next day, embryos were washed with PBS and photographed with a transmitted light base microscope.

5.1.3.2. Immunofluorescent staining procedures

Cryosections from non-prefixed organs were dried one hour, fixed in acetone or in 4% PFA (for nuclei staining) for 10 min at RT, rinsed in PBS and permeabilized in 0.1% PBS + Triton X-100 for 3 min in case of nuclei staining. Autofluorescence was quenched with 50 mM NH_4Cl for 15 min and epitopes were blocked with 10% FCS/ PBS for 60min. The incubation with a biotinylated primary antibody required an avidin/biotin block. For this purpose, sections were incubated with avidin solution for 15 min after regular blocking, rinsed with PBS and incubated then with biotin solution for another 15 min. Sections were then treated with first antibody over night at 4 °C, washed three times with PBS and secondary antibody was applied. Primary and secondary antibodies were diluted in 0.01% FCS/PBS and incubated in a humidity chamber. Finally, sections were washed three times with PBS, once with dH2O and mounted with fluorescent mounting medium.

Cryosections from PFA prefixed tissue were treated as follows. Epitopes were blocked in immunofluorescent block buffer for 60 min and first antibody was incubated over night at 4 °C. After three washing steps, secondary antibody was applied for 45 min. Primary and secondary antibodies were diluted in 20% immunofluorescent block buffer/ PBS and incubated in a humidity chamber. Sections were washed three times with PBS, once with dH2O and mounted in fluorescence mounting medium. Fluorescent specimens were imaged with a multi-photon laser scanning microscope or confocal laser scanning microscope.

5.1.3.3. Immunohistochemical staining procedures

Cryosections were dried one hour, fixed in acetone for 10 min at RT and rinsed in PBS. Endogenous peroxidase activity was blocked with peroxidase block for 10 min and epitopes were blocked with 10% FCS/ PBS for 60 min. After incubation with first antibody over night at 4 °C, sections were washed three times with PBS and secondary antibody was applied Primary and secondary antibodies were diluted in 0.01% FCS and incubated in a humidity chamber. Sections were then incubated in AEC substrate until desired signal intensity was produced (5 to 20 min depending on the tissue and antibody) and counterstained with Mayer's Haematoxylin. Finally, sections were washed three times with PBS, once with dH2O and mounted with aqueous mounting medium. Images were captured with an upright microscope Eclipse Ci-E or an upright motorized microscope Eclipse Ni-E.

5.1.3.4. Histological staining

H&E and Sirius Red staining was carried out on paraffin sections according to routine protocols in the local pathology department.

5.1.3.5. Electron microscopy

Experiments were carried out in cooperation with the electron microscopy core facility (K. Richter) from German Cancer Research Centre (Heidelberg). FLs from embryos were dissected and immediately immersed in fresh fixative for epoxy-embedding for several hours. Post-fixation in buffered 1% osmium tetroxide, dehydration, and resin-embedding were carried out according to standard protocols at the core facility. Ultrathin sections (60 nm) were contrast-stained with lead citrate and uranyl acetate and observed in an electron microscope at 100 kV. Micrographs were taken with image-plates, scanned at 30 µm resolution (Ditabis).

5.1.4. Cell isolation procedures

5.1.4.1. Isolation of peripheral blood mononuclear cells

Mice were anesthetized with 5% isoflurane and 400 ml/min oxygen flow rate. Blood was sampled from the retrobulbar venous plexus with a 20 µl micropipette into Lithium Heparin microvettes. Blood was diluted in an equal volume with PBS and was added slowly on top of 2 ml of Biocoll solution and centrifuged for 20 min at 300 x g at room temperature (RT). The intermediate cloudy phase was transferred into a new tube and washed once with PBS.

5.1.4.2. Isolation of cells from spleen, thymus, and bone marrow

For isolation of splenic and thymic cells, organs were minced in PBS, filtered through a 70 µm cell strainer and washed once in PBS.
For isolation of BM cells, tibia and femur were flushed with PBS via a 26 G needle and cell suspension was passed through a 70 µm cell strainer.

5.1.4.3. FACS

FACS experiments were either performed according to our protocol or in cooperation with the AG Rodewaldt from German Cancer Research Centre (Heidelberg).

5.1.4.3.1. Analysis of the reporter mice

Results in Figure 8 G, H, Figure 11 B, E, H, Figure 12 I were obtained from experiments carried out in cooperation with the group of Prof. H. R. Rodewaldt, DKFZ, Heidelberg. The FLs of embryos were harvested (see section 5.1.1.3) and resuspended in 1 ml 10% FCS in Hanks' Balanced Salt Solution (HBSS), centrifuged at 500 x g for 1 min and the pellet incubated in 1 ml Calcium deprived medium supplemented with 25 µl collagenase IV (Sigma C2675, 50 mg/ml) and 15 µl DNAse I (Fermentas #EN0521, 1 U/µl) at 37 °C for 30 min. Single cell suspensions were then incubated with directly labelled antibodies (CD146 PE 1:100, CD45 PE Cy7 1:400, CD117 APC 1:400, Sca1 PCPCy5-5 1:200) for 30 min at 4 °C. Single cell suspensions of BM, spleen, thymus and blood from adult f2;YFP and f3;YFP were prepared as described in section 5.1.4.1 and 5.1.4.2. Cells were washed in 10% FCS/HBSS, blocked in purified mouse IgG (500 µg/ml in 10% FCS/HBSS) for 20 min on ice and washed in 10% FCS/HBSS. Single cell suspensions from spleen were incubated with directly labelled antibodies (CD3 APC-Cy7, CD19 Qdot, CD11b PE-Cy7, and Gr1 APC) for 30 min at 4 °C. Cells from thymus were incubated with directly labelled antibodies (CD3 APC-Cy7, CD4 PE Cy7, and CD8 APC) for 30 min at 4 °C. Cells from BM and blood were first incubated with primary antibodies (CD3, CD4, CD8, CD11b, CD19, Gr1, Ter119; all biotinylated) for 30 min at 4 °C. Cells were then washed with 10% FCS/HBSS and incubated with streptavidin APC-Cy7 secondary antibody for lineage negative gating and with directly labelled antibodies (CD117 A700 1:400, CD48 PE 1:200, Sca1 PerCP-Cy5.5

1:200, CD150 BV605 1:100, CD16/32 PE-Cy7 1:400, CD34 APC 1:25) for 30 min at 4 °C. Cells were washed once with 10% FCS/HBSS, resuspended in 100 µl 10% FCS/HBSS supplemented with 100 µl Sytox and analysed on a FACS Fortessa (BD) and data were evaluated using FACS Diva software (BD).
Results in Figure 11 A, C, D, F, G, I and Figure 17 were obtained from experiments carried out in our facility. Single cell suspensions were prepared as described in section 5.1.4.1 and 5.1.4.2 and incubated in 100 µl (pBMCs, BM) or 200 µl (spleen) of 10% Fc block/FACS buffer for 20 min on ice. After that, the cell concentration was adjusted with FACS buffer to one million cells per ml and incubated in 100 µl FACS buffer containing 1 µl of the respective antibody for 20 min on ice protected from light. Cells were washed once in FACS buffer, analysed with FACS-Canto™ II and data were evaluated using FlowJo V 10.1 software.

5.1.4.3.2. Analysis of GATA4 knockout embryos

Results in Figure 26 and Figure 27 were obtained from experiments carried out in cooperation with the group of Prof. H. R. Rodewaldt, DKFZ (Heidelberg). YS were harvested and digested in HBSS/10% FCS containing collagenase IV (60 U/ml f.c., Sigma) and DNase I (25 µg/ml f.c., Sigma) for 1 h at 37 °C. FLs were harvested, mechanically dissociated and passed through a 100 µm cell strainer (BD). Embryo remnants were exsanguinated into defined volumes of HBSS/10% FCS and blood samples were washed twice with PBS/5% FCS. Single cell suspensions were washed with PBS/5% FCS and Fc receptors were blocked by incubating cells with purified mouse IgG (500 mg/ml, Jackson ImmunoResearch Laboratories). All stainings were performed in PBS with 5% FCS on ice for 30 min with optimal dilutions of commercially-prepared antibodies. Reagents used were CD3e phycoerythrin (PE) (clone 145-C11, #12-0031-80), CD11b PerCP-Cy5.5 (clone M1/70, #45-0112-80), CD16/32 PE-Cy7 (clone 93, #25-0161-81), CD34 eFluor660 (RAM34, #50-0341-80), CD45 PE-Cy7 (clone 30-F11), CD45APC-eFlour780 (clone 30-F11, #47-0451-80), CD48 APC (clone HM 48-1, # 17-0481-80), CD117 A700 (ACK-2, #56-1172-80), F4/80 APC (clone BM8, # 17-4801-80), Sca-1 PerCP-Cy5.5 (clone D7, #45-5981-80), Ter119 PE-Cy7 (Ter119, # 25-5921-81) (all eBioscience), CD4 PE (H129.19, # 553652), CD8 PE (53-6.7, #553032), CD19 PE (clone 1D3, #553786), Gr-1 PE (clone RB6-8C5, # 561084), Ter119 PE (clone Ter119, # 553673), streptavidin APC-Alexa750 (#565144) (all BD) CD150 BV605 (clone TC15-12F12.2, #115927, BioLegend), streptavidin Qdot605 (#Q10001MP, Invitrogen). Stainings for apoptosis detection were performed using Annexin V Fitc apoptosis detection kit (BD) according to manufacturer's instruction. Before FACS measurement, cells were washed once with 10% FCS/HBSS, resuspended in 100 µl 10% FCS/HBSS supplemented with 100 µl Sytox and analysed on a FACS Fortessa (BD) and data were evaluated using FACS Diva software (BD).

5.1.5.Molecular biology techniques

5.1.5.1. Genotyping

DNA was extracted from the YS or tail of the embryos or from the tail tip of adult mice. The tissue was incubated in 50 µl tail lysis buffer supplemented with 1.5 µl proteinase K over night at 56 °C. The next day 500 µl dH2O was added, the mixture boiled at 95 °C for 10 min and stored at 4 °C. For polymerase chain reaction (PCR) 1 µl of the DNA mixture was added to 19 µl of master mix for genotyping. Thermocycler conditions were: 3 min at 95 °C, followed by 34 cycles of 20 s at 95 °C, 30 s at 60 °C and 45 s at 72 °C, finished with 5 min 72 °C and hold at 12 °C. The finalized PCR product was complemented with 4 µl of 6x loading dye and 12 µl of the mixture was subjected to a 1% agarose gel for electrophoresis. Electrophoresis was carried out at 100V for 25 – 30 min. The agarose gel was photographed with Azure Imager.

5.1.5.2. Protein isolation

The FL was harvested as described above, incubated in 10 µl protein lysis buffer for 45 min on ice and centrifuged at 4 °C at 300 g for 10 min to remove cellular debris. The protein containing supernatant was transferred to a new tube, snap frozen and stored at -80 °C. Colorimetric quantification of protein concentration was determined by Protein Assay Kit, a method based on Lowry-Assay. The standard curve was prepared using bovine serum albumin (BSA) diluted in the corresponding lysis buffer, absorbance was measured at λ = 650 nm with a plate reader.

5.1.5.3. Sodium dodecyl sulphate polyacrylamide gel electrophoresis (SDS-PAGE)

Protein samples were mixed with 2x Laemmli Buffer and boiled at 95 °C for 5 min. The SDS-gels were placed in electrophoresis chambers and covered with Tris base, acetic acid and EDTA buffer (TAE) buffer. 50 µg of FL lysates were loaded on the gels and samples were then subjected to gel electrophoresis at 20 mA until the protein size of interest was separated properly.

5.1.5.4. Western Blot

The proteins were transferred to nitrocellulose membranes in a semi-dry manner for 35 minutes at 0.45 A in the Trans-Blot Turbo. After blotting, the membrane was blocked in 5% milk block for 1 h at RT followed by incubation with primary antibody diluted in 5% milk block for 2 h at RT or overnight at 4 °C. Membrane were washed three times with PBS and incubated with horseradish-peroxidase (HRP)-conjugated secondary antibody diluted in 5% milk block for 1 h at RT. The membrane was washed extensively with PBS and

treated with Luminate Forte Western HRP Substrate for 3 minutes. The signal was detected by chemiluminescence on an Azure Imaging System.

5.1.6.Statistics

Statistical analysis was performed with SigmaPlot or GraphPad Prism. For comparisons unpaired two-tailed Student's t-test was used. Differences between data sets with $p < 0.05$ were considered statistically significant. Data are presented as means with error bars indicating standard deviation. Statistical significance is indicated by $*p < 0.05$, $**p < 0.01$, $***p < 0.001$.

5.2. Material

Antibodies

Table 3: Antibodies

Primary antibody	Company	Catalogue Number
CD11b	BioLegend	101202
CD146	Milteny Biotec	130-101-866
CD3	BioLegend	100202
CD31	BD Biosciences	102502
CD32b	R&D Systems	AF1460
CD68	BioLegend	137002
cKit/CD117	R&D Systems	AF1356
Cre recombinase	Synaptic systems	257003
Desmin	Abcam	ab15200
F4/80	BioLegend	123102
Gata4	Santa Cruz	sc-9053
GFP/YFP	Molecular Probes	A-11122
Liv2	MBL	D118-3
Lyve1	Reliatech	103-PA50S
Stab2	Martens *et al.* [8]	clone 3.1
Ter119	BD Pharmingen	550565

Secondary antibody	Company	Catalogue Number
donkey anti-rabbit Cy2	Dianova	711-225-152
goat anti-rat Cy3	Dianova	112-165-044
donkey anti-goat Cy3	Dianova	705-165-147
donkey anti-rat Cy3	Dianova	712-165-153
bovine anti-goat Cy3	Dianova	805-165-180
donkey anti-mouse Cy3	Dianova	715-165-151
donkey anti-goat Cy5	Dianova	705-175-147
sheep anti-mouse Cy5	Dianova	515-175-072
donkey anti-rabbit Cy5	Dianova	711-175-152
donkey anti-mouse Cy5	Dianova	715-175-151
donkey anti-mouse Alexa Fluor 488	Dianova	715-485-150
bovine anti-goat Alexa Fluor 488	Dianova	805-485-180
donkey anti-mouse Alexa Fluor 488	Dianova	715-485-151
goat anti-mouse HRP	Dianova	115-035-166
mouse anti-goat HRP	Dianova	205-035-108
donkey anti-rabbit HRP	GE-Healthcare	NA934
Streptavidin labelled Alexa Fluor 488	Life Technologies	S11223
donkey anti-rat Cy2	Jackson Immunoresearch	712-225-153
goat anti-rat Cy5	Jackson Immunoresearch	112-175-003
Streptavidin labelled HRP	Jackson Immunoresearch	016-030-084

Directly labelled antibody	Company	Catalogue Number
CD11b-PE	BD Pharmingen	553311
CD11b-PerCP	BioLegend	101230
CD11c-APC	BD Pharmingen	550261
CD19-PerCP	BioLegend	115532
CD45.2-PE	BD Pharmingen	560694
F4/80-PE	R&D Systems	5580P
GFP/YFP-A488	Molecular Probes	A-21311
Ly6C-APC	BioLegend	108412
Ly6G-PE-Cy7	BD Pharmingen	560601

Buffers and buffer recipes

Ketamine/Xylazine anaesthesia

10% Ketamine	1.2 ml
2% Xylazine	0.8 ml
PBS	ad 10 ml

Tail lysis buffer

100 mM Tris HCL pH 8.0 - pH 8.5	20 ml
0.5 mM EDTA	2 ml
0.2% SDS	4 ml
200 mM NaCl	8 ml
dH2O	ad 200 ml

Master mix for genotyping

Reaction Buffer Set for Taq DNA Polymerase (10X)	2 µl
Deoxynucleoside triphosphate (dNTPs) mix, 10 mM each	0.4 µl
Each Primer	0.6 µl
DFS Taq DNA Polymerase	0.2 µl
dH2O	ad 19 µl

1% Agarose gel

In an Erlenmeyer flask agarose and 1x TAE buffer were mixed and heated in the microwave until gently boiling. After cooling down, Nancy was added and a gel was poured in an appropriate chamber.

Agarose	1 g
Nancy-520	10 µl
1x TAE buffer	100 ml

4% PFA pH 7.2
The PFA powder were weighted carefully under the laminar flow and added to dH2O. The mixture was stirred; the pH value was measured and increased by adding NaOH to pH 11. After a few minutes, the PFA powder has dissolved and 10x PBS was added. The pH value was adjusted to pH 7.2 by adding HCl. The 4% PFA solution was short term stored at 4 °C or aliquoted in 50 ml falcon tubes and stored at -20 °C.

PFA powder	40 g
10x PBS	100 ml
dH2O	900 ml

30% Sucrose

Sucrose	150 g
NaN_3 10%	500 µl
PBS	500 ml

Peroxidase block

H_2O_2 30%	100 µl
NaN_3 10%	200 µl
PBS	30 ml

β-galactosidase staining solution

Reagent A	10 µl
Reagent B	10 µl
Reagent C	10 µl
X-Gal solution 20 µg/ml in DMF	50 µl
PBS	920 µl

Immunofluorescent block buffer

BSA	500 µg
Donkey serum	500 µl
NaN_3 10%	10 µl
PBS	10 ml

Fixative for electron microscopy

Formaldehyde	2%
Glutaraldehyde	2%
Tannic acid	0.5%
$MgCl_2$	1 mM
Sucrose	2%

in Sodium cacodylate 100 mM, pH 7.2

FACS buffer

NaN_3, 10%	500 µl
FCS	50 ml
Dulbecco's phosphate buffered saline	500 ml

Protein lysis buffer

NaCl	150 mM
NP-40	1%
Sodium deoxycholate	0.5%
SDS	0.1%
Tris / HCl (pH 8.0)	50 mM
Sodium fluoride	10 mM
EDTA	2 mM
Protease inhibitor cocktail	4%

Resolving gel

During polymerization the resolving gel was covered carefully with isopropanol to avoid drying up.

dH2O	5.0 mL
30% Acrylamide	6.0 mL
1.5 M Tris / HCl (pH 8.8)	3.8 mL
10% SDS	0.15 mL
10% APS	0.15 mL
TEMED	6 µl

Stacking gel

After completion of the polymerization of the resolving gel, the isopropanol was demounted, the stacking gel was casted on top of the resolving gel and a comb was inserted.

dH2O	1.72 mL
30% Acrylamide	0.5 mL
0.5 M Tris, pH = 6,8	0.76 mL
10% SDS	0.03 mL
10% APS	0.03 mL
TEMED	3 µl

Milk block

Milk powder	5 g
PBS	100 ml

Chemicals and reagents

Table 4: Chemicals and reagents

Name	Company
4',6-Diamidino-2-Phenylindole, Dihydrochloride (DAPI)	Life Technologies
Acetone	Roth
Acrylamide, 30%	Bio-Rad
AEC Substrate Chromogen	DAKO
Agarose	Sigma
Ammonium persulfate	Sigma
Ammonium chloride NH4Cl	Roth
Biocoll	Biochrom
Bovine serum albumin (BSA)	Fitzgerald
DFS Taq DNA Polymerase	Bioron
DNA Gel Loading Dye (6X)	Thermo Fisher
DNA Ladder	Thermo Scientific
dNTPs mix, 10 mM each	Fermentas
Donkey serum	Dianova
DPBS [-]$CaCl_2$ [-]$MgCl_2$	Life Technologies
Ethanol	Roth
Ethylenediaminetetraacetic acid (EDTA)	Sigma
Faramount aquaeus mounting medium	DAKO
Faramount mounting medium, aqueous	DAKO
Fetal calf serum (FCS)	Life Technologies
Fluorescent mounting medium	DAKO
Hydrogen peroxide H_2O_2	Sigma
Isofluorane (Forene® 100%)	Abbot
Ketamine 10%	Medistar
Laemmli Buffer	Bio-Rad
Milk powder	Roth
Nancy-520	Sigma
NP-40	Fluka
PageRuler prestained protein ladder	Fermentas
Paraffin	Roth
Paraformaldehyde	Roth
PBS powder without Ca^{2+}, Mg^{2+}	Life Technologies
Protease inhibitor cocktail	Roche
Proteinase K (10 mg/ml)	Sigma
Reaction Buffer Set for Taq DNA Polymerase (10X)	Bioron
Rompun 2% (Xylazine)	Bayer
Sodium azide NaN_3	Sigma
Sodium chloride NaCl	Sigma
Sodium deoxycholate	Sigma
Sodium dodecyl sulphate (SDS)	BioRad

Sucrose	BioFroxx
TAE buffer 10x	Roth
Tetramethylethylenediamine (TEMED)	GenAxxon
Tri-HCl	Sigma
Triton X-100	Sigma
Tween	Sigma
Xylene	Sigma

Consumables

Table 5: Consumables

Name	Company
Adhesion microscope slides SuperFrost Plus®	Langenbrinck
Butterfly needle, 25 G	Seidel Medizin
Cell strainer70 µm and 100 µm	BD Biosciences
Cryomolds	Sakura
Falcon tubes	Becton Dickinson
Lithium/Heparin microvettes 500 µl	Sarstedt
Micropipettes, intraEND, 20 µl	Blaubrand
Nitrocellulose membrane	Bio-Rad
OCT compound	Sakura
Paraffin embedding cassettes	Sarstedt

Instruments

Table 6: Instruments

Name	Company
Analytical balance R300S	Sartorius
Azure Imager C400	Azure Biosystems
Confocal laser scanning microscope SP5 DS	Leica
Cryotome CM3050S	Leica
Electron microscope 910	Carl Zeiss
FACS-Canto™ II	BD Biosciences
Gel electrophoresis system	Mupid One
Microtome RM2065	Leica
Multi-photon laser scanning microscope SP MP	Leica
Nanodrop 2000	Thermo Scientific
pH Meter FG2/EL2	Mettler Toledo
Plate reader infinite 200pro	Tecan
Table centrifuge 5415D	Eppendorf
Thermoblock Thermomixer C	Eppendorf
Thermocycler T100	BioRad
Top-loading balance PT2100	Sartorius

Trans-Blot Turbo	BioRad
Transmitted Light Bases TL3000 Ergo microscope	Leica
Upright microscope Eclipse Ci-E	Nikon
Upright motorized microscope Eclipse Ni-E	Nikon
Vortex Genie-2	Scientific Industries

Kits

Table 7: Kits

Name	Company	Catalogue number
Avidin/biotin blocking kit	Vector Laboratories	#SP-2001
Protein Assay Kit	BioRad	5000112
β - Galactosidase Reporter Gene Staining Kit	Sigma	#GALS-1KT

Mouse strains

Table 8: Mouse strains

Name	Official name	Company / reference
Gata4 [79]	Gata4$^{tm1.1Sad}$	The Jackson Laboratory / #008194
R26LacZ [92]	Gt(ROSA)26Sor^{tm1Sor}	The Jackson Laboratory / #003474
R26YFP [93]	Gt(ROSA)26Sor$^{tm1(EYFP)Cos}$	The Jackson Laboratory / #006148
Stab2-cre	B6.Stab2$^{tg1.2cre}$	
	B6.Stab2$^{tg1.3cre}$	
Clec4g-cre	B6.Clec4g$^{tg1.1cre}$	
Rag2$^{-/-}$;γc$^{-/-}$;Kit$^{W/Wv}$	Rag2$^{-/-}$;γc$^{-/-}$;Kit$^{W/Wv}$	Waskow *et al.* [117]

Primer

Table 9: Primer

Name	Sequence 5' -> 3'
Gata4_forward	CCC AGT AAA GAA GTC AGC ACA AGG AAA C
Gata4_reverse	AGA CTA TTG ATC CCG GAG TGA ACA TT
iCre_forward	AAG AAC CTG ATG GAC ATG TTC AGG
iCre_reverse	TCT GTC AGA GTT CTC CAT CAG GGA
LacZ_common	AAA GTC GCT CTG AGT TGT TAT
LacZ_mutant	GCG AAG AGT TTG TCC TCA ACC
LacZ_wildtype	GGA GCG GGA GAA ATG GAT ATG
YFP_common	AAA GTC GCT CTG AGT TGT TAT
YFP_mutant	AAG ACC GCG AAG AGT TTG TC
YFP_wildtype	GGA GCG GGA GAA ATG GAT ATG

Software

Table 10 Software

Name	Version	Company
FlowJo	Version 10.4.2	Tree Star, Inc.
GraphPad Prism	Prism 5	GraphPad Software
ImageJ	ImageJ 1.50i	National Institutes of Health [255]
SigmaPlot	SigmaPlot 11.0	Systat Software

References

1. Potente, M. & Mäkinen, T. Vascular heterogeneity and specialization in development and disease. *Nat. Rev. Mol. Cell Biol.* (2017). doi:10.1038/nrm.2017.36
2. Aird, W. C. Phenotypic heterogeneity of the endothelium: II. Representative vascular beds. *Circ. Res.* **100,** 174–90 (2007).
3. Aird, W. C. Spatial and temporal dynamics of the endothelium. *J Thromb Haemost* **3,** 1392–406 (2005).
4. Ulvmar, M. H. & Mäkinen, T. Heterogeneity in the lymphatic vascular system and its origin. *Cardiovasc. Res.* **111,** 310–321 (2016).
5. Sarin, H. Physiologic upper limits of pore size of different blood capillary types and another perspective on the dual pore theory of microvascular permeability. *J. Angiogenesis Res.* **2,** 14 (2010).
6. Aird, W. C. Phenotypic heterogeneity of the endothelium: I. Structure, function, and mechanisms. *Circ. Res.* **100,** 158–73 (2007).
7. Itkin, T. *et al.* Distinct bone marrow blood vessels differentially regulate haematopoiesis. *Nature* **advance online publication,** (2016).
8. Martens, J. H. *et al.* Differential expression of a gene signature for scavenger/lectin receptors by endothelial cells and macrophages in human lymph node sinuses, the primary sites of regional metastasis. *J Pathol* **208,** 574–89 (2006).
9. Iftakhar-E-Khuda, I. *et al.* Gene-expression profiling of different arms of lymphatic vasculature identifies candidates for manipulation of cell traffic. *Proc. Natl. Acad. Sci. U. S. A.* **113,** 10643–10648 (2016).
10. Murphy, K., Travers, P., Walport, M. & Janeway, C. *Janeway's immunobiology*. (Garland Science, 2012).
11. Mebius, R. E. & Kraal, G. Structure and function of the spleen. *Nat. Rev. Immunol.* **5,** 606–616 (2005).
12. Trefts, E., Gannon, M. & Wasserman, D. H. The liver. *Curr. Biol.* **27,** R1147–R1151 (2017).
13. Iwakiri, Y., Shah, V. & Rockey, D. C. Vascular pathobiology in chronic liver disease and cirrhosis – Current status and future directions. *J. Hepatol.* **61,** 912–924 (2014).
14. Elvevold, K., Smedsrod, B. & Martinez, I. The liver sinusoidal endothelial cell: a cell type of controversial and confusing identity. *Am J Physiol Gastrointest Liver Physiol* **294,** G391-400 (2008).
15. Svistounov, D. *et al.* The Relationship between Fenestrations, Sieve Plates and Rafts in Liver Sinusoidal Endothelial Cells. *PLoS ONE* **7,** e46134 (2012).
16. *Molecular cell biology*. (W.H. Freeman, 2008).
17. Tokairin, T. *et al.* A highly specific isolation of rat sinusoidal endothelial cells by the immunomagnetic bead method using SE-1 monoclonal antibody. *J. Hepatol.* **36,** 725–733 (2002).
18. Katz, S. C., Pillarisetty, V. G., Bleier, J. I., Shah, A. B. & DeMatteo, R. P. Liver sinusoidal endothelial cells are insufficient to activate T cells. *J. Immunol. Baltim. Md 1950* **173,** 230–235 (2004).

19. Onoe, T. *et al.* Liver Sinusoidal Endothelial Cells Tolerize T Cells across MHC Barriers in Mice. *J. Immunol.* **175,** 139–146 (2005).
20. Rauen, U. *et al.* Injury to cultured liver endothelial cells during cold preservation: energy-dependent versus energy-deficiency injury. *Transpl. Int.* **6,** 218–222 (1993).
21. Krause, P. *et al.* Hepatocyte-supported serum-free culture of rat liver sinusoidal endothelial cells. *J. Hepatol.* **32,** 718–726 (2000).
22. March, S., Hui, E. E., Underhill, G. H., Khetani, S. & Bhatia, S. N. Microenvironmental Regulation of the Sinusoidal Endothelial Cell Phenotype In Vitro. *Hepatology* **50,** 920–8 (2009).
23. DeLeve, L. D., Wang, X., Hu, L., McCuskey, M. K. & McCuskey, R. S. Rat liver sinusoidal endothelial cell phenotype is maintained by paracrine and autocrine regulation. *Am J Physiol Gastrointest Liver Physiol* **287,** G757-763 (2004).
24. Geraud, C. *et al.* Liver sinusoidal endothelium: a microenvironment-dependent differentiation program in rat including the novel junctional protein liver endothelial differentiation-associated protein-1. *Hepatology* **52,** 313–26 (2010).
25. Elvevold, K., Nedredal, G. I., Revhaug, A., Bertheussen, K. & Smedsrød, B. Long-term preservation of high endocytic activity in primary cultures of pig liver sinusoidal endothelial cells. *Eur. J. Cell Biol.* **84,** 749–764 (2005).
26. Geraud, C. *et al.* Unique cell type-specific junctional complexes in vascular endothelium of human and rat liver sinusoids. *PLoS One* **7,** e34206 (2012).
27. Falkowski, M., Schledzewski, K., Hansen, B. & Goerdt, S. Expression of stabilin-2, a novel fasciclin-like hyaluronan receptor protein, in murine sinusoidal endothelia, avascular tissues, and at solid/liquid interfaces. *Histochem Cell Biol* **120,** 361–9 (2003).
28. Bankston, P. W. & Pino, R. M. The development of the sinusoids of fetal rat liver: Morphology of endothelial cells, Kupffer cells, and the transmural migration of blood cells into the sinusoids. *Am. J. Anat.* **159,** 1–15 (1980).
29. Enzan, H. *et al.* Development of hepatic sinusoidal structure with special reference to the Ito cells. *Microsc Res Tech* **39,** 336–49 (1997).
30. Couvelard, A. *et al.* Structural and functional differentiation of sinusoidal endothelial cells during liver organogenesis in humans. *Blood* **87,** 4568–4580 (1996).
31. Nonaka, H., Tanaka, M., Suzuki, K. & Miyajima, A. Development of murine hepatic sinusoidal endothelial cells characterized by the expression of hyaluronan receptors. *Dev Dyn* **236,** 2258–67 (2007).
32. Zhang, H. *et al.* Genetic lineage tracing identifies endocardial origin of liver vasculature. *Nat. Genet.* **48,** 537–543 (2016).
33. Smedsrød, B. Clearance function of scavenger endothelial cells. *Comp. Hepatol.* **3,** 22 (2004).
34. Martinez-Pomares, L. The mannose receptor. *J. Leukoc. Biol.* **92,** 1177–1186 (2012).
35. Sondermann, P. Crystal structure of the soluble form of the human Fcgamma - receptor IIb: a new member of the immunoglobulin superfamily at 1.7Aresolution. *EMBO J.* **18,** 1095–1103 (1999).
36. PrabhuDas, M. *et al.* Standardizing Scavenger Receptor Nomenclature. *J. Immunol.* **192,** 1997–2006 (2014).

37. Kelley, J. L., Ozment, T. R., Li, C., Schweitzer, J. B. & Williams, D. L. Scavenger receptor-A (CD204): a two-edged sword in health and disease. *Crit. Rev. Immunol.* **34,** 241–261 (2014).
38. Plüddemann, A., Neyen, C. & Gordon, S. Macrophage scavenger receptors and host-derived ligands. *Methods San Diego Calif* **43,** 207–217 (2007).
39. Pepino, M. Y., Kuda, O., Samovski, D. & Abumrad, N. A. Structure-function of CD36 and importance of fatty acid signal transduction in fat metabolism. *Annu. Rev. Nutr.* **34,** 281–303 (2014).
40. Stewart, C. R. *et al.* CD36 ligands promote sterile inflammation through assembly of a Toll-like receptor 4 and 6 heterodimer. *Nat. Immunol.* **11,** 155–161 (2010).
41. Adachi, H. & Tsujimoto, M. FEEL-1, a novel scavenger receptor with in vitro bacteria-binding and angiogenesis-modulating activities. *J Biol Chem* **277,** 34264–70 (2002).
42. Hansen, B. *et al.* Stabilin-1 and stabilin-2 are both directed into the early endocytic pathway in hepatic sinusoidal endothelium via interactions with clathrin/AP-2, independent of ligand binding. *Exp Cell Res* **303,** 160–73 (2005).
43. Kim, S., Bae, D. J., Hong, M., Park, S. Y. & Kim, I. S. The conserved histidine in epidermal growth factor-like domains of stabilin-2 modulates pH-dependent recognition of phosphatidylserine in apoptotic cells. *Int J Biochem Cell Biol* **42,** 1154–63 (2010).
44. Kzhyshkowska, J., Gratchev, A. & Goerdt, S. Stabilin-1, a homeostatic scavenger receptor with multiple functions. *J Cell Mol Med* **10,** 635–49 (2006).
45. Schledzewski, K. *et al.* Deficiency of liver sinusoidal scavenger receptors stabilin-1 and -2 in mice causes glomerulofibrotic nephropathy via impaired hepatic clearance of noxious blood factors. *J Clin Invest* **121,** 703–14 (2011).
46. Cao, Z. *et al.* Angiocrine Factors Deployed by Tumor Vascular Niche Induce B Cell Lymphoma Invasiveness and Chemoresistance. *Cancer Cell* **25,** 350–365 (2014).
47. Ding, B. S. *et al.* Divergent angiocrine signals from vascular niche balance liver regeneration and fibrosis. *Nature* **505,** 97–102 (2014).
48. Hu, J. *et al.* Endothelial cell-derived angiopoietin-2 controls liver regeneration as a spatiotemporal rheostat. *Science* **343,** 416–9 (2014).
49. Poisson, J. *et al.* Liver sinusoidal endothelial cells: physiology and role in liver diseases. *J. Hepatol.* (2016). doi:10.1016/j.jhep.2016.07.009
50. Lao, Y. *et al.* Proteomic Analysis Reveals Dab2 Mediated Receptor Endocytosis Promotes Liver Sinusoidal Endothelial Cell Dedifferentiation. *Sci. Rep.* **7,** (2017).
51. Klein, D. *et al.* Wnt2 acts as a cell type-specific, autocrine growth factor in rat hepatic sinusoidal endothelial cells cross-stimulating the VEGF pathway. *Hepatology* **47,** 1018–31 (2008).
52. DeLeve, L. D. Liver sinusoidal endothelial cells in hepatic fibrosis. *Hepatology* **61,** 1740–6 (2015).
53. Bataller, R. & Brenner, D. A. Liver fibrosis. *J. Clin. Invest.* **115,** 209–218 (2005).
54. Deleve, L. D., Wang, X. & Guo, Y. Sinusoidal endothelial cells prevent rat stellate cell activation and promote reversion to quiescence. *Hepatology* **48,** 920–930 (2008).
55. Geraud, C. *et al.* Endothelial transdifferentiation in hepatocellular carcinoma: loss of Stabilin-2 expression in peri-tumourous liver correlates with increased survival. *Liver Int* **33,** 1428–40 (2013).

56. Orban, P. C., Chui, D. & Marth, J. D. Tissue- and site-specific DNA recombination in transgenic mice. *Proc. Natl. Acad. Sci. U. S. A.* **89,** 6861–6865 (1992).
57. Kisanuki, Y. Y. *et al.* Tie2-Cre transgenic mice: a new model for endothelial cell-lineage analysis in vivo. *Dev Biol* **230,** 230–42 (2001).
58. Alva, J. A. *et al.* VE-Cadherin-Cre-recombinase transgenic mouse: a tool for lineage analysis and gene deletion in endothelial cells. *Dev Dyn* **235,** 759–67 (2006).
59. Licht, A. H., Raab, S., Hofmann, U. & Breier, G. Endothelium-specific Cre recombinase activity in flk-1-Cre transgenic mice. *Dev Dyn* **229,** 312–8 (2004).
60. Zorn, A. M. Liver development. in *StemBook* (Harvard Stem Cell Institute, 2008).
61. Edgar, R. *et al.* LifeMap Discovery™: the embryonic development, stem cells, and regenerative medicine research portal. *PloS One* **8,** e66629 (2013).
62. Watt, A. J., Zhao, R., Li, J. & Duncan, S. A. Development of the mammalian liver and ventral pancreas is dependent on GATA4. *BMC Dev Biol* **7,** 37 (2007).
63. Si-Tayeb, K., Lemaigre, F. P. & Duncan, S. A. Organogenesis and Development of the Liver. *Dev. Cell* **18,** 175–189 (2010).
64. Rossi, J. M., Dunn, N. R., Hogan, B. L. M. & Zaret, K. S. Distinct mesodermal signals, including BMPs from the septum transversum mesenchyme, are required in combination for hepatogenesis from the endoderm. *Genes Dev.* **15,** 1998–2009 (2001).
65. Matsumoto, K., Yoshitomi, H., Rossant, J. & Zaret, K. S. Liver organogenesis promoted by endothelial cells prior to vascular function. *Science* **294,** 559–63 (2001).
66. Mikkola, H. K. & Orkin, S. H. The journey of developing hematopoietic stem cells. *Development* **133,** 3733–44 (2006).
67. Crawford, L. W., Foley, J. F. & Elmore, S. A. Histology atlas of the developing mouse hepatobiliary system with emphasis on embryonic days 9.5-18.5. *Toxicol Pathol* **38,** 872–906 (2010).
68. Guo, Y. *et al.* Relationships between hematopoiesis and hepatogenesis in the midtrimester fetal liver characterized by dynamic transcriptomic and proteomic profiles. *PloS One* **4,** e7641 (2009).
69. Dartsch, N., Schulte, D., Hagerling, R., Kiefer, F. & Vestweber, D. Fusing VE-cadherin to alpha-catenin impairs fetal liver hematopoiesis and lymph but not blood vessel formation. *Mol Cell Biol* **34,** 1634–48 (2014).
70. Rocha, A. S. *et al.* The Angiocrine Factor Rspondin3 Is a Key Determinant of Liver Zonation. *Cell Rep.* **13,** 1757–1764 (2015).
71. Evans, T., Reitman, M. & Felsenfeld, G. An erythrocyte-specific DNA-binding factor recognizes a regulatory sequence common to all chicken globin genes. *Proc. Natl. Acad. Sci. U. S. A.* **85,** 5976–5980 (1988).
72. Lowry, J. A. & Atchley, W. R. Molecular evolution of the GATA family of transcription factors: conservation within the DNA-binding domain. *J. Mol. Evol.* **50,** 103–115 (2000).
73. Arceci, R. J., King, A. A., Simon, M. C., Orkin, S. H. & Wilson, D. B. Mouse GATA-4: a retinoic acid-inducible GATA-binding transcription factor expressed in endodermally derived tissues and heart. *Mol. Cell. Biol.* **13,** 2235–2246 (1993).

74. Pilon, N., Raiwet, D., Viger, R. S. & Silversides, D. W. Novel pre- and post-gastrulation expression of Gata4 within cells of the inner cell mass and migratory neural crest cells. *Dev Dyn* **237,** 1133–43 (2008).
75. Kuo, C. T. *et al.* GATA4 transcription factor is required for ventral morphogenesis and heart tube formation. *Genes Dev.* **11,** 1048–1060 (1997).
76. Molkentin, J. D., Lin, Q., Duncan, S. A. & Olson, E. N. Requirement of the transcription factor GATA4 for heart tube formation and ventral morphogenesis. *Genes Dev.* **11,** 1061–72 (1997).
77. Rivera-Feliciano, J. *et al.* Development of heart valves requires Gata4 expression in endothelial-derived cells. *Development* **133,** 3607–3618 (2006).
78. Crispino, J. D. *et al.* Proper coronary vascular development and heart morphogenesis depend on interaction of GATA-4 with FOG cofactors. *Genes Dev.* **15,** 839–844 (2001).
79. Watt, A. J., Battle, M. A., Li, J. & Duncan, S. A. GATA4 is essential for formation of the proepicardium and regulates cardiogenesis. *Proc. Natl. Acad. Sci.* **101,** 12573–12578 (2004).
80. Delgado, I. *et al.* GATA4 loss in the septum transversum mesenchyme promotes liver fibrosis in mice. *Hepatology* **59,** 2358–2370 (2014).
81. Wandzioch, E., Kolterud, A., Jacobsson, M., Friedman, S. L. & Carlsson, L. Lhx2-/- mice develop liver fibrosis. *Proc. Natl. Acad. Sci.* **101,** 16549–16554 (2004).
82. Yu, Y. *et al.* Functional mutant GATA4 identification and potential application in preimplantation diagnosis of congenital heart diseases. *Gene* **641,** 349–354 (2018).
83. Zhang, Y., Ai, F., Zheng, J. & Peng, B. Associations of GATA4 genetic mutations with the risk of congenital heart disease: A meta-analysis. *Medicine (Baltimore)* **96,** e6857 (2017).
84. McCulley, D. J. & Black, B. L. Transcription factor pathways and congenital heart disease. *Curr. Top. Dev. Biol.* **100,** 253–277 (2012).
85. Enane, F. O. *et al.* GATA4 loss of function in liver cancer impedes precursor to hepatocyte transition. *J. Clin. Invest.* (2017). doi:10.1172/JCI93488
86. Holtzinger, A. & Evans, T. Gata4 regulates the formation of multiple organs. *Development* **132,** 4005–4014 (2005).
87. Torregroza, I. *et al.* Regulation of a vascular plexus by gata4 is mediated in zebrafish through the chemokine sdf1a. *PloS One* **7,** e46844 (2012).
88. Jung, M. Y., Park, S. Y. & Kim, I. S. Stabilin-2 is involved in lymphocyte adhesion to the hepatic sinusoidal endothelium via the interaction with alphaMbeta2 integrin. *J Leukoc Biol* **82,** 1156–65 (2007).
89. Lee, S. J., Park, S. Y., Jung, M. Y., Bae, S. M. & Kim, I. S. Mechanism for phosphatidylserine-dependent erythrophagocytosis in mouse liver. *Blood* **117,** 5215–23 (2011).
90. Li, R. *et al.* Role of liver sinusoidal endothelial cells and stabilins in elimination of oxidized low-density lipoproteins. *Am J Physiol Gastrointest Liver Physiol* **300,** G71-81 (2011).
91. Qian, H. *et al.* Stabilins are expressed in bone marrow sinusoidal endothelial cells and mediate scavenging and cell adhesive functions. *Biochem Biophys Res Commun* **390,** 883–6 (2009).

92. Soriano, P. Generalized lacZ expression with the ROSA26 Cre reporter strain. *Nat Genet* **21,** 70–1 (1999).
93. Srinivas, S. *et al.* Cre reporter strains produced by targeted insertion of EYFP and ECFP into the ROSA26 locus. *BMC Dev. Biol.* **1,** 4 (2001).
94. Trifonov, S., Yamashita, Y., Kase, M., Maruyama, M. & Sugimoto, T. Overview and assessment of the histochemical methods and reagents for the detection of β-galactosidase activity in transgenic animals. *Anat. Sci. Int.* **91,** 56–67 (2016).
95. Nierhoff, D., Ogawa, A., Oertel, M., Chen, Y.-Q. & Shafritz, D. A. Purification and characterization of mouse fetal liver epithelial cells with high in vivo repopulation capacity. *Hepatology* **42,** 130–139 (2005).
96. *The atlas of mouse development*. (Elsevier Acad. Press, 2010).
97. Nitou, M., Ishikawa, K. & Shiojiri, N. Immunohistochemical analysis of development of desmin-positive hepatic stellate cells in mouse liver. *J Anat* **197,** 635–46 (2000).
98. Altschul, S. F. *et al.* Gapped BLAST and PSI-BLAST: a new generation of protein database search programs. *Nucleic Acids Res.* **25,** 3389–3402 (1997).
99. Altschul, S. F. *et al.* Protein database searches using compositionally adjusted substitution matrices. *FEBS J.* **272,** 5101–5109 (2005).
100. Liu, W. *et al.* Characterization of a Novel C-type Lectin-like Gene, LSECtin. *J. Biol. Chem.* **279,** 18748–18758 (2004).
101. Tang, L. *et al.* Liver Sinusoidal Endothelial Cell Lectin, LSECtin, Negatively Regulates Hepatic T-Cell Immune Response. *Gastroenterology* **137,** 1498-1508.e5 (2009).
102. Pipirou, Z. *et al.* Mouse LSECtin as a model for a human Ebola virus receptor. *Glycobiology* **21,** 806–812 (2011).
103. Liu, B. *et al.* Liver Sinusoidal Endothelial Cell Lectin Inhibits CTL-Dependent Virus Clearance in Mouse Models of Viral Hepatitis. *J. Immunol.* **190,** 4185–4195 (2013).
104. Petryszak, R. *et al.* Expression Atlas update--a database of gene and transcript expression from microarray- and sequencing-based functional genomics experiments. *Nucleic Acids Res.* **42,** D926-932 (2014).
105. Qu, C., Brinck-Jensen, N.-S., Zang, M. & Chen, K. Monocyte-derived dendritic cells: targets as potent antigen-presenting cells for the design of vaccines against infectious diseases. *Int. J. Infect. Dis.* **19,** 1–5 (2014).
106. Kohrgruber, N. *et al.* Survival, Maturation, and Function of CD11c– and CD11c+ Peripheral Blood Dendritic Cells Are Differentially Regulated by Cytokines. *J. Immunol.* **163,** 3250–3259 (1999).
107. van Lochem, E. G. *et al.* Immunophenotypic differentiation patterns of normal hematopoiesis in human bone marrow: Reference patterns for age-related changes and disease-induced shifts. *Cytometry* **60B,** 1–13 (2004).
108. Swamydas, M. & Lionakis, M. S. Isolation, purification and labeling of mouse bone marrow neutrophils for functional studies and adoptive transfer experiments. *J. Vis. Exp. JoVE* e50586 (2013). doi:10.3791/50586
109. Wang, K., Wei, G. & Liu, D. CD19: a biomarker for B cell development, lymphoma diagnosis and therapy. *Exp. Hematol. Oncol.* **1,** 36 (2012).
110. Hey, Y. Y. & O'Neill, H. C. Murine spleen contains a diversity of myeloid and dendritic cells distinct in antigen presenting function. *J. Cell. Mol. Med.* **16,** 2611–2619 (2012).

111. Hey, Y.-Y., Tan, J. K. H. & O'Neill, H. C. Redefining Myeloid Cell Subsets in Murine Spleen. *Front. Immunol.* **6,** (2016).
112. Mowat, A. M. & Bain, C. C. Mucosal Macrophages in Intestinal Homeostasis and Inflammation. *J. Innate Immun.* **3,** 550–564 (2011).
113. Gordon, S., Plüddemann, A. & Martinez Estrada, F. Macrophage heterogeneity in tissues: phenotypic diversity and functions. *Immunol. Rev.* **262,** 36–55 (2014).
114. Misharin, A. V., Morales-Nebreda, L., Mutlu, G. M., Budinger, G. R. S. & Perlman, H. Flow Cytometric Analysis of Macrophages and Dendritic Cell Subsets in the Mouse Lung. *Am. J. Respir. Cell Mol. Biol.* **49,** 503–510 (2013).
115. Warren, A. *et al.* Marked changes of the hepatic sinusoid in a transgenic mouse model of acute immune-mediated hepatitis. *J. Hepatol.* **46,** 239–246 (2007).
116. Mori, T. *et al.* Defenestration of the sinusoidal endothelial cell in a rat model of cirrhosis. *Hepatology* **17,** 891–897 (1993).
117. Waskow, C. *et al.* Hematopoietic stem cell transplantation without irradiation. *Nat Meth* **6,** 267–269 (2009).
118. Géraud, C. *et al.* GATA4-dependent organ-specific endothelial differentiation controls liver development and embryonic hematopoiesis. *J. Clin. Invest.* (2017). doi:10.1172/JCI90086
119. Katsuno, T. *et al.* Deficiency of zonula occludens-1 causes embryonic lethal phenotype associated with defected yolk sac angiogenesis and apoptosis of embryonic cells. *Mol. Biol. Cell* **19,** 2465–2475 (2008).
120. Wyss, L. *et al.* Junctional Adhesion Molecule (JAM)-C Deficient C57BL/6 Mice Develop a Severe Hydrocephalus. *PLoS ONE* **7,** e45619 (2012).
121. Gossen, M. & Bujard, H. Tight control of gene expression in mammalian cells by tetracycline-responsive promoters. *Proc. Natl. Acad. Sci.* **89,** 5547–5551 (1992).
122. Shockett, P. E. & Schatz, D. G. Diverse strategies for tetracycline-regulated inducible gene expression. *Proc. Natl. Acad. Sci. U. S. A.* **93,** 5173–5176 (1996).
123. Sauer, B. & Henderson, N. Site-specific DNA recombination in mammalian cells by the Cre recombinase of bacteriophage P1. *Proc. Natl. Acad. Sci. U. S. A.* **85,** 5166–5170 (1988).
124. Feil, R. *et al.* Ligand-activated site-specific recombination in mice. *Proc. Natl. Acad. Sci. U. S. A.* **93,** 10887–10890 (1996).
125. Metzger, D. & Chambon, P. Site- and time-specific gene targeting in the mouse. *Methods* **24,** 71–80 (2001).
126. Gory, S. *et al.* The vascular endothelial-cadherin promoter directs endothelial-specific expression in transgenic mice. *Blood* **93,** 184–192 (1999).
127. Crosswhite, P. L. *et al.* CHD4-regulated plasmin activation impacts lymphovenous hemostasis and hepatic vascular integrity. *J. Clin. Invest.* **126,** (2016).
128. Tang, Y., Bai, H., Urs, S., Wang, Z. & Liaw, L. Notch1 activation in embryonic VE-cadherin populations selectively blocks hematopoietic stem cell generation and fetal liver hematopoiesis. *Transgenic Res.* **22,** 403–410 (2013).
129. Chen, M. J., Yokomizo, T., Zeigler, B. M., Dzierzak, E. & Speck, N. A. Runx1 is required for the endothelial to haematopoietic cell transition but not thereafter. *Nature* **457,** 887–891 (2009).

130. Lv, J., Wang, L., Gao, Y., Ding, Y.-Q. & Liu, F. 5-hydroxytryptamine synthesized in the aorta-gonad-mesonephros regulates hematopoietic stem and progenitor cell survival. *J. Exp. Med.* **214,** 529–545 (2017).
131. Ambrosi, T. H. *et al.* Adipocyte Accumulation in the Bone Marrow during Obesity and Aging Impairs Stem Cell-Based Hematopoietic and Bone Regeneration. *Cell Stem Cell* **20,** 771-784.e6 (2017).
132. Frame, J., Fegan, K. H., Conway, S. J., McGrath, K. E. & Palis, J. Definitive Hematopoiesis in the Yolk Sac Emerges from Wnt-Responsive Hemogenic Endothelium Independently of Circulation and Arterial Identity. *Stem Cells* **34,** 431–444 (2015).
133. Song, Y., Jiang, J., Vermeren, S. & Tong, W. ARAP3 Functions in Hematopoietic Stem Cells. *PLOS ONE* **9,** e116107 (2014).
134. Imanirad, P. *et al.* HIF1α is a regulator of hematopoietic progenitor and stem cell development in hypoxic sites of the mouse embryo. *Stem Cell Res.* **12,** 24–35 (2014).
135. Chanda, B., Ditadi, A., Iscove, N. N. & Keller, G. Retinoic Acid Signaling Is Essential for Embryonic Hematopoietic Stem Cell Development. *Cell* **155,** 215–227 (2013).
136. Scholz, B. *et al.* Endothelial RSPO3 Controls Vascular Stability and Pruning through Non-canonical WNT/Ca2+/NFAT Signaling. *Dev. Cell* **36,** 79–93 (2016).
137. Shoham, A. B. *et al.* Deposition of collagen type I onto skeletal endothelium reveals a new role for blood vessels in regulating bone morphology. *Development* **143,** 3933–3943 (2016).
138. Stan, R. V. *et al.* The Diaphragms of Fenestrated Endothelia: Gatekeepers of Vascular Permeability and Blood Composition. *Dev. Cell* **23,** 1203–1218 (2012).
139. Yang, M. *et al.* MiR-497~195 cluster regulates angiogenesis during coupling with osteogenesis by maintaining endothelial Notch and HIF-1α activity. *Nat. Commun.* **8,** 16003 (2017).
140. Park, S. O. *et al.* ALK5- and TGFBR2-independent role of ALK1 in the pathogenesis of hereditary hemorrhagic telangiectasia type 2. *Blood* **111,** 633–642 (2008).
141. Hong, K.-H. *et al.* Genetic ablation of the BMPR2 gene in pulmonary endothelium is sufficient to predispose to pulmonary arterial hypertension. *Circulation* **118,** 722–730 (2008).
142. Motoike, T., Markham, D. W., Rossant, J. & Sato, T. N. Evidence for novel fate of Flk1+ progenitor: Contribution to muscle lineage. *Genesis* **35,** 153–159 (2003).
143. Terry, R. W., Kwee, L., Baldwin, H. S. & Labow, M. A. Cre-mediated generation of a VCAM-1 null allele in transgenic mice. *Transgenic Res* **6,** 349–56 (1997).
144. Braren, R. *et al.* Endothelial FAK is essential for vascular network stability, cell survival, and lamellipodial formation. *J. Cell Biol.* **172,** 151–162 (2006).
145. Kano, A. *et al.* Endothelial Cells Require STAT3 for Protection against Endotoxin-induced Inf lammation. *J. Exp. Med.* **198,** 1517–1525 (2003).
146. Koni, P. A. *et al.* Conditional vascular cell adhesion molecule 1 deletion in mice: impaired lymphocyte migration to bone marrow. *J. Exp. Med.* **193,** 741–754 (2001).
147. Theis, M. *et al.* Endothelium-specific replacement of the connexin43 coding region by a lacZ reporter gene. *Genesis* **29,** 1–13 (2001).
148. Constien, R. *et al.* Characterization of a novel EGFP reporter mouse to monitor Cre recombination as demonstrated by a Tie2 Cre mouse line. *Genesis* **30,** 36–44 (2001).

149. Lan, Y. *et al.* Essential role of endothelial Smad4 in vascular remodeling and integrity. *Mol. Cell. Biol.* **27,** 7683–7692 (2007).
150. Gustafsson, E., Brakebusch, C., Hietanen, K. & Fässler, R. Tie-1-directed expression of Cre recombinase in endothelial cells of embryoid bodies and transgenic mice. *J. Cell Sci.* **114,** 671–676 (2001).
151. Olsson, A.-K., Dimberg, A., Kreuger, J. & Claesson-Welsh, L. VEGF receptor signalling - in control of vascular function. *Nat. Rev. Mol. Cell Biol.* **7,** 359–371 (2006).
152. Iwama, A. *et al.* Molecular cloning and characterization of mouse TIE and TEK receptor tyrosine kinase genes and their expression in hematopoietic stem cells. *Biochem Biophys Res Commun* **195,** 301–309 (1993).
153. Li, W.-L. *et al.* Endothelial cell-specific expression of Cre recombinase in transgenic mice. *Yi Chuan Xue Bao* **32,** 909–915 (2005).
154. Schlaeger, T. M. *et al.* Uniform vascular-endothelial-cell-specific gene expression in both embryonic and adult transgenic mice. *Proc. Natl. Acad. Sci. U. S. A.* **94,** 3058–3063 (1997).
155. Hou, Y., Li, F., Karin, M. & Ostrowski, M. C. Analysis of the IKKbeta/NF-kappaB signaling pathway during embryonic angiogenesis. *Dev. Dyn. Off. Publ. Am. Assoc. Anat.* **237,** 2926–2935 (2008).
156. Tan, Z. *et al.* Lineage tracing reveals conversion of liver sinusoidal endothelial cells into hepatocytes. *Dev. Growth Differ.* (2016). doi:10.1111/dgd.12307
157. Verhagen-Oldenampsen, J. H. E. *et al.* Loss of Ercc1 Results in a Time- and Dose-Dependent Reduction of Proliferating Early Hematopoietic Progenitors. *Anemia* **2012,** 1–9 (2012).
158. Zhu, B.-M. *et al.* Hematopoietic-specific Stat5-null mice display microcytic hypochromic anemia associated with reduced transferrin receptor gene expression. *Blood* **112,** 2071–2080 (2008).
159. Monvoisin, A. *et al.* VE-cadherin-CreERT2 transgenic mouse: a model for inducible recombination in the endothelium. *Dev Dyn* **235,** 3413–22 (2006).
160. Okabe, K. *et al.* Neurons limit angiogenesis by titrating VEGF in retina. *Cell* **159,** 584–596 (2014).
161. Sörensen, I., Adams, R. H. & Gossler, A. DLL1-mediated Notch activation regulates endothelial identity in mouse fetal arteries. *Blood* **113,** 5680–5688 (2009).
162. Forde, A., Constien, R., Gröne, H.-J., Hämmerling, G. & Arnold, B. Temporal Cre-mediated recombination exclusively in endothelial cells using Tie2 regulatory elements. *Genesis* **33,** 191–197 (2002).
163. Korhonen, H. *et al.* Anaphylactic shock depends on endothelial Gq/G11. *J. Exp. Med.* **206,** 411–420 (2009).
164. Claxton, S. *et al.* Efficient, inducible Cre-recombinase activation in vascular endothelium. *Genesis* **46,** 74–80 (2008).
165. Higashi, A. Y. *et al.* Direct Hematological Toxicity and Illegitimate Chromosomal Recombination Caused by the Systemic Activation of CreERT2. *J. Immunol.* **182,** 5633–5640 (2009).
166. Guo, C., Yang, W. & Lobe, C. G. A Cre recombinase transgene with mosaic, widespread tamoxifen-inducible action. *Genesis* **32,** 8–18 (2002).

167. Patel, S. H. *et al.* Low-dose tamoxifen treatment in juvenile males has long-term adverse effects on the reproductive system: implications for inducible transgenics. *Sci. Rep.* **7,** (2017).
168. Huang, Y. W. & Meng, X. J. Identification of a porcine DC-SIGN-related C-type lectin, porcine CLEC4G (LSECtin), and its order of intron removal during splicing: comparative genomic analyses of the cluster of genes CD23/CLEC4G/DC-SIGN among mammalian species. *Dev. Comp. Immunol.* **33,** 747–760 (2009).
169. Domínguez-Soto, A. *et al.* The pathogen receptor liver and lymph node sinusoidal endotelial cell C-type lectin is expressed in human Kupffer cells and regulated by PU.1. *Hepatology* **49,** 287–296 (2009).
170. Leibing, T. *et al.* Angiocrine Wnt signaling controls liver growth and metabolic maturation in mice. *Hepatology* (2017). doi:10.1002/hep.29613
171. Wang, B., Zhao, L., Fish, M., Logan, C. Y. & Nusse, R. Self-renewing diploid Axin2(+) cells fuel homeostatic renewal of the liver. *Nature* **524,** 180–185 (2015).
172. Koch, P.-S. *et al.* Angiocrine Bmp2 signaling in murine liver controls normal iron homeostasis. *Blood* **129,** 415–419 (2017).
173. Zhou, L. *et al.* Murine peripherin gene sequences direct Cre recombinase expression to peripheral neurons in transgenic mice. *FEBS Lett.* **523,** 68–72 (2002).
174. Henikoff, S. Conspiracy of silence among repeated transgenes. *BioEssays News Rev. Mol. Cell. Dev. Biol.* **20,** 532–535 (1998).
175. Xin, H.-B., Deng, K.-Y., Rishniw, M., Ji, G. & Kotlikoff, M. I. Smooth muscle expression of Cre recombinase and eGFP in transgenic mice. *Physiol. Genomics* **10,** 211–215 (2002).
176. Bianchi, R. *et al.* A Transgenic Prox1-Cre-tdTomato Reporter Mouse for Lymphatic Vessel Research. *PLOS ONE* **10,** e0122976 (2015).
177. Van Keuren, M. L., Gavrilina, G. B., Filipiak, W. E., Zeidler, M. G. & Saunders, T. L. Generating transgenic mice from bacterial artificial chromosomes: transgenesis efficiency, integration and expression outcomes. *Transgenic Res.* **18,** 769–785 (2009).
178. Dominguez-Soto, A. *et al.* The DC-SIGN-related lectin LSECtin mediates antigen capture and pathogen binding by human myeloid cells. *Blood* **109,** 5337–5345 (2007).
179. Banks, W. A. From blood–brain barrier to blood–brain interface: new opportunities for CNS drug delivery. *Nat. Rev. Drug Discov.* **15,** 275–292 (2016).
180. Zlokovic, B. V. The Blood-Brain Barrier in Health and Chronic Neurodegenerative Disorders. *Neuron* **57,** 178–201 (2008).
181. Wilhelm, I., Fazakas, C. & Krizbai, I. A. In vitro models of the blood-brain barrier. *Acta Neurobiol. Exp. (Warsz.)* **71,** 113–128 (2011).
182. Meng, F. *et al.* Surfactant protein A promoter directs the expression of Cre recombinase in brain microvascular endothelial cells of transgenic mice. *Matrix Biol.* **26,** 54–57 (2007).
183. Li, F. *et al.* Endothelial Smad4 Maintains Cerebrovascular Integrity by Activating N-Cadherin through Cooperation with Notch. *Dev. Cell* **20,** 291–302 (2011).
184. Li, Z. *et al.* Mouse Embryonic Head as a Site for Hematopoietic Stem Cell Development. *Cell Stem Cell* **11,** 663–675 (2012).
185. Guo, S.-L. *et al.* Akt-p53-miR-365-cyclin D1/cdc25A axis contributes to gastric tumorigenesis induced by PTEN deficiency. *Nat. Commun.* **4,** (2013).

186. Ridder, D. A. *et al.* TAK1 in brain endothelial cells mediates fever and lethargy. *J. Exp. Med.* **208,** 2615–2623 (2011).
187. Wilhelms, D. B. *et al.* Deletion of Prostaglandin E2 Synthesizing Enzymes in Brain Endothelial Cells Attenuates Inflammatory Fever. *J. Neurosci.* **34,** 11684–11690 (2014).
188. Eskilsson, A. *et al.* Immune-Induced Fever Is Mediated by IL-6 Receptors on Brain Endothelial Cells Coupled to STAT3-Dependent Induction of Brain Endothelial Prostaglandin Synthesis. *J. Neurosci.* **34,** 15957–15961 (2014).
189. Storck, S. E. *et al.* Endothelial LRP1 transports amyloid-β1–42 across the blood-brain barrier. *J. Clin. Invest.* **126,** 123–136 (2015).
190. Iwakiri, Y. & Groszmann, R. J. Vascular endothelial dysfunction in cirrhosis. *J. Hepatol.* **46,** 927–934 (2007).
191. Lin, L. *et al.* Amelioration of cirrhotic portal hypertension by targeted cyclooxygenase-1 siRNA delivery to liver sinusoidal endothelium with polyethylenimine grafted hyaluronic acid. *Nanomedicine Nanotechnol. Biol. Med.* **13,** 2329–2339 (2017).
192. Yang, Z. F. & Poon, R. T. P. Vascular Changes in Hepatocellular Carcinoma. *Anat. Rec. Adv. Integr. Anat. Evol. Biol.* **291,** 721–734 (2008).
193. Ishikawa, H. *et al.* Antiangiogenic gene therapy for hepatocellular carcinoma using angiostatin gene. *Hepatology* **37,** 696–704 (2003).
194. Aravalli, R. N., Belcher, J. D. & Steer, C. J. Liver-Targeted Gene Therapy: Approaches and Challenges. *Liver Transpl.* **21,** 718–737 (2015).
195. Abel, T. *et al.* Specific gene delivery to liver sinusoidal and artery endothelial cells. *Blood* **122,** 2030–2038 (2013).
196. Scherphof, G. L., Koning, G., Bartsch, M., Yan, X. & Kamps, J. Targeting liposomes and lipoplexes to cells in the liver. *Cell. Mol. Biol. Lett.* **7,** 251–254 (2002).
197. Kim, M. J. & Ahituv, N. The Hydrodynamic Tail Vein Assay as a Tool for the Study of Liver Promoters and Enhancers. in *Pharmacogenomics* (eds. Innocenti, F. & van Schaik, R. H. N.) **1015,** 279–289 (Humana Press, 2013).
198. Suda, T. & Liu, D. Hydrodynamic Gene Delivery: Its Principles and Applications. *Mol. Ther.* **15,** 2063–2069 (2007).
199. Kamps, J. A., Morselt, H. W., Swart, P. J., Meijer, D. K. & Scherphof, G. L. Massive targeting of liposomes, surface-modified with anionized albumins, to hepatic endothelial cells. *Proc. Natl. Acad. Sci. U. S. A.* **94,** 11681–11685 (1997).
200. Marquez, J. *et al.* Targeting liver sinusoidal endothelial cells with miR-20a-loaded nanoparticles reduces murine colon cancer metastasis to the liver. *Int. J. Cancer* (2018). doi:10.1002/ijc.31343
201. Pankowicz, F. P., Jarrett, K. E., Lagor, W. R. & Bissig, K.-D. CRISPR/Cas9: at the cutting edge of hepatology. *Gut* **66,** 1329–1340 (2017).
202. Yin, H. *et al.* Genome editing with Cas9 in adult mice corrects a disease mutation and phenotype. *Nat. Biotechnol.* **32,** 551–553 (2014).
203. Yin, H. *et al.* Therapeutic genome editing by combined viral and non-viral delivery of CRISPR system components in vivo. *Nat. Biotechnol.* **34,** 328–333 (2016).
204. Yang, Y. *et al.* A dual AAV system enables the Cas9-mediated correction of a metabolic liver disease in newborn mice. *Nat. Biotechnol.* **34,** 334–338 (2016).

205. Engelholm, L. H. *et al.* CRISPR/Cas9 Engineering of Adult Mouse Liver Demonstrates That the Dnajb1 – Prkaca Gene Fusion Is Sufficient to Induce Tumors Resembling Fibrolamellar Hepatocellular Carcinoma. *Gastroenterology* **153,** 1662-1673.e10 (2017).
206. Pu, W. T., Ishiwata, T., Juraszek, A. L., Ma, Q. & Izumo, S. GATA4 is a dosage-sensitive regulator of cardiac morphogenesis. *Dev. Biol.* **275,** 235–244 (2004).
207. Holtzinger, A., Rosenfeld, G. E. & Evans, T. Gata4 directs development of cardiac-inducing endoderm from ES cells. *Dev. Biol.* **337,** 63–73 (2010).
208. Zheng, R. *et al.* Function of GATA factors in the adult mouse liver. *PLoS One* **8,** e83723 (2013).
209. Pierre, M., Yoshimoto, M., Huang, L., Richardson, M. & Yoder, M. C. VEGF and IHH rescue definitive hematopoiesis in Gata-4 and Gata-6-deficient murine embryoid bodies. *Exp. Hematol.* **37,** 1038–1053 (2009).
210. Cañete, A. *et al.* A population of hematopoietic stem cells derives from GATA4-expressing progenitors located in the placenta and lateral mesoderm of mice. *Haematologica* haematol.2016.155812 (2017). doi:10.3324/haematol.2016.155812
211. Hosoya-Ohmura, S. *et al.* GATA-4 incompletely substitutes for GATA-1 in promoting both primitive and definitive erythropoiesis in vivo. *J. Biol. Chem.* **281,** 32820–32830 (2006).
212. Agnihotri, S., Wolf, A., Picard, D., Hawkins, C. & Guha, A. GATA4 is a regulator of astrocyte cell proliferation and apoptosis in the human and murine central nervous system. *Oncogene* **28,** 3033–3046 (2009).
213. Walker, E. M., Thompson, C. A. & Battle, M. A. GATA4 and GATA6 regulate intestinal epithelial cytodifferentiation during development. *Dev Biol* **392,** 283–94 (2014).
214. Zhao, R. *et al.* GATA6 is essential for embryonic development of the liver but dispensable for early heart formation. *Mol Cell Biol* **25,** 2622–31 (2005).
215. Tevosian, S. G. *et al.* FOG-2: A novel GATA-family cofactor related to multitype zinc-finger proteins Friend of GATA-1 and U-shaped. *Proc. Natl. Acad. Sci. U. S. A.* **96,** 950–955 (1999).
216. Tevosian, S. G. *et al.* FOG-2, a cofactor for GATA transcription factors, is essential for heart morphogenesis and development of coronary vessels from epicardium. *Cell* **101,** 729–739 (2000).
217. Ding, B.-S. *et al.* Inductive angiocrine signals from sinusoidal endothelium are required for liver regeneration. *Nature* **468,** 310–315 (2010).
218. Yim, S. H. *et al.* Disruption of the Arnt gene in endothelial cells causes hepatic vascular defects and partial embryonic lethality in mice. *Hepatology* **44,** 550–60 (2006).
219. Cuervo, H. *et al.* Endothelial notch signaling is essential to prevent hepatic vascular malformations in mice. *Hepatology* **64,** 1302–1316 (2016).
220. Xing, Y., Zhao, T., Gao, X. & Wu, Y. Liver X receptor α is essential for the capillarization of liver sinusoidal endothelial cells in liver injury. *Sci. Rep.* **6,** 21309 (2016).
221. Antoniv, T. T. *et al.* Identification of a Repressor in the First Intron of the Human α2(I) Collagen Gene. *J. Biol. Chem.* **280,** 35417–35423 (2005).

222. Wang, L., Tanaka, S. & Ramirez, F. GATA-4 binds to an upstream element of the human α2(I) collagen gene (COL1A2) and inhibits transcription in fibroblasts. *Matrix Biol.* **24,** 333–340 (2005).
223. Wells, R. G. Cellular Sources of Extracellular Matrix in Hepatic Fibrosis. *Clin Liver Dis* **12,** 759–viii (2008).
224. Teichert, A.-M. *et al.* Endothelial nitric oxide synthase gene expression during murine embryogenesis: commencement of expression in the embryo occurs with the establishment of a unidirectional circulatory system. *Circ. Res.* **103,** 24–33 (2008).
225. Guillot, P. V. *et al.* Targeting of human eNOS promoter to the Hprt locus of mice leads to tissue-restricted transgene expression. *Physiol. Genomics* **2,** 77–83 (2000).
226. Manavski, Y. *et al.* Endothelial transcription factor KLF2 negatively regulates liver regeneration via induction of activin A. *Proc. Natl. Acad. Sci.* 201613392 (2017). doi:10.1073/pnas.1613392114
227. Marrone, G. *et al.* The transcription factor KLF2 mediates hepatic endothelial protection and paracrine endothelial-stellate cell deactivation induced by statins. *J. Hepatol.* **58,** 98–103 (2013).
228. Gressner, A. M., Weiskirchen, R., Breitkopf, K. & Dooley, S. Roles of TGF-beta in hepatic fibrosis. *Front. Biosci. J. Virtual Libr.* **7,** d793-807 (2002).
229. Rantakari, P. *et al.* Fetal liver endothelium regulates the seeding of tissue-resident macrophages. *Nature* (2016). doi:10.1038/nature19814
230. Kajikhina, K., Melchers, F. & Tsuneto, M. Chemokine polyreactivity of IL7Ralpha+CSF-1R+ lympho-myeloid progenitors in the developing fetal liver. *Sci Rep* **5,** 12817 (2015).
231. Wigle, J. T. & Oliver, G. Prox1 function is required for the development of the murine lymphatic system. *Cell* **98,** 769–778 (1999).
232. Wigle, J. T. *et al.* An essential role for Prox1 in the induction of the lymphatic endothelial cell phenotype. *EMBO J.* **21,** 1505–1513 (2002).
233. Hong, Y.-K. *et al.* Prox1 is a master control gene in the program specifying lymphatic endothelial cell fate. *Dev. Dyn. Off. Publ. Am. Assoc. Anat.* **225,** 351–357 (2002).
234. Petrova, T. V. *et al.* Lymphatic endothelial reprogramming of vascular endothelial cells by the Prox-1 homeobox transcription factor. *EMBO J.* **21,** 4593–4599 (2002).
235. Lawson, N. D. *et al.* Notch signaling is required for arterial-venous differentiation during embryonic vascular development. *Dev. Camb. Engl.* **128,** 3675–3683 (2001).
236. Zhong, T. P., Rosenberg, M., Mohideen, M. A., Weinstein, B. & Fishman, M. C. gridlock, an HLH gene required for assembly of the aorta in zebrafish. *Science* **287,** 1820–1824 (2000).
237. Zhong, T. P., Childs, S., Leu, J. P. & Fishman, M. C. Gridlock signalling pathway fashions the first embryonic artery. *Nature* **414,** 216–220 (2001).
238. Duarte, A. *et al.* Dosage-sensitive requirement for mouse Dll4 in artery development. *Genes Dev.* **18,** 2474–2478 (2004).
239. You, L.-R. *et al.* Suppression of Notch signalling by the COUP-TFII transcription factor regulates vein identity. *Nature* **435,** 98–104 (2005).
240. Sang, M. *et al.* LIM-domain-only proteins: multifunctional nuclear transcription coregulators that interacts with diverse proteins. *Mol. Biol. Rep.* **41,** 1067–1073 (2014).

241. Olsavszky, V. *et al.* GATA4 and LMO3 balance angiocrine signaling and autocrine inflammatory activation by BMP2 in liver sinusoidal endothelial cells. *Gene* **627,** 491–499 (2017).
242. Tse, E. *et al.* Null mutation of the Lmo4 gene or a combined null mutation of the Lmo1/Lmo3 genes causes perinatal lethality, and Lmo4 controls neural tube development in mice. *Mol. Cell. Biol.* **24,** 2063–2073 (2004).
243. Zhao, G. Q., Zhao, Q., Zhou, X., Mattei, M. G. & de Crombrugghe, B. TFEC, a basic helix-loop-helix protein, forms heterodimers with TFE3 and inhibits TFE3-dependent transcription activation. *Mol. Cell. Biol.* **13,** 4505–4512 (1993).
244. Steingrimsson, E. *et al.* Mitf and Tfe3, two members of the Mitf-Tfe family of bHLH-Zip transcription factors, have important but functionally redundant roles in osteoclast development. *Proc. Natl. Acad. Sci. U. S. A.* **99,** 4477–4482 (2002).
245. Steingrímsson, E., Tessarollo, L., Reid, S. W., Jenkins, N. A. & Copeland, N. G. The bHLH-Zip transcription factor Tfeb is essential for placental vascularization. *Dev. Camb. Engl.* **125,** 4607–4616 (1998).
246. Mahony, C. B., Fish, R. J., Pasche, C. & Bertrand, J. Y. tfec controls the hematopoietic stem cell vascular niche during zebrafish embryogenesis. *Blood* **128,** 1336–1345 (2016).
247. Ogata, A., Shimizu, T., Abe, R., Shimizu, H. & Sakai, M. Expression of c-maf and mafB genes in the skin during rat embryonic development. *Acta Histochem.* **106,** 65–67 (2004).
248. MacLean, H. E. *et al.* Absence of transcription factor c-maf causes abnormal terminal differentiation of hypertrophic chondrocytes during endochondral bone development. *Dev. Biol.* **262,** 51–63 (2003).
249. Ogino, H. & Yasuda, K. Induction of lens differentiation by activation of a bZIP transcription factor, L-Maf. *Science* **280,** 115–118 (1998).
250. DePianto, D. J., Blankenship, T. N., Hess, J. F. & FitzGerald, P. G. Analysis of non-crystallin lens fiber cell gene expression in c-Maf -/- mice. *Mol. Vis.* **9,** 288–294 (2003).
251. Imaki, J. *et al.* Developmental contribution of c-maf in the kidney: distribution and developmental study of c-maf mRNA in normal mice kidney and histological study of c-maf knockout mice kidney and liver. *Biochem Biophys Res Commun* **320,** 1323–1327 (2004).
252. Kusakabe, M. *et al.* c-Maf plays a crucial role for the definitive erythropoiesis that accompanies erythroblastic island formation in the fetal liver. *Blood* **118,** 1374–1385 (2011).
253. Shimshek, D. R. *et al.* Codon-improved Cre recombinase (iCre) expression in the mouse. *Genesis* **32,** 19–26 (2002).
254. Lee, E. C. *et al.* A highly efficient Escherichia coli-based chromosome engineering system adapted for recombinogenic targeting and subcloning of BAC DNA. *Genomics* **73,** 56–65 (2001).
255. Schindelin, J., Rueden, C. T., Hiner, M. C. & Eliceiri, K. W. The ImageJ ecosystem: An open platform for biomedical image analysis. *Mol. Reprod. Dev.* **82,** 518–529 (2015).

Appendix

List of figures

List of tables

List of abbreviations

Name	Abbreviation
Aorta-gonad-mesonephros	AGM
Bacterial artificial chromosome	BAC
Base pairs	bp
Bone marrow	BM
Bone morphogenetic protein	BMP
Caudal hematopoietic tissue	CHT
Central vein	CV
Clustered regularly interspaced short palindromic repeats	CRISPR
Complementary DNA	cDNA
CRISPR-associated protein 9	Cas9
C-type lectin domain family 4 member G	CLEC4G
C-X-C chemokine receptors	CXCR
Day postpartum	Dpp
Deoxynucleotide triphosphate	dNTPs
Disabled homolog 2	Dab2
Embryonic day	E
Endothelial cell	EC
Epidermal growth factor	EGF
Epithelial–mesenchymal transition	EMT
Extracellular matrix	ECM
Fetal calf serum	FCS
Fetal liver	FL
Fibroblast growth factor	FGF
Fluorescent activated cell sorting	FACS
Friend of GATA	FOG
Haematopoietic stem and progenitor cells	HSPCs
Haematopoietic progenitor cells	HPCs
Haematopoietic stem cells	HSCs
Haematoxylin & eosin	H&E
Hanks' Balanced Salt Solution	HBSS
Hepatocellular carcinoma	HCC
Hepatocyte growth factor	HGF
Hepatocyte nuclear factor	HNF
High-endothelial venule	HEV
Hypoxia-inducible transcription factor 1 subunit β	Hif-1β
Immunofluorescence	IF
LIM-domain-only	LMO
Lineage- Sca-1+ cKit+	LSK
Liver sinusoidal endothelial cells	LSEC
Long term-HSC	lt-HSC
Lymph node	LN
Lymphatic vessel endothelial hyaluronan receptor 1	LYVE1

Messenger RNA	mRNA
Multipotent progenitor cells	MPP
Optimal cutting temperature	OCT
P1-derived artificial chromosome	PAC
Paraformaldehyde	PFA
Peripheral blood mononuclear cells	pBMCs
Phosphate buffered saline	PBS
Phycoerythrin	PE
Plasmalemma vesicle-associated protein	PLVAP
Polymerase chain reaction	PCR
Portal vein	PV
Protein wntless homolog	Wls
Ribonucleic acid	RNA
Room temperature	RT
Rspondin	Rspo
Septum transversum mesenchyme	STM
Short term HSC	st-HSC
Small interfering RNA	siRNA
Stabilin	Stab
Transcription factor	TF
Transcription factor EC/TF EC	Tfec
Tris base, acetic acid and EDTA buffer	TAE buffer
Vascular endothelial	VE
Vascular endothelial growth factor	VEGF
Yellow fluorescent protein	YFP
Yolk sac	YS